NEW MEASUREMENTS ON THE
ABSOLUTE COSMIC RAY IONIZATION
FROM SEA LEVEL TO 1540 KILOMETERS ALTITUDE

Thesis by

Michael James George

CALIFORNIA INSTITUTE OF TECHNOLOGY

PASADENA, CALIFORNIA

NEW MEASUREMENTS ON THE

ABSOLUTE COSMIC RAY IONIZATION

FROM SEA LEVEL TO 1540 KILOMETERS ALTITUDE

Thesis by

Michael James George

NEW MEASUREMENTS ON THE

ABSOLUTE COSMIC RAY IONIZATION

FROM SEA LEVEL TO 1540 KILOMETERS ALTITUDE

Thesis by

Michael James George

In Partial Fulfillment of the Requirements

For the Degree of

Doctor of Philosophy

California Institute of Technology

Pasadena, California 91109

1969

(Submitted April 25, 1969)

ACKNOWLEDGMENTS

mention for their help in integrating the experiment onto the spacecraft.

Thanks are due Dr. Anderson and Dr. James McCoy of Rice University

for their efforts in the tedious process of performing the initial reduction

of the POGO ion chamber data. Finally, the author acknowledges Dr.

K. A. Anderson of the University of California, Berkeley, and Dr. S.

R. Kane of the University of Minnesota for making available their data

from the ion chambers on the IMP-III and OGO-I satellites. NASA

contract numbers involved in this research were NGL 05-002-007,

NAS 5-3095, NAS 5-9317 (Rice University), and NAS 7-100 (Jet Propulsion

Laboratory).

ABSTRACT

An air filled ionization chamber has been constructed with a volume of 552 liters and a wall consisting of 12.7 mg/cm^2 of plastic wrapped over a rigid, lightweight aluminum frame. A calibration in absolute units, independent of previous Caltech ion chamber calibrations, was applied to a sealed Neher electrometer for use in this chamber. The new chamber was flown along with an older, argon filled, balloon type chamber in a C-135 aircraft from 1,000 to 40,000 feet altitude, and other measurements of sea level cosmic ray ionization were made, resulting in the value of 2.60 ± .03 ion pairs/(cm^3 sec atm) at sea level. The calibrations of the two instruments were found to agree within 1 percent, and the airplane data were consistent with previous balloon measurements in the upper atmosphere. Ionization due to radon gas in the atmosphere was investigated. Absolute ionization data in the lower atmosphere have been compared with results of other observers, and discrepancies have been discussed.

Data from a polar orbiting ion chamber on the OGO-II, IV spacecraft have been analyzed. The problem of radioactivity produced on the spacecraft during passes through high fluxes of trapped protons has been investigated, and some corrections determined. Quiet time ionization averages over the polar regions have been plotted as function of altitude, and an analytical fit is made to the data that gives a value of 10.4 ± 2.3 percent for the fractional part of the ionization at the top of the atmosphere due to splash albedo particles, although this result is shown to depend on an assumed angular distribution for the albedo particles.

Comparisons with other albedo measurements are made. The data are shown to be consistent with balloon and interplanetary ionization measurements. The position of the cosmic ray knee is found to exhibit an altitude dependence, a North-South effect, and a small local time variation.

CONTENTS

Contents, cont'd.

1

Part I

THE ABSOLUTE VALUE OF COSMIC RAY

IONIZATION IN THE LOWER ATMOSPHERE

Introduction

The ionization in the upper atmosphere due to cosmic radiation has been studied extensively since the use of high altitude balloons became practical in the middle 1930's. Its dependence on atmospheric depth, geomagnetic latitude, and solar activity are now well known (1,2). These studies have involved the use of integrating ionization chambers, which are noted for their convenience and accuracy.

The ionization in the lower atmosphere and at various depths in lakes was first investigated extensively by Millikan and Cameron (3) in 1931. Recently there has been renewed interest in the ionization at sea level and in the lower atmosphere, particularly in connection with the problem of man-made radioactivity in various earth environments. Measurements on sea level cosmic ray ionization by Shamos and Liboff (4) and the ionization in the lower atmosphere by Lowder and Beck (5) have shown significant disagreement with the earlier Millikan values.

Disagreements among various ion chamber results are thought to be due in large measure to the different properties of the chambers themselves and to the method by which the chambers are calibrated in absolute units. We decided to undertake some experiments with the following two objectives as our goal: 1) a new absolute ionization cali- bration, independent of previous Caltech calibrations, measured with a new instrument but compared with the old ones; and 2) a new deter- mination of the ionization vs. depth curve in the lower atmosphere and comparison with results obtained with the Caltech balloon chambers. We would try to make our new measurements as directly as possible. Where perturbing effects occurred, we would try to eliminate them rather than

correct for them.

Johnston (6) also made an independent calibration check on the Caltech ionization standards. However, the instrumentation that he used was quite similar to that which was already existing, so the effects due to chamber walls, fill gas, etc. were not changed significantly. He then proceeded to discuss extensively the cosmic ray ionization in the upper atmosphere, deriving various corrections to be applied to the Caltech 8.8 liter ion chamber results from balloon flights. Many of his calculations will be of significance in the analysis of our results in the lower atmosphere.

The present Caltech ion chamber calibration has been carried along from an original absolute ionization determination made by Millikan in 1931. Johnston's check in 1955 agreed with it, so it has been maintained unchanged through the use of "standard" ionization chambers, which have been kept especially for the purpose of intercalibrating the chambers to be used for balloon flights. It is very important to point out that the Caltech absolute calibration and all published Caltech ion-ization values are expressed in terms of Millikan's original standard atmosphere, which is air at $24°C$ and 74 cm Hg, the typical Pasadena laboratory atmosphere. This unique standard atmosphere has led to considerable confusion among readers of the literature who have tried to compare Caltech absolute values to those reported from other institutions, which relate to STP air. In the hope of avoiding such confusion, all ionization values given in the following text, including previously published Caltech results, will be expressed in terms of STP air. The conversion factor is 1.1173.

An Air Filled, Thin Walled Ionization Chamber

A. Construction.

Two problems inherent in almost all reported ionization chamber results are the effect of the chamber walls on the measured ionization and the reduction of the ionization from the chamber fill gas to STP air. No measurements have ever been reported based on ion chambers that were not subject to at least one, and usually both, of these difficulties. Lowder and Beck (5) have used an air filled chamber, but its walls were 1.08 gm/cm^2, mostly aluminum. Shamos and Liboff (4) have used chambers with plastic walls of approximately 0.5 gm/cm^2 thickness, but they are filled with $C C\ell_2 F_2$. Most other ion chambers have steel walls and are argon filled.

Thus we found it desirable to build an ion chamber that eliminates both of these problems. It must have a very large volume, since fewer ion pairs are formed in air than in more commonly used fill gases, resulting in a loss of sensitivity, compounded by the fact that it must operate at ambient pressure, since the very thin walls will be able to support essentially no internal pressure. A frame having the shape of an icosahedron was constructed from $\frac{1}{4}$ " diameter aluminum tubing. This particular shape was chosen because the triangular faces make the structure very strong and rigid, and the volume could easily be determined from accurate measurements of the 30 edges. The length of each edge turned out to be 81.20 cm, corresponding to a volume of 1168 liters, perhaps the largest ion chamber ever used. The walls of the chamber were then formed from .0005" aluminized mylar plastic, pulled

sufficiently tight over each face to ensure a plane surface except for some small ripples. It was found that Scotch No. 850 silver coated tape adhered very well to the clean aluminum surfaces and held the mylar securely in place. For reasons to be explained later, this wall eventually proved to be too thin for practical use, yet with it we obtained valuable information which helped us gain confidence in our final results.

A Neher quartz electrometer (7, 8) was intended for use in the ion chamber. However, for initial investigations and absolute value calibrations, an Applied Physics, Model 30 Vibrating Reed Electrometer was employed. The input circuit to the electrometer is shown in Figure 1. The ion collector was introduced through one of the vertices of the chamber. Several collectors were used for these experiments, usually a metal rod or tube of diameter $\frac{3}{16}$" and of a meter or more in length. The distance between opposite vertices of the chamber was 1.55 m.

The ion collector was kept near ground potential, and the chamber wall at a high negative potential. To minimize leakage current across the teflon insulator, a grounded guard ring was inserted, so there would be little difference in voltage across the insulator between it and the ion collector. V_c, the ion collecting voltage, was supplied by dry batteries and could be varied from 0 to 1225 volts.

The standard capacitor C_s was used for measurement of the absolute value of the ion current by a null method. By varying the voltage V_s on the capacitor, it is possible to keep the ion collector at constant, usually zero, voltage by sucking all the ion current into C_s. Thus we can measure the time required to change the voltage on C_s a known amount. V_s was measured with the 10 volt scale of a voltmeter,
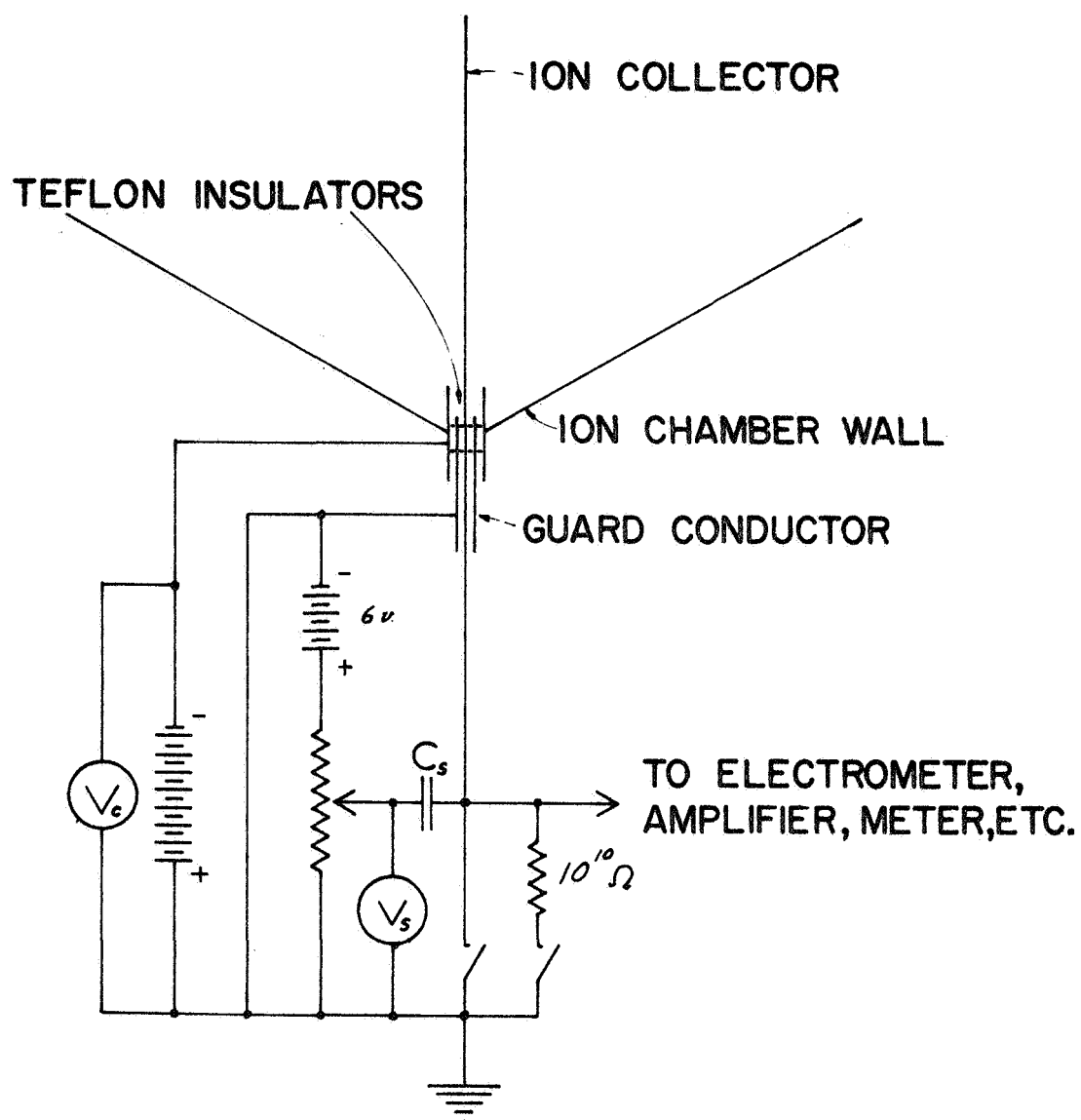
ION COLLECTOR

TEFLON INSULATORS

ION CHAMBER WALL

GUARD CONDUCTOR

6 v.

C_s

V_c

V_s

TO ELECTROMETER,
AMPLIFIER, METER, ETC.

$10^{10} \Omega$

Figure 1.

Circuit for measuring absolute value of the ion current,
for use with vibrating reed electrometer.

which could be read or set to about 0.1 percent. Its calibration was checked against a differential voltmeter. C_s is a cylindrical capacitor which can be used in either of two configurations, short (C_1) or long (C_2). The difference between the two is an extension section C whose dimensions are accurately known. Let a be the inner diameter (outer diameter of internal conductor), b be the outer diameter (inner diameter of external conductor), and ℓ be the length. Then

$$C = 2\pi\epsilon_0 \, \ell/\ln(\frac{b}{a}). \tag{1}$$

The central element was supported from one end directly by the ion collector assembly, with the other end free, so that no insulators were needed between the elements of C_s. It was visually evident that the two cylinders were sufficiently concentric to cause negligible error in the capacitance. The dimensions of C were found to be

$$a = 0.4498 \pm 0.0002 \text{ in}$$

$$b = 0.6252 \pm 0.0002 \text{ in}$$

$$\ell = 3.9165 \pm 0.0005 \text{ in} = 9.948 \pm 0.0001 \text{ cm.}$$

If we use $2\pi\epsilon_0 = 0.5561$ pf/cm, we get

$$C = 16.80 \pm 0.03 \text{ pf.}$$

Now for an ionization current i, let t_1 be the time required to charge C_1 to voltage V_s, and let t_2 be the time required to charge C_2 to the same voltage. Then

$$i t_1 = C_1 V_s , \tag{2}$$

$$i\,t_2 = C_2\,V_s \ . \tag{3}$$

Subtracting, we get

$$i(t_2 - t_1) = (C_2 - C_1)V_s = CV_s \ , \tag{4}$$

$$i = \frac{CV_s}{t_2 - t_1} \ . \tag{5}$$

If the ion chamber contains STP air and has volume A, the absolute ionization in ion pairs/$(cm^3 \sec atm)$ is given by

$$I = \frac{i}{Ae} = \frac{CV_s}{Ae(t_2 - t_1)} \ , \tag{6}$$

where e is the electron charge. The quantities A and C can be determined to within an error of about 0.2 percent; all others 0.1 percent or better. If we always use the same V_s, then for a given ionization chamber we can write (6) as

$$I = \frac{K}{\Delta t} \ , \tag{7}$$

where $K = \dfrac{CV_s}{Ae}$ is a constant and Δt is the time required to charge the standard capacitor, or any configuration of C_s provided the corresponding value is incorporated into K. Eq. (7) is also used to determine the ionization when a Neher quartz electrometer is used, except that K must be determined by measuring Δt in a known ionization field I. In practice the conditions inside the ion chamber will be somewhat different from STP, so the ionization will have to be adjusted accordingly.

An alternate method of determining the ion current is to connect the 10^{10} ohm resistor in Fig. 1 to ground and measure the voltage across it. The voltage can be observed directly on the electrometer output

meter, or it can be recorded continuously by a chart recorder. This method is useful for continuous monitoring of the ion current, but it is not considered nearly so good for measuring absolute currents. The value of the resistor, nominally 10^{10} ohms, is subject to calibration errors as well as changes due to atmospheric temperature and humidity. There is also a noise signal super-imposed upon the d.c. ion current. It is due partly to the discrete number of particles passing through the chamber and partly due to small changes in capacitance between the ion collector and the chamber walls. If the ion current is 10^{-12} amp and V_c is 1000 volts, then such capacitance changes, of characteristic times less than the RC time constant of the ion collector to ground (somewhat greater than 0.1 sec), and of the order of one part in 10^6, will introduce a noise signal of 1 millivolt, or 10 percent of the d.c. signal due to the ion current itself. Even in relatively quiet air the very thin chamber walls were observed to shimmer slightly, and such motion was probably responsible for a large fraction of the noise signals seen. This noise is integrated out when the standard capacitor is used, because the charging times are usually of the order of 100 sec.

B. Analysis of Preliminary Test Data.

The problem of ion recombination has always been a deterrent to the use of air in ionization chambers. The negative ions are normally negative oxygen molecules, and thus it takes much longer to collect them than it does in argon, where they are free electrons. Another important difficulty is the contribution to the total ion current due to alpha particles emitted from radioactive impurities in the ion chamber walls. It will be

shown below that these two problems are intimately related in our thin walled chamber and must be treated simultaneously.

Since the large chamber was ultimately intended to be used to measure low ionization intensities, namely the ionization due to cosmic radiation in the lower atmosphere, we endeavored to do most of our testing and trouble shooting using only the natural background radiation in the lab. Past experience with standard Caltech balloon-type ion chambers (8.8 liter, $\frac{1}{2}$ gm/cm^2 steel wall, filled with 8 atm of argon) indicated the background in the lab was about 8 ion pairs/(cm^3 sec atm), about one third of which was due to cosmic rays and the rest due to local radiation, mostly γ-rays. It soon became apparent, however, that the background ionization that we were measuring in our new ion chamber was considerably more than that, and it was quite variable in time, which was not expected from previous experience.

The hypothesis was advanced that a significant contribution to our ion current was due to α-particles from the decay of radon and its daughters in the atmosphere. These nuclei are known to escape into the atmosphere from materials containing uranium, thorium, and other parent nuclei. The principle isotope involved is probably the gas, ^{222}Rn, which is the direct decay product of ^{226}Ra and has the original parent ^{238}U. It has a half life of 3.8 days and decays through four successive short-lived daughter nuclei until ^{210}Pb is reached, which has a half life of 22 years and probably escapes from the atmosphere before decay in rain, snow, etc. The α-particles from these decays can easily penetrate the thin ion chamber wall and proceed a few centimeters into the active volume, leaving very heavily ionized tracks. Even if only a

small fraction of these ions were collected, a large increase in the ion current could occur. The number of α-particle contributors in the local atmosphere at any time will depend upon the history of that air over periods perhaps as long as several weeks, but with emphasis on the few days preceding the observation.

In order to screen out these α-particles, a housing of polyethylene sheet was built around the ion chamber to enclose sufficient dead air to absorb the α-particles. We began feeding the ion chamber and the surrounding space with air from cylinders of compressed air that had been in storage for several weeks prior to use in order to get rid of possible radioactive contaminants inside the ion chamber itself. This air was claimed by the manufacturer to be oil free, dry, fit for breathing, and composed of 79 percent N_2 and 21 percent O_2. It was used as our standard fill gas in all further experiments. No correction has been used for any possible difference between the ionization in this mixture and that in normal air (approximately 78 percent N_2, 21 percent O_2, 1 percent A), which may be about 0.5 percent greater because the argon contributes $\sim$ 1.5 times as many ions as an equal amount of air. After flushing the chamber and housing with this air for several days, the ion current was observed to have decreased by almost a factor of two, and it became much less variable. It now became possible to make accurate quantitative measurements of the ion current as a function of collecting voltage.

Several typical ion current vs. collecting voltage curves are shown in Figs. 2 and 3. Fig. 2 shows data obtained with only the natural background radiation in the lab. In each of the three cases it is possible
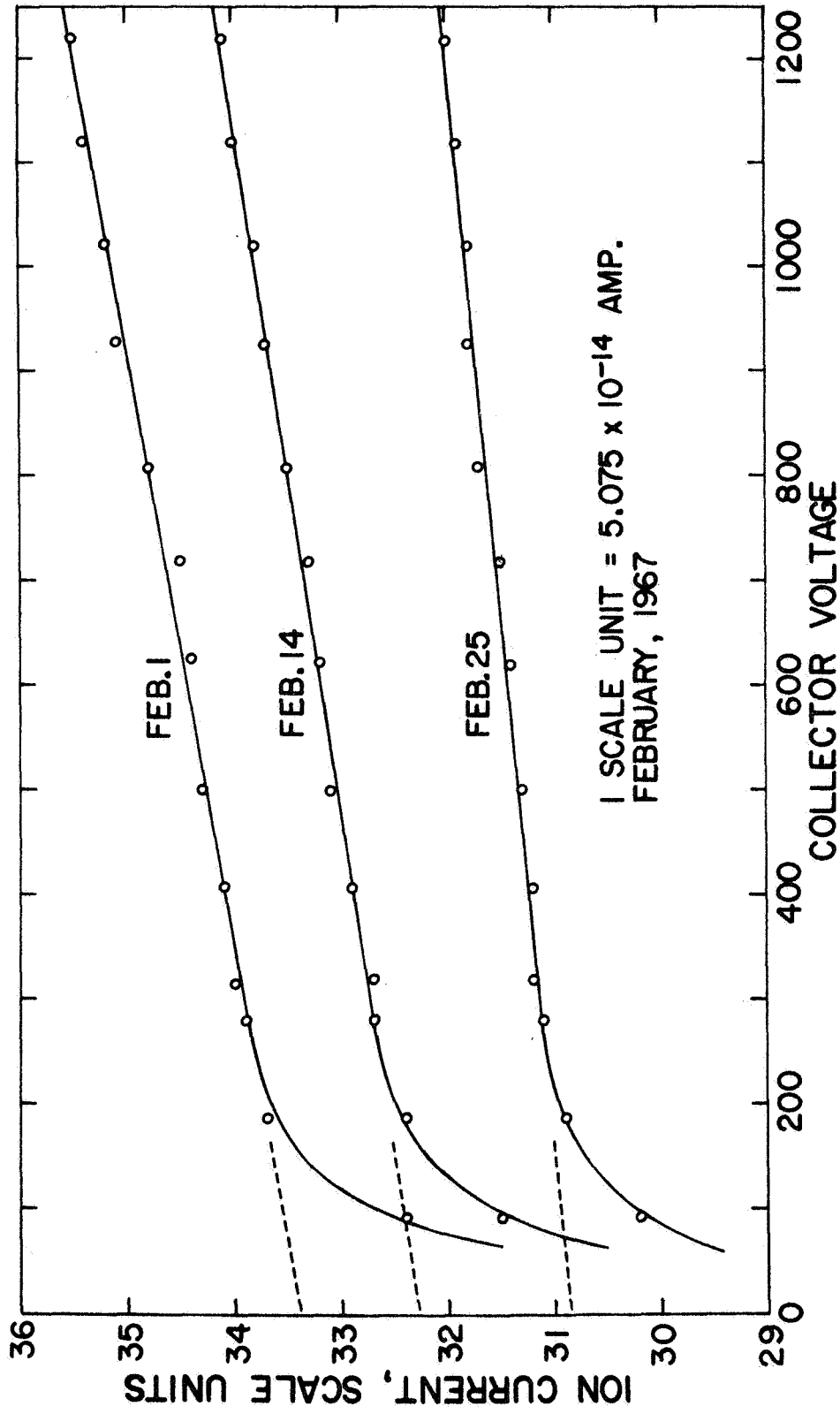
12

Figure 2.

Saturation characteristics of 1168 liter air filled ion chamber for lab background radiation. Data accurate to 0.1 scale unit.
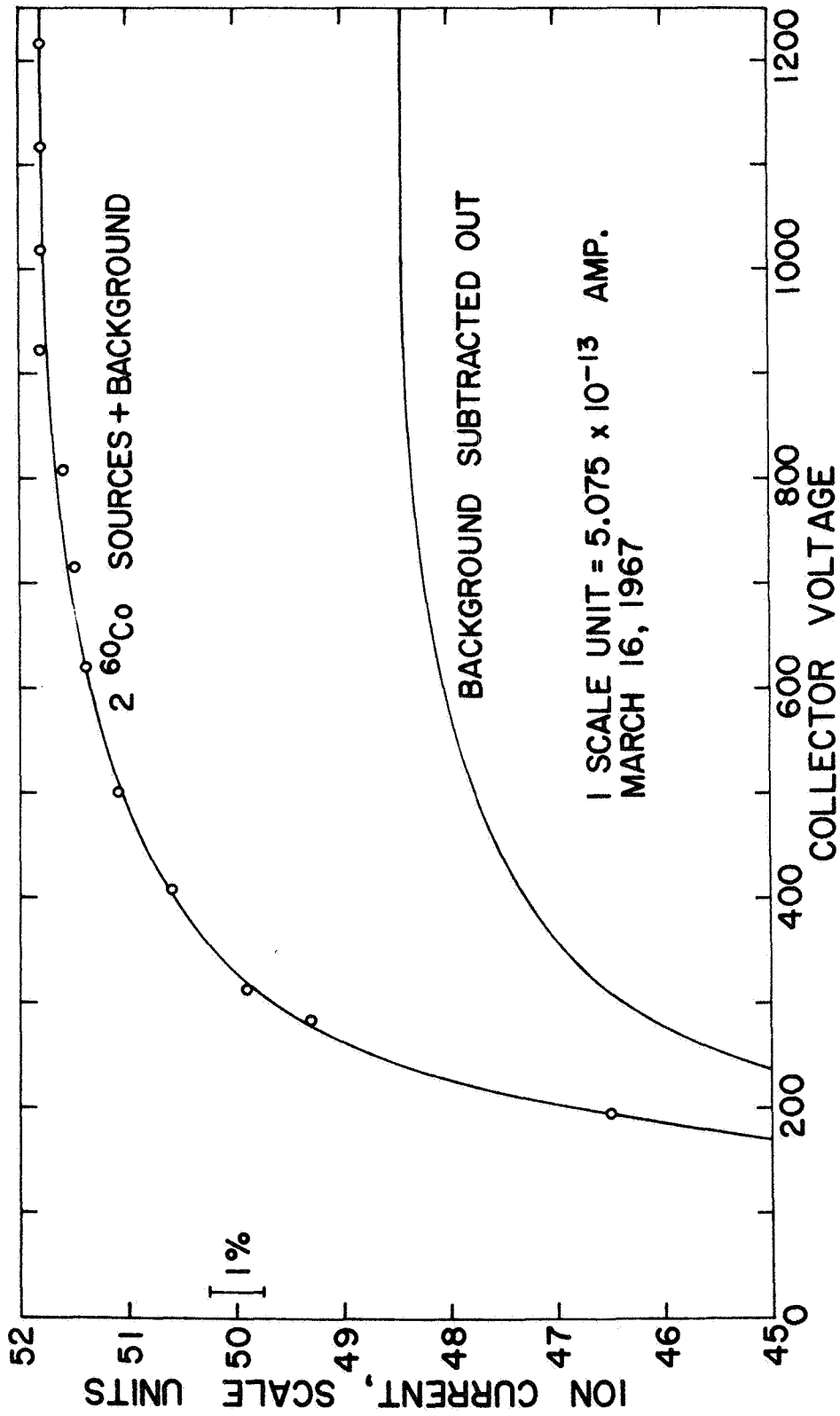
Figure 3.

Saturation characteristics of 1168 liter air filled ion chamber for ^{60}Co γ-rays of ionization strength approximately 15 times the lab background. Data accurate to 0.05 scale unit.

to fit the data obtained with a straight line from 300 volts upward to 1220 volts, the greatest collecting voltage used. The positive slope indicates the ion chamber is not saturated, but the amount of unsaturation seems to be decreasing with time, as is the total ion current. If these curves had been extended to higher voltages, one might expect them eventually to level off and become independent of voltage, but there is no indication here of how far one would have to go. An alternate explanation for the positive slope is a leakage current across the teflon insulator which is proportional to the collecting voltage, but this has been ruled out because of the presence of the guard ring (see Fig. 1).

Fig. 3 shows some results obtained using ^{60}Co γ-rays to increase the ionization to about 15 times the normal background. The shape of these curves is considerably different from that of the background curves. Almost complete saturation seems to have been reached above 1000 volts, especially if one first subtracts out the background ionization. However, at the lower voltages the fraction of ions being collected is less than that for the background results. We assume this is due to volume recombination of the ions at the higher ionization rate. At a collecting voltage of 1000 volts, the electric field at the chamber wall is approximately 1.5 volts/cm.

We were thus led to believe that the positive slopes of the background curves of Fig. 2 are due to α-particles penetrating the chamber walls from the outside or emanating directly from the walls themselves Such α-particles will leave dense tracks of ions in just the part of the chamber where the electric field is weakest, namely near the walls. These ion tracks will therefore be subject to severe columnar

recombination. The Jaffe theory (9) agrees with experiment reasonab.y well for electric fields strong enough to allow collection of 50 percent or more of the ions, but does not seem to work very well in our case, where the field strengths are of the order of 1 to 2 volts/cm, and probably only 10 to 20 percent of the ions are collected. It seems reasonable that for low field strengths the number of ions collected should be approximately proportional to the field if the field is nearly uniform throughout the volume of interest, which in our case is the volume within a few centi-meters of the ion chamber wall. This will explain the fact that we can fit our low intensity ion current vs. voltage curves with positively sloped straight lines, the slope of each line then being a measure of the α-particle contribution present at the time of each measurement. The fact that the intercept of the line also decreases with the slope indicates that we are also getting contributions from β- and γ-rays associated with the same decay process. The same effect is no doubt present in the data taken with the ^{60}Co sources, but it is much harder to see because it is relatively 15 times less.

The February 25 data in Fig. 2 represent about the lowest level of ionization that we were able to obtain with the 1168 liter ion chamber. Similar levels were recorded on two other runs. The apparent residual contamination may be due to one or more of several causes. 1) A small amount of radon-containing air is still entering the polyethylene house and producing α-particles which penetrate the chamber walls. 2) The chamber walls may have contained α-emitting impurities from the beginning. This is a standard problem with ion chambers, and one we hoped yet to eliminate. 3) The outside surface of the chamber may have

become contaminated during exposure to the atmosphere before the protective housing was built. Such contaminants might include dust containing α-emitters, or radioactive nuclei that have adhered themselves to the chamber wall directly from the air. In order to estimate the magnitude of the effect, observe that the difference between the ion current at 1250 volts and the 0 volt intercept is about 4×10^{-14} amp, or about 2.5×10^{5} electrons/sec. If each α-particle deposits 10^{5} ions in the chamber, and if we collect 10 percent of them, then 25 α-particles are required per second. Since the area of chamber wall is almost $6 \, m^{2}$, this is a flux through the chamber walls of about 4 α-particles per m^{2} per sec. They contribute 2.5 percent of the total ion current at 1250 volts.

Fig. 4 shows the relation between the slopes and intercepts of the ion current vs. voltage curves for background ionization. The data have been fit with a least squares straight line. Most of the scatter is probably due to changes in the background radiation that are still taking place in the lab, from which the ion chamber is still sensitive to the β- and γ-radiations. The extrapolated value at zero slope represents an estimate of the background ion current that we would get if the chamber were completely shielded from the α-particles and associated β- and γ-rays. It corresponds to an ionization of 8.34 ± 0.18 pairs/(cm^{3} sec atm). The Caltech standard 8.8 liter ion chambers in nearly the same position gave 9.01 ion pairs, and a set of calibrated balloon chambers gave 9.10 ion pairs. It should be pointed out that this comparison is important only in a qualitative sense, and the result of 8.34 ion pairs is not used in any of the work that follows. It is given here only because it was our first opportunity to compare the large chamber with the balloon chambers.

However, the slope-intercept relation is significant because it provides evidence that the positive slopes are indeed due to α-particles and not some other effect that is merely proportional to the collector voltage.

It should be mentioned that Shamos and Liboff (4) also try to separate out the α-particle contribution from the saturation characteristics of their freon, $CC\ell_2F_2$, filled chambers. However, they observe a transition region after complete saturation of lightly ionizing particles and before the α-particle contribution appears, in which the ion current is independent of collecting voltage. They eliminated the α-contribution from their field measurements by operating in this voltage region. We observe no such flat region in our data.

C. An Improved Ionization Chamber.

The 1168 liter ion chamber had been designed with the idea that it would be flown under a balloon. However, since we were primarily interested in measuring the ionization in the lower atmosphere, it became clear that we should be able to get much better data by flying the chamber in an airplane, where we could have much better control over the chamber environment. Also, the balloon traverses the lower atmosphere rather quickly, whereas the airplane would allow us much more time at selected altitudes. The most suitable aircraft available seemed to be one of three C-135's based in Albuquerque, New Mexico and operated by the U.S. Air Force and Los Alamos Scientific Laboratory. We might expect the radiation inside the plane to be slightly altered by the aircraft skin and other matter inside the plane, but most of these things are aluminum, which should not have too much effect
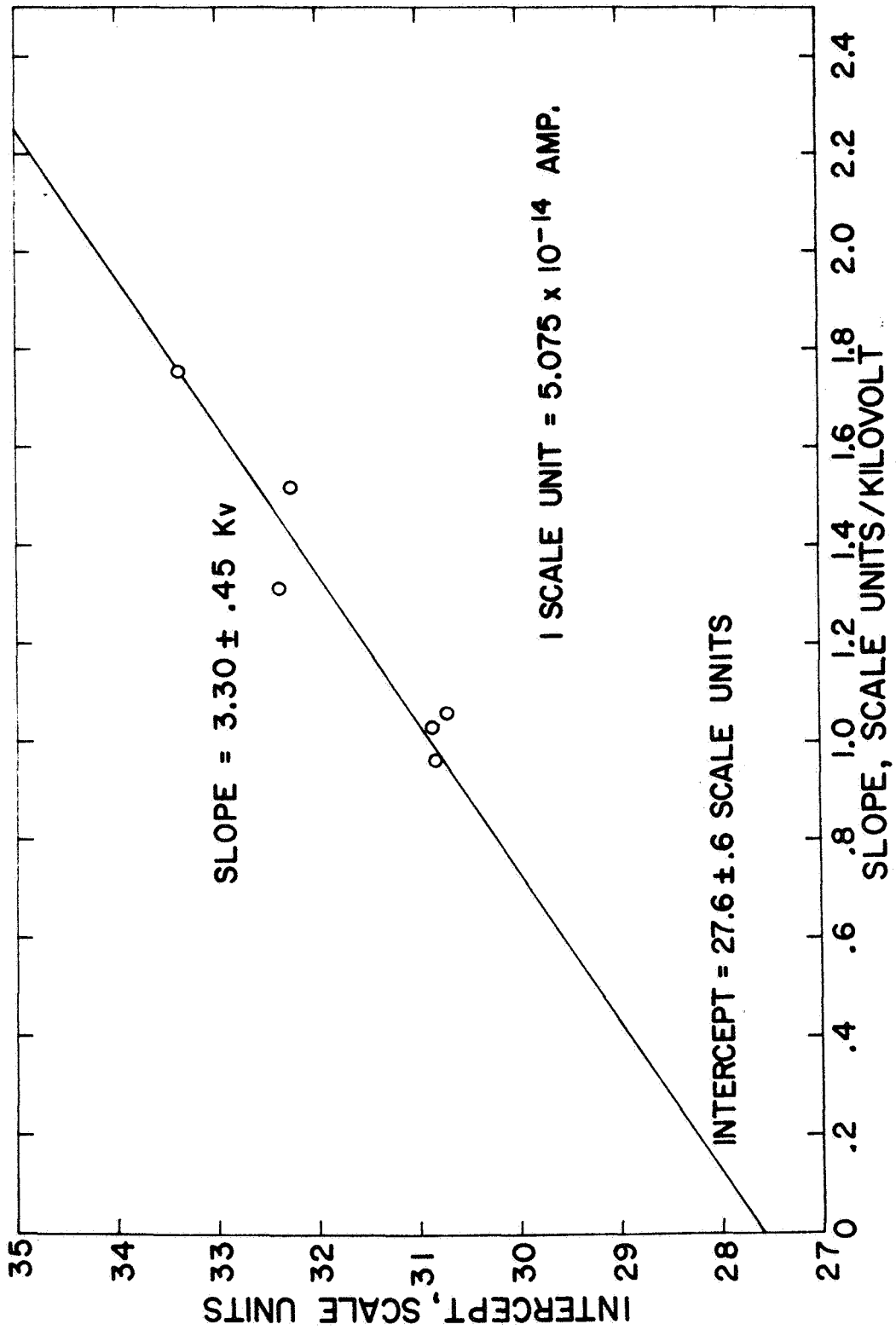
SLOPE = 3.30 ± .45 Kv

I SCALE UNIT = 5.075 x 10^{-14} AMP.

INTERCEPT = 27.6 ± .6 SCALE UNITS

SLOPE, SCALE UNITS/KILOVOLT

INTERCEPT, SCALE UNITS

Figure 4.

Relation of slopes and intercepts of saturation curves of 1168 liter ion chamber for background radiation.

because of its low Z. One of our primary objectives was a comparison of ionizations measured by the 8.8 liter balloon chamber and the large, thin walled chamber, which will be unchanged provided the character of the radiation is not significantly altered by the plane. The 1168 liter chamber was too big to fit through the 3' × 6' aircraft door, however, so it became necessary to design and build a new model.

The geometrical design of the new chamber is shown in Fig. 5. It is the same as the first chamber except for an extra equatorial section. Thus it has 30 equilateral triangular faces instead of 20. The ion collector is to be inserted along the long axis from the lower vertex. The frame was constructed from $\frac{3}{16}$" diameter tubing, and each of the 45 edges turned out to be 53.18 cm long. The volume was 552 ± 2 liters, the surface area 3.67 m^2, and the distance between extreme vertices 1.47 m. It would go through a door of width 33" or more. The mylar walls were covered with epoxy resin to a total average thickness of 12.7 mg/cm^2, determined by weighing the chamber before and after application of the epoxy. Epoxycon C-65 resin was used because it could be applied with a spray gun. Assuming a possible variation of ± 20 percent (some test panels were checked with a micrometer and found good to ± 14 percent) in the wall thickness, the minimum thickness of 10.4 mg/cm^2 is sufficient to stop 8 MeV α-particles, about the most energetic found in natural radioactivity. The epoxy coating also increased the rigidness of the walls and greatly reduced shimmer, so the new chamber ought to withstand mechanical vibrations much better than did the old one. It was eventually determined that vibrations encountered during field experiments had less than 0.1 percent effect on the output current.
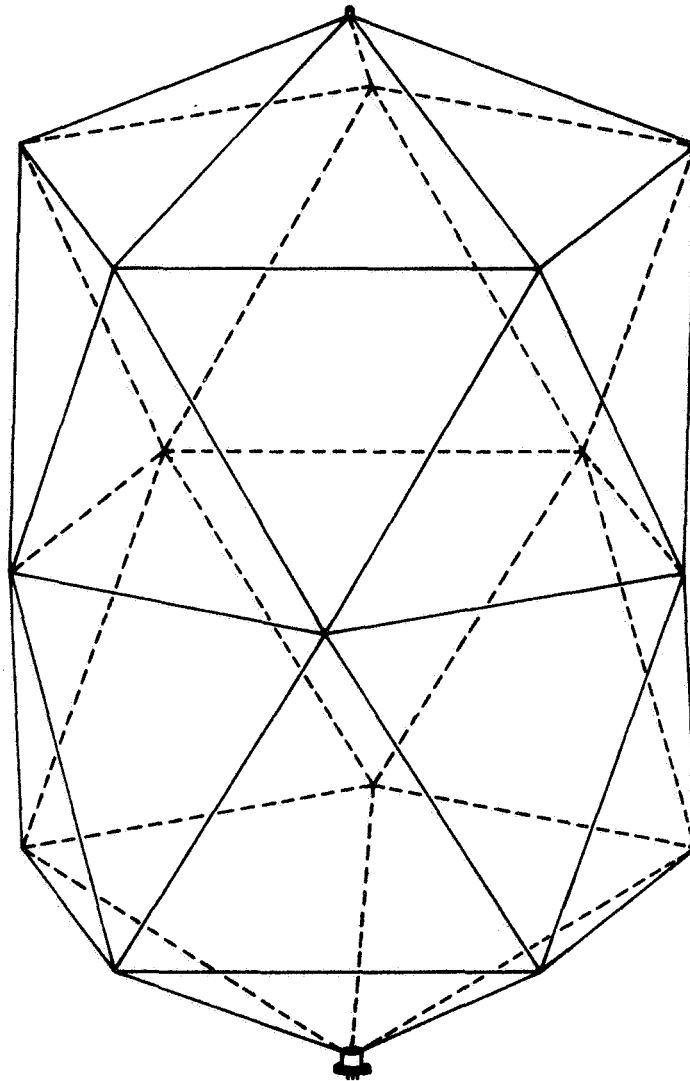
Figure 5.

Geometrical design for 552 liter ionization chamber.
Each of the 45 edges is 53.18 cm long, and the length (top to bottom,
excluding neck) is 146.5 cm. The Neher electrometer is inserted
through the neck at bottom. Gas inlet/outlet is provided
at the bottom/top.

Preliminary experiments with the vibrating reed electrometer produced saturation curves which indicated that the contribution of wall α-particles to the total background ion current at 1250 volts collecting potential was no more than 1 percent, and it could be very much less than that within the error limits of our data. We still encountered variations in the background of a few percent. We assumed this was due to β- and γ-radiations from the radon decays in the room air. We were pleased to find out that there seemed to be little or no α-contamination of the materials used in the ion chamber itself. According to the data given by Sharpe (10) for the emission of α-particles from commercial aluminum surfaces, we might expect one α-particle every 5 to 10 seconds to be emitted into the chamber from the aluminum frame. This would contribute an average of 2×10^{-16} amp to the total ion current of nearly 10^{-12} amp. The chamber walls themselves provide about 20 times the effective surface area of the frame. However, it seems reasonable to expect their α-contribution to be much less than 20 times that of the frame, since they are mostly plastic and have refinement and production chemistries so much different from that of the metals. We do not have to worry about ^{14}C β-rays from the wall, since mylar, epoxy, and most other plastics are made from petroleum, which contains only fossil carbon.

D. An Electrometer for the Ionization Chamber.

The Neher quartz electrometer (7) used in the Caltech 8.8 liter ionization chambers is completely exposed to the chamber fill gas, which is argon. The electrometer was modified (11) for use in the

1 liter POGO satellite chambers to provide a second mode of operation which is roughly 10 times more sensitive than the normal mode. The extra electrical sensitivity was needed to compensate for the decrease in chamber volume in order to keep about the same time resolution. Such an electrometer of the unmodified type had been tried with initial success in the 1168 liter chamber, but its performance rapidly deteriorated. The deterioration was thought to be due to loss of conductivity at the point where the quartz fibre makes contact with the ion collector, because of two reasons. 1) The charge dumped per pulse was much larger than what is encountered in the 8.8 liter chamber, due to the much larger capacitance of the ion collector in the large chamber. This may have caused excessive sparking. 2) The exposure to the ion chamber air probably caused deterioration of the contact point through oxidation or deposit of organic impurities. We concluded that if the electrometer were to be reliable for long periods of time, it would have to be sealed in a casing that was filled with inert gas.

A schematic diagram of the new electrometer is shown in Fig. 6. The maximum outer diameter of the assembly was one inch, so that it could be inserted through the ion chamber neck. The electrometer was of the dual sensitivity type, so that we would be able to measure low ionization intensities with reasonably short integration times. The high voltage shield surrounding the electrometer assembly keeps the electric fields in the sensitive region independent of collecting voltage. Thus we could still study the saturation characteristics of the chamber.

The system was baked out under vacuum at 300°C. It was then filled with argon to 60 psi absolute pressure and sealed by freezing the

ION COLLECTOR 3/16"
STAINLESS STEEL

AQUADAG COATED QUARTZ TUBE

FRICTION FIT

TUNGSTEN FEED-THROUGH

SPRING CONTACTS

QUARTZ INSULATION (OUTSIDE
& INSIDE)

GROUNDED SHIELD
STAINLESS STEEL

QUARTZ-GLASS GRADED SEAL

4 ATM. ARGON FILLED
QUARTZ ELECTROMETER INPUT

GLASS HOUSING

HIGH VOLTAGE CONDUCTOR
SURROUNDS ELECTROMETER
ASSEMBLY

3 HIGH VOLTAGE PINS PROVIDE
SUPPORT FOR ELECTROMETER
ASSEMBLY AND SHIELD

TUNGSTEN FEED THROUGHS

6 ELECTRICAL LEADS ALSO PROVIDE
MECHANICAL SUPPORT

GLASS FILL TUBE

BASE, FITS INTO ION
CHAMBER NECK

EXTERIOR ELECTRICAL
CONNECTIONS

Figure 6.

Sealed electrometer (Neher type) for use in 552 liter air filled
ion chamber. See references 7, 8, 11.

argon out at the quartz end with liquid nitrogen. Based on a tensile strength of 1000 psi for the glass, we calculated that the housing could stand 240 psi, but we only tested it to 80 psi. The internal pressure was found to be necessary in order to damp out oscillations of the quartz electrometer fibre. Leaks were looked for by immersing the whole assembly in kerosene and looking for small bubbles. In one case bubbles were detected coming from a flaw in the glass near one of the tungsten leads. The leak was sealed with wax. When this electrometer was used we kept the ion chamber shell at circuit ground and the ion collector at a high positive potential. It is important that no electrical leakage occurs across the quartz insulator. The interior surface was assumed good because it was baked out and sealed. The exterior surface was heated with a gas or hydrogen flame before inserting the system into the ion chamber where it was exposed only to clean, dry air. Such leakage, or contamination of the chamber walls with α-particles as already discussed, could be detected by observing changes in the apparent saturation characteristics of the ion chamber as one went to lower ionization strengths. Except for the expected effect of volume recombination, no such changes were ever observed with the 552 liter chamber, even at the lowest ionization intensities.

Since its calibration depends on the relative strengths of mechanical and electrical forces, the Neher electrometer depends on the direction of gravity and other accelerations which may be applied to the system. For example, the gravitational coefficient for the high sensitivity mode of the POGO ion chambers was approximately 30 percent/g (12) in the most sensitive direction. The normal calibration and operation

position of the system in Fig. 6 was vertical, along the long axis of the ion chamber. Care was always taken to ensure that the axis of the chamber was always vertical within a degree or less. Since it was to be used in an aircraft, the electrometer was designed so that it would be least sensitive to vertical accelerations, next least sensitive to lateral accelerations, and most sensitive to thrust and drag accelerations. From experience in flying in commercial jet airplanes, we believed that during normal, level flight the forward-backward accelerations were least severe, and vertical accelerations were likely to be most severe. The low sensitivity mode of the electrometer is much less sensitive to accelerations than the high sensitivity mode (about 3 percent/g). In practice we used the low sensitivity mode as our standard calibration, and we planned to check the high sensitivity mode against it at various times during our experiments.

The ion chamber now completed, we list the weight data for the various components.

frame and neck	1100 gm
walls (mylar and epoxy)	465 gm
mylar tape	24 gm
quartz electrometer	85 gm
ion collector	19 gm
complete ion chamber	1693 gm

Two of the sealed electrometers were built. The No. 1 unit was calibrated with ^{60}Co γ-rays producing a total ionization intensity of about 6 times background, the ionization first having been determined

by use of the vibrating reed electrometer and the standard capacitor.
The No. 2 unit was calibrated against the No. 1 unit and held in reserve.

E. Final Test Results.

As already mentioned, the shape of the saturation curves for the
new chamber appeared to be independent of ionization intensity except
for effects which we attribute to volume recombination. Two examples
are given in Fig. 7. The electric field at the chamber wall in volts/cm
is given approximately by the collector voltage divided by 400. For the
comparison given, the volume recombination effect becomes important
only below 250 volts. Higher ionization strengths were investigated
only with the quartz electrometer, where we had only three collector
voltages available from the power supply: 315, 630, and 945 volts. The
radio of ion currents $i(315) / i(945)$ was down about 0.5 percent at
$I = 200$ ion pairs/cm^3 sec atm) and down 2 percent at $I = 800$ ion pairs/
$(cm^3$ sec atm), while the $i(630) / i(945)$ ratio was essentially unaffected
even at 800 ion pairs/$(cm^3$ sec atm). We conclude there is no detectable
contribution of wall α-particles to our data.

The linearity of the quartz system was checked in the following
manner. Using ^{60}Co sources and 945 volts collecting potential, we
measured the separate ionizations due to source configurations I_1 and
I_2, approximately equal to each other. We then measured the ionization
due to $I_1 + I_2$ and compared it to the sum of the first two results,
always subtracting the background out of each measurement. The cycle
was then repeated at higher ionization strengths. Since we have shown
in the preceding paragraph that volume recombination is not important
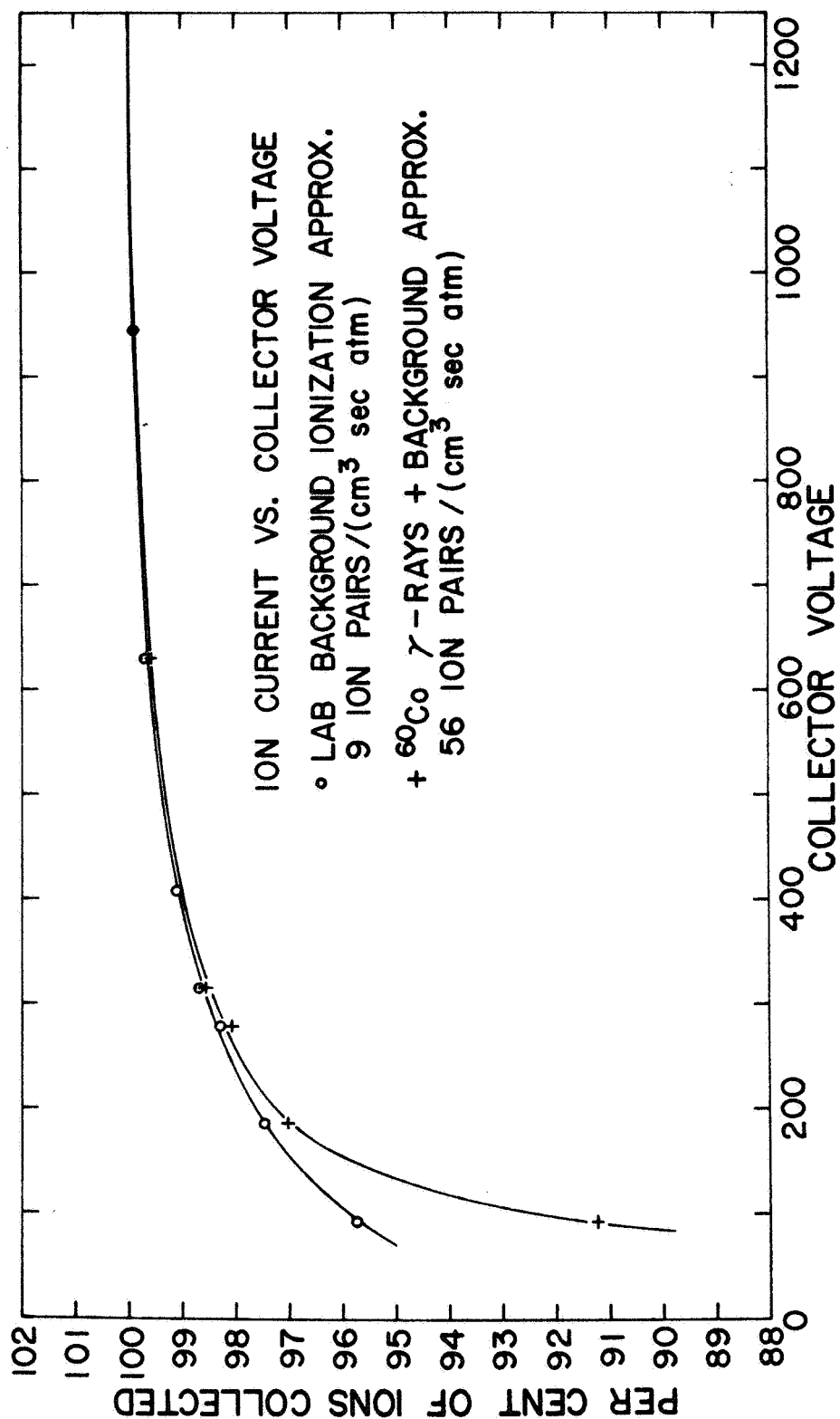
27

Figure 7.

Saturation characteristics of 552 liter air filled ion chamber.
Errors in data points are approximately 0.1 percent.

above 630 volts, the results here are a measure of the linearity of the system at constant voltage. With the electrometer in the low sensitivity mode (hereafter called Mode I) the system was found to be linear to $\pm$ 0.3 percent up to ionizations of 900 ion pairs/$(\text{cm}^3 \sec \text{atm})$. In the high sensitivity mode (hereafter called Mode II) the situation was different. The measured ionization was found to be too low by the amounts given in Table 1. The results are qualitatively similar to

Table 1

Ionization ion pairs/$(\text{cm}^3 \sec \text{atm})$	Departure from Linearity Percent
30	0.0
65	0.2
133	0.6
253	1.3
867	2.9

observations with the POGO ion chambers, but the ionizations are much higher. For Flight Unit No. 1, for example, Mode II remained linear to 6×10^4 ion pairs/$(\text{cm}^3 \sec \text{atm})$, while Mode I remained linear to 3×10^6 ion pairs/$(\text{cm}^3 \sec \text{atm})$. In our case we hope to be able to use Mode I at ionizations where Mode II is non-linear. Quartz system No. 2 was not checked for linearity in as detailed a manner as was used for No. 1, but its similar behavior was verified by comparing the ratio of different radiation strengths with the same ratios determined with system No. 1.

The effect of noise on the ion chamber was investigated in a preliminary sort of way by blowing air over the chamber with a fan. The

integration time in Mode II was unaffected at 315 volts but decreased by 0.3 percent at 945 volts. No effect at all was observed in Mode I, which we plan to use as the calibration standard. In order to prevent external air from entering the chamber, we found it desirable to feed air from our compressed air cylinder through the chamber. A rate of about 1 liter/min seemed to be sufficient. At this rate the measured ionization increased less than 0.1 percent at the background radiation level, where effects due to ions in the entering air might be expected to have the greatest relative contribution.

Cosmic Ray Measurements with the Thin Walled Ionization Chamber

A. The C-135 Aircraft Flight

The objectives of the aircraft flight were twofold: 1) to measure the absolute cosmic ray ionization as a function of altitude in the lower atmosphere using the thin walled, air filled ion chamber and 2) to compare the results so obtained with those obtained using the regular Caltech steel walled, argon filled, balloon type ion chamber. The C-135 aircraft promised to be very well suited to our needs. It could fly to 40,000 ft. altitude with a well controlled cabin atmosphere and had a range long enough to allow time for data acquisition at all our desired altitudes.

The airplane to be used had been used by the Atomic Energy Commission for monitoring of nuclear bomb tests in the atmosphere, but Dr. Robert Peterson of the Los Alamos Scientific Laboratory claimed it was free from radioactive contamination. We checked it with a survey meter and found no hot spots or radiation levels higher than what we could attribute to the normal background, which we expected was due to the concrete below the airplane. Nor did we find any radio-active instrument dials, which used to be a problem in the early history of cosmic ray measurements in airplanes. Our two ion chambers, the large plastic-covered one and the balloon type, were installed on the right side of the cabin, approximately two meters behind the point where the trailing edge of the wing meets the fuselage. That area of the cabin was fairly free from electronic gear or heavy equipment; most of the surrounding matter was aluminum or organic, except for some over-

head electrical cables. The 552 liter ion chamber was suspended inside a special aluminum frame, using ten small shock absorbers which we designed and built to minimize vibration or possible jerky movements of the aircraft. The frame was then fastened rigidly to the interior of the aircraft. The more easily handled 8.8 liter chamber was simply suspended in the cabin for data acquisition and tied down during takeoffs and landings.

A combination power supply and data recording unit had been built for each ion chamber. These allowed us to record our data on paper tape in the same manner as is used for telemetered balloon flight data, except that the ion chamber pulses were transmitted directly by cable rather than by radio. Power was supplied by dry batteries for everything except the synchronous recorder motor, which used 60 cps aircraft power. Timing marks were put on the tape by a mechanical clock. The units were mounted in electronic racks on the left side of the cabin, sufficiently far behind the chambers to be easily accessible to an operator.

Before the flight we determined from our test data that the saturation characteristics of the 552 liter chamber were essentially the same as we had previously observed in the lab, which indicated that the quartz insulator had not become contaminated. All during transportation, installation, testing, and the flight itself we fed the chamber from a compressed air cylinder in order to keep out external air. This was especially necessary when the cabin pressure was increasing. We determined the bias voltage required to make Mode II approximately ten times as sensitive as Mode I. The 8.8 liter chamber had only one mode, giving

about half the integration time of the 552 liter chamber in Mode I at the same ionization strength.

The course to be flown had to meet four basic requirements. 1) It could not exceed mechanical limitations of the aircraft. 2) It must be consistent with military security restrictions in certain areas. 3) In order for our data to show the effect of altitude variation only, we should fly as near as possible to a line of constant geomagnetic cutoff rigidity. 4) The lower altitude portions of the flight must be made over water, so we would not get any contribution from ground radiation. The portions of the actual flight during which data were obtained are shown in Fig. 8, along with the altitude for each run. Also shown are a few cities for reference and lines of constant geomagnetic cutoff rigidity P_c = 4.0 Bv and 4.4 Bv. The latter were determined from 1966 values of Shea and Smart (13).

The flight was made in two parts. The first portion began at 16:13 GMT January 10, 1968 at Albuquerque, New Mexico and ended at 22:40 GMT at Travis Air Force Base, near San Francisco, where a refueling stop was made. Data acquisition proceeded according to a pre-arranged schedule, and runs were made at seven different altitudes. The second portion began at 1:02 GMT January 11, the last two altitudes were completed, and we landed back at Albuquerque at 3:02 GMT.

At the beginning of the flight, we attempted to make sure that the aircraft vibration did not affect the ion chambers. Before the flight we measured the ionization in the presence of two ^{60}Co γ-ray sources, with the electrometer in Mode I. After takeoff the airplane leveled off briefly at 15,000 ft., where we made another measurement with the sources in
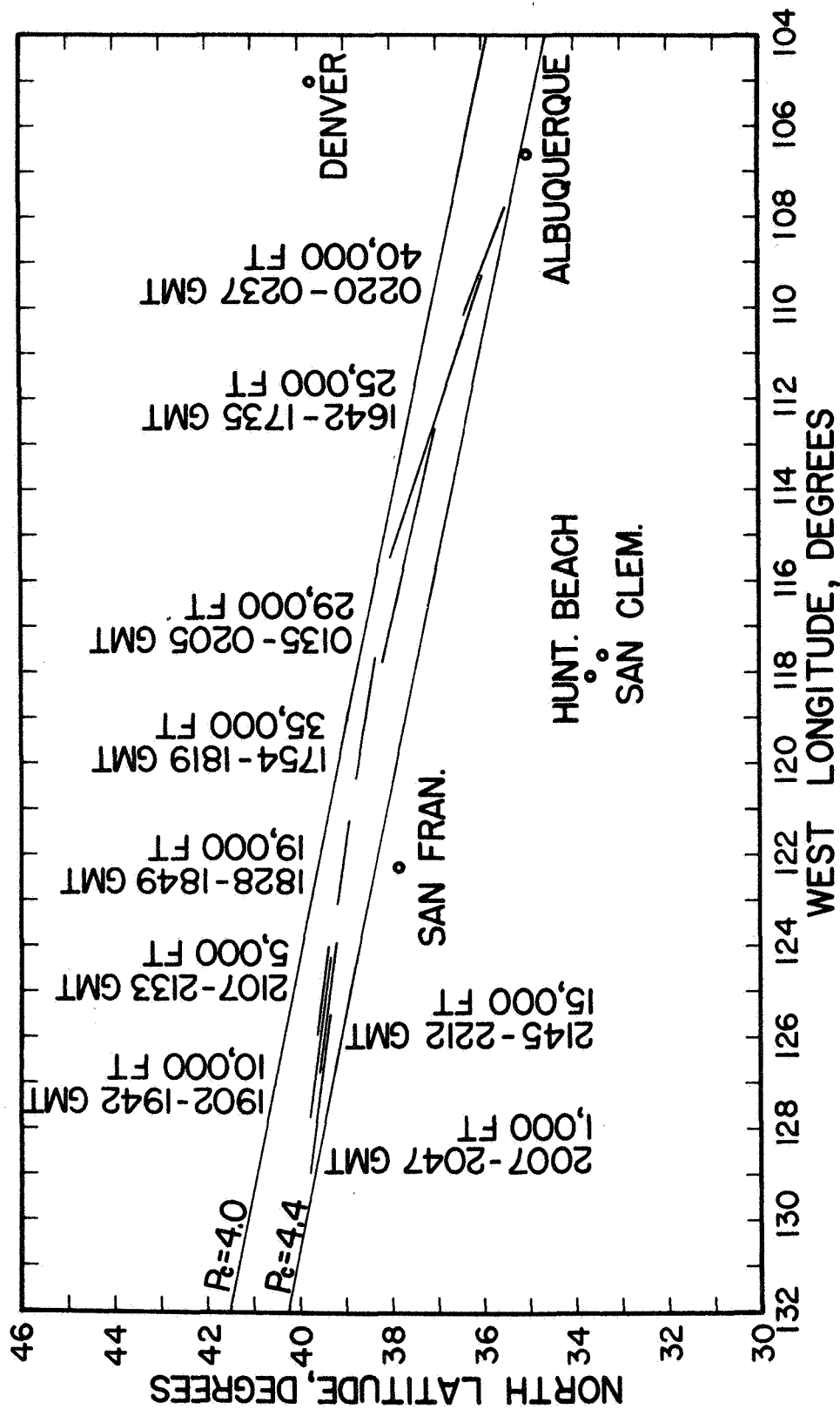
Figure 8.

Route of C-135 aircraft flight, January 10-11, 1968. Line segments indicate data acquisition portions of the flight, with times and altitudes. 29,000 and 40,000 ft runs were made on January 11, all others January 10. Later sea level measurements were made at San Clemente and Huntington Beach, California.

the same position. No change was observed in the ionization as measured by either chamber, so we concluded that vibration did not affect the chambers to a measurable degree. The sources were used in order to make the effects of ground or cosmic radiation negligibly small. They were then stowed in lead blocks far forward in the aircraft, where their presence had previously been found not to affect the radiation at the position of the ion chambers. We did not make this comparison for Mode II, but we intended to calibrate Mode II against Mode I later in the flight.

Of course the output data from the 552 liter chamber had to be corrected according to the temperature and pressure in the cabin. Temperatures at the position of the ion chamber were measured with an ordinary lab thermometer. The cabin pressure was monitored with an aircraft altimeter that had been calibrated against a mercury manometer in the lab. The aircraft pressure altitude was determined to ± 10 ft from the average of three altimeters on board the plane. Corrections were applied for scale error and air speed. During each data acquisition period, the altitude usually remained constant to ± 20 ft.

The ionizations measured at the nine different altitudes are given in Table 2. The estimated errors in the ionizations are standard deviations of the mean at each altitude and do not include errors in the calibration constants. The calibration error for the 552 liter chamber is estimated to be 0.6 percent, while that for the 8.8 liter chamber is probably about 1 percent.

Table 2

Altitude feet	Pressure gm/cm²	Ion pairs/(cm³ sec atm)	
		552 liter	8.8 liter
40,570	188	171.3 ± 0.3	177.1 ± 0.4
35,380	239	126.4 ± 0.2	131.8 ± 0.3
29,530	313	78.46 ± 0.18	81.73 ± 0.21
25,400	375	53.07 ± 0.10	54.18 ± 0.13
19,250	489	27.18 ± 0.13	26.94 ± 0.10
15,120	581	17.27 ± 0.18	15.99 ± 0.05
10,030	715	9.66 ± 0.09	8.19 ± 0.08
5,050	868	6.59 ± 0.09	4.97 ± 0.05
1,040	1010	4.92 ± 0.06	3.45 ± 0.04

Data were obtained from the 552 liter chamber in both Mode I and Mode II at the four highest altitudes. The ratio Δt (Mode I)/Δt (Mode II) was thus determined to be 10.50 ± .05, and that value was used to calibrate the chamber at the remaining altitudes, where only Mode II was used. Only one time interval was recorded for the 8.8 liter chamber at each of the three lowest altitudes, which was assumed to be good to 1.0 percent. In fact for the 1000 ft. and 5000 ft. runs the time interval was not quite complete but extended into portions of the flight where the altitude was changing. However, only small corrections were necessary to reduce each time interval to the desired altitude.

The thin walled chamber was still sensitive to the β and γ components of the radiation from radon decays in the atmosphere. The steel walled chamber may also show some response to these radiations,

but probably much less. These radiations are most important at the lower altitudes, where their contribution relative to the cosmic ray ionization may be significant. However, the data at the four lowest altitudes of our flight were all obtained over the Pacific Ocean, west of the California coast. The winds in this region blow predominately from the west, so the air we encountered in that portion of the flight should have been over the water for several weeks, and almost all the radon that might have been in it should have decayed during that time. This idea will be investigated in more detail in the next section on sea level cosmic ray measurements. Now it is sufficient to say that we expected no contribution from atmospheric radioactivity at the lower altitudes, and at the upper altitudes it would be negligibly small, even if there were any. The air conditioning system of the airplane exchanged the cabin air for fresh air about once every three minutes, so the cabin air could be expected to have the same composition as the outside air.

The data for the seven lower altitudes are plotted in Fig. 9. We can immediately notice a marked difference in the response of the two ion chambers as a function of atmospheric depth. The ionization values near sea level are also higher than what might be expected on the basis of measurements by other observers. We began to suspect that the airplane contained a small amount of radioactivity that was appearing in our results. Such a level of radiation would be rather hard to detect except with a measurement of the kind we made, since the intensity is fairly low, even in comparison with natural background radiation. The thin walled chamber appears to be much more affected by it than the 8.8 liter chamber, which means the contaminating radiation must be of
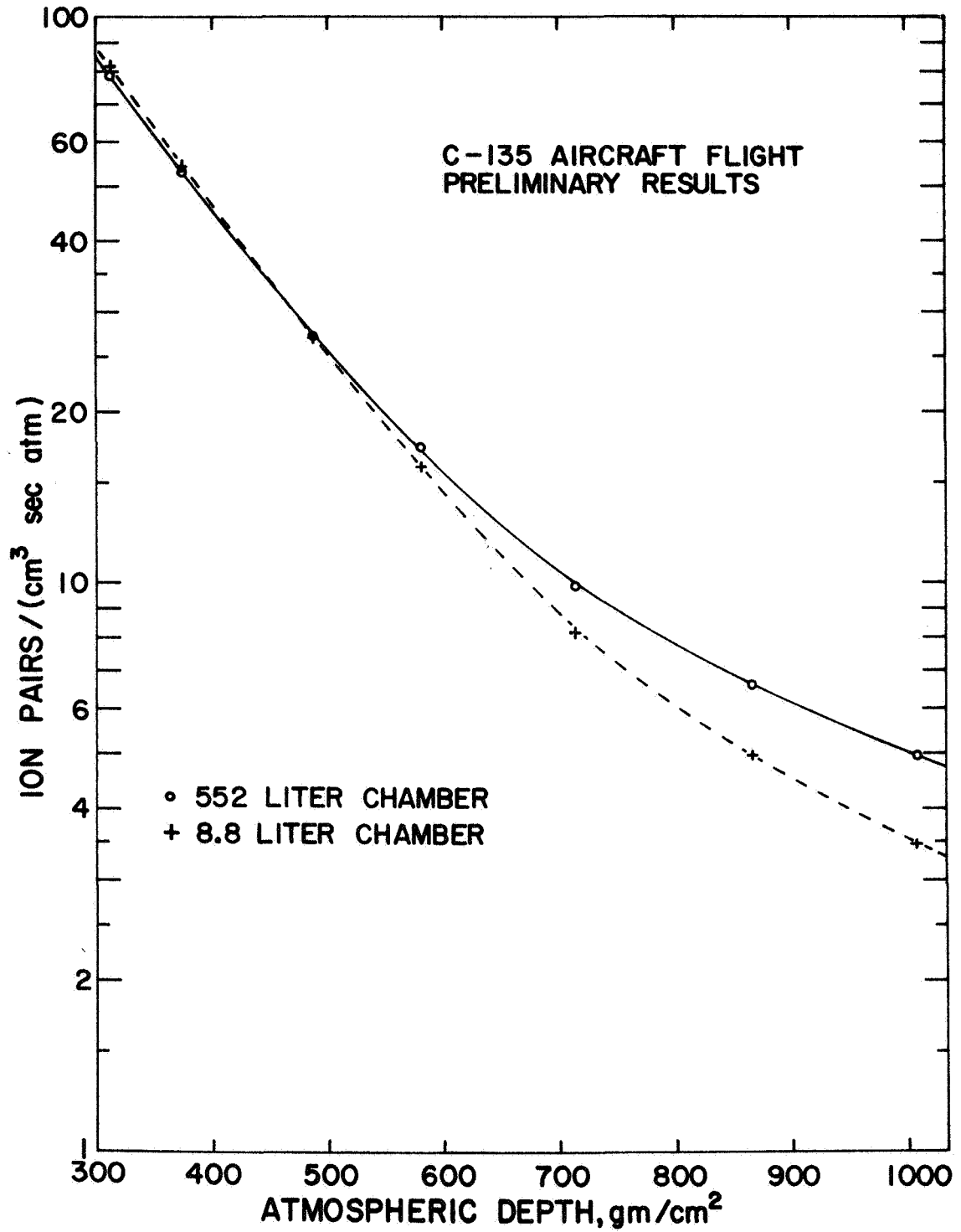
Figure 9.

Ionization vs. atmospheric depth as measured in the C-135 aircraft
with two different ion chambers.

low energy, such a β-particles of energy less than 1 MeV or γ-rays of energy less than 30 keV, both of which are not very likely to penetrate the wall of the 8.8 liter chamber. In order to try to find out if we did have contamination, it was decided to make some independent sea level ionization measurements to supplement the airplane data. Ultimately we might determine a constant ionization, independent of altitude but different for the two ion chambers, to subtract out of the airplane data. These measurements will be described before further analysis of the ionization as a function of altitude.

B. Sea Level Ionization Measurements.

The major problem associated with measurement of sea level cosmic ray ionization is eliminating the effects due to terrestrial radiations. Usually the measurement is made over a reasonably large body of water, where one can get several hundred meters or more from the shore. The measuring instrument is usually mounted in some kind of a boat, which may itself be contaminated.

In view of our previous problems with atmospheric radon, our obvious choice of a measurement site was somewhere off the Pacific coast, preferably near southern California so we would not have to transport our big ion chamber too far. However, we wanted to avoid the use of boats if possible. Our acceleration-sensitive instruments might be affected by the motions of a small boat, while the use of a large ship would increase the probability of getting radiation from sources other than cosmic rays. Also our operating schedule might be severely limited. A stable platform was desirable if one could be found.

Using one of the 8.8 liter chambers, which are easily portable, we made some survey measurements on some long piers along the southern California coast. The lowest ionization level, about 2.83 ion pairs/(cm³ sec atm), was found on the pier at San Clemente, the only pier we could find that was constructed entirely of wood, which is not expected to contain very much radioactivity. This measurement was made about 300 meters from the shore but not at the end of the pier, where there was a stucco covered concession building.

We decided to bring the 552 liter chamber down to the San Clemente pier and compare its output with that of the 8.8 liter chamber. For this purpose we built a housing for the large chamber, using $\frac{1}{8}$" masonite panels mounted on the same aluminum frame that was used for the airplane flight. It was then sealed with a layer of polyethylene sheet. Thus we further reduced the sensitivity of the large chamber to atmospheric radon and at the same time protected it from the weather. The effective wall thickness of the chamber was now 400 mg/cm², compared with the previous 12.7 mg/cm². During testing of the system, the No. 1 quartz electrometer failed, and we began using the No. 2 unit.

The comparison measurement was made on February 28, 1968. The ionization was found to vary slowly with time, probably due to atmospheric radon. The lowest ionization recorded was 2.70 ± .01 ion pairs/(cm³ sec atm) with the 552 liter chamber, and simultaneously 2.69 ± .01 ion pairs/(cm³ sec atm) with the 8.8 liter chamber. Whether or not this was really the true sea level cosmic ray ionization, the results seemed to confirm our suspicions that there was contamination present in the airplane data.

We considered the possibility of tethering a balloon to the pier in order to get an ion chamber about 100 meters into the air. In this way we might find out if there was a contribution to the ionization from the pier itself. We actually tried doing it, but without very much success. The first time a strong wind came up and caused too much motion of the instrument, resulting in meaningless data. On the second attempt we did get some data under calm conditions; then the balloon broke, dropping the instrument into the ocean. The radiation at the balloon was indeed a little lower than on the pier, but both results were higher than the 2.69 ion pairs/$(cm^3 sec atm)$ recorded during the comparison measurement. We could not draw any definite conclusions other than the fact that it seemed necessary to investigate further the effect of atmospheric radon on our measurements.

An off-shore oil drilling platform $2\frac{1}{4}$ miles off the coast of Huntington Beach was chosen as the site for continued observations. It was much more isolated than the San Clemente pier, so we would be able to leave our instrument unattended for long periods of time without fear of it being disturbed. For a check out run we set up an 8.8 liter ion chamber on the helicopter deck, which was not being used. The only structure above us was a crane and derrick, both of which were on the opposite side of the rig and subtended very little solid angle. The plat- form, which extended approximately 100 ft above the water,was made almost entirely of steel, which is expected to contain very little radio- activity but may scatter some of the cosmic radiation in the backward direction. Fortunately there was about an inch of wood planking on the helicopter deck, which would help to attenuate backscattered radiation.

During a six hour run the ionization was found to decrease from 2.84 to 2.60 ion pairs/(cm^3 sec atm), the lowest value yet observed in our measurements. A strong sea breeze began to blow near the beginning of the run and continued for its duration, so at the end the air might have been nearly free from radon.

A few days later the same ion chamber was again set up on the platform and left to run continuously for six days. The recorder pen failed after $4\frac{1}{2}$ days, but the data obtained up to then turned out to be quite interesting. The ionization is plotted in Fig. 10 as a function of date and time. Weather records for the same period were obtained from the U.S. Weather Bureau station at Long Beach, only a few miles away. We were especially interested in correlating the ionization variations with the direction of the wind. The following facts were noticed. 1) If the wind began blowing off the land, the ionization began to increase soon thereafter and continued to rise until the wind shifted to come from the sea. 2) When the wind blew from the sea, the ionization always eventually decreased, but not always immediately. 3) Ionization minima generally occurred late in the day, after the wind had been blowing from the sea for many hours. 4) The magnitude of the ionization fluctuations seemed to decrease with the ionization itself. Normal instrumental statistical fluctuations are about 0.5 percent. 5) There seemed to be a minimum value below which the ionization would not go. The four lowest values are listed in Table 3.
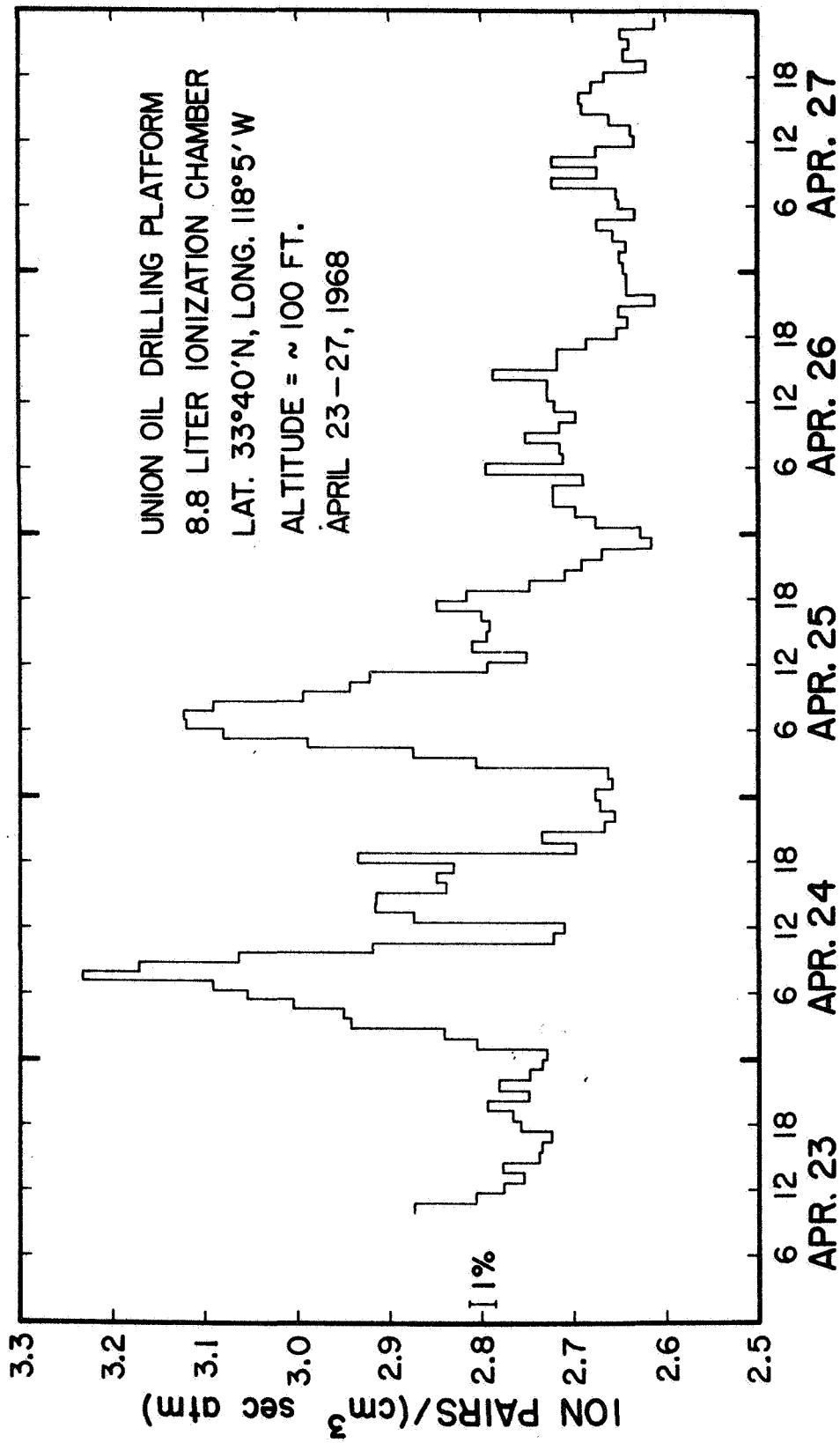
UNION OIL DRILLING PLATFORM
8.8 LITER IONIZATION CHAMBER
LAT. 33°40'N, LONG. 118°5'W
ALTITUDE = ~ 100 FT.
APRIL 23-27, 1968

Figure 10.

Ionization vs. date and local time (PST) on off-shore oil drilling platform, $2\frac{1}{4}$ miles off the coast of Huntington Beach, California.

Table 3

Date of Measurement	Ionization ion pairs/(cm^3 sec atm)	Barometric Pressure gm/cm^2
April 4	2.60	1033
April 25	2.62	1030
April 26	2.61	1031
April 27	2.61	1034

We conclude that our original hope, that at certain times we can find air near the California coast that has been over the ocean for several weeks and contains little or no radioactivity, has been realized. The average of the results in Table 3 is 2.61 ion pairs/(cm^3 sec atm) at 1032 gm/cm^2. No experiments have been done to determine what, if any, correction is necessary to account for radiation from the drilling platform, but we believe it is constructed of materials (mostly steel) which contain little or no contamination. Shamos and Liboff (4) subtracted 0.035 ion pair/cm^3 sec atm) from all their data obtained over sea water to account for the presence of ^{40}K at a concentration of 7.6×10^{14} nuclei/cm^3 of sea water. Based on crude estimates of the amount of matter between our ion chamber and the ocean surface, and the solid angle of unobstructed ocean visible from the ion chamber, we believe only 0.01 ion pair/(cm^3 sec atm) should be subtracted from our result for this correction. Roughly an equal amount should be subtracted

from our result to account for the remaining 1 gm/cm^2 to sea level (1033 gm/cm^2). Thus we present $2.59 \pm .01$ ion pairs/(cm^3 sec atm) as the sea level ionization given by the 8.8 liter ion chamber.

The difference between this result and the San Clemente result is only 0.10 ion pair/(cm^3 sec atm) for the 8.8 liter chamber. Since it is fairly small, we assume that the corresponding difference for the 552 liter chamber will be essentially the same within the limits of our errors. Considering the agreement between the two instruments found earlier at or near sea level, it was not felt necessary to actually make the measurement with the 552 liter chamber, especially since the problem of transporting it by boat to the platform and raising it to the helicopter deck would have been by no means trivial. The sea level value for the thin walled chamber is therefore to be given as $2.60 \pm .01$ ion pairs/(cm^3 sec atm).

C. Discussion of Lower Atmosphere Data.

We can now proceed to determine the amount of ionization to be subtracted from the C-135 data of Table 2. From Fig. 9 the change of ionization with atmospheric depth near sea level is estimated to be -0.008 ion pair/(cm^3 sec atm) / (gm/cm^2). The ionization at 1010 gm/cm^2 must then be 0.18 ion pair/(cm^3 sec atm) higher than our sea level value, namely 2.78 ion pairs/(cm^3 sec atm) for the 552 liter chamber and 2.77 ion pairs/(cm^3 sec atm) for the 8.8 liter chamber. Comparing these values to those for the same depth in Table 2 we find that the amounts to be subtracted from the airplane data are 2.14 and 0.68 ion pairs/(cm^3 sec atm), respectively, from the results of the large and small chambers.

The values so obtained are listed in Table 4.

All the data in Table 4 are shown in Fig. 11, which is a plot of ionization vs. atmospheric depth. Also shown are the lower atmosphere

Table 4

Atm. Depth gm/cm²	Ion pairs/(cm³ sec atm) 552 liter	8.8 liter	Difference percent
188	169.2 ± 0.3	176.4 ± 0.4	+ 4.3
239	124.3 ± 0.2	131.1 ± 0.3	+ 5.5
313	76.32 ± 0.18	81.05 ± 0.21	+ 4.9
375	50.93 ± 0.10	53.50 ± 0.13	+ 5.1
489	25.04 ± 0.13	26.26 ± 0.10	+ 4.9
581	15.13 ± 0.18	15.31 ± 0.05	+ 1.2
715	7.52 ± 0.09	7.51 ± 0.08	- 0.1
868	4.45 ± 0.09	4.29 ± 0.05	- 3.6
1010	2.78 ± 0.06	2.77 ± 0.04	- 0.4
1033	2.60 ± 0.01	2.59 ± 0.01	- 0.4

data of Millikan and Cameron (3), Lowder and Beck (5), and Shamos and Liboff (4). During the 1965 latitude survey of Neher (1), a balloon flight with an 8.8 liter ion chamber was made on July 17 from the geographic location 30.2°N, 74.3°W, where the geomagnetic cutoff rigidity is 3.87 Bv, close to the value of 4.2 which applies to the C-135 data. The data for this balloon flight are also included in Fig. 11, extended as far up to the top of the atmosphere as data were obtained. Notice that the sea level latitude effect has been neglected in the comparison to remove the
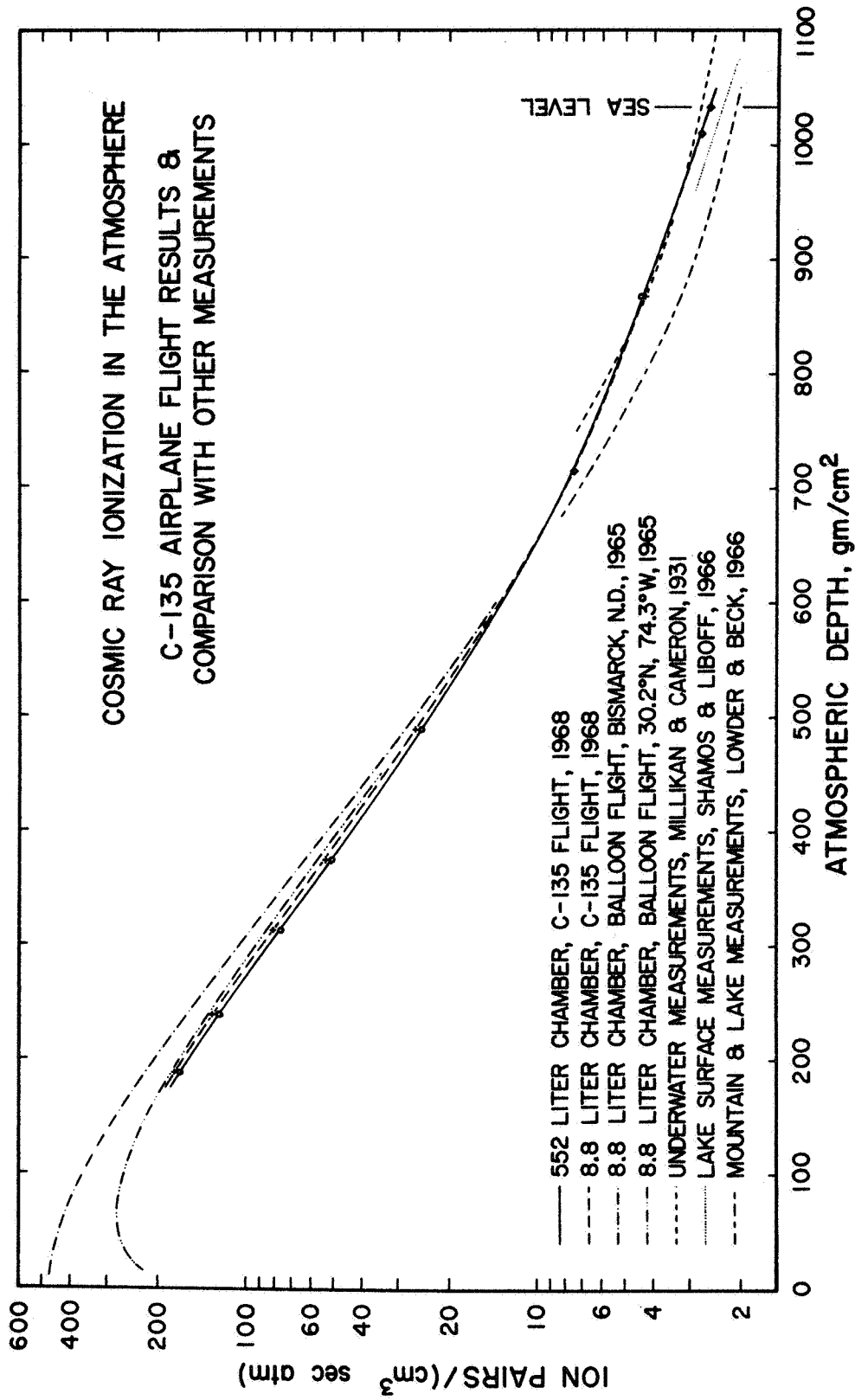
Figure 11.

Cosmic ray ionization in the atmosphere as determined at different times by various observers.

contamination ionization from the airplane data, even though the cutoff

rigidity is 5.48 Bv at the point where the sea level measurements were

made. Finally we include a curve showing balloon results at Bismarck,

North Dakota, the reference station for the 1965 latitude survey. The

Bismarck data can be extended farther down into the atmosphere, since

many flights can be averaged. The vertical cutoff rigidity at Bismarck

is 1.26 Bv, considerably less than that for our other data in Fig. 11,

which is responsible for the higher values of the ionization, especially

at the top of the atmosphere.

We expect the 1965 balloon-recorded ionizations to be somewhat

higher than those measured in the airplane in 1968, since the amount of

solar modulation was much lower in 1965. Otherwise we believe that the

airplane results for the 8.8 liter ion chamber are consistent with the

balloon results for the same chamber. We thus conclude that the air-

craft skin had little influence on our measurement except for the extra

mass of about 1 gm/cm^2, which has already been added to the atmosphere

depths listed in Table 4 and plotted in Fig. 11.

It should be pointed out that the absolute calibrations of the 552

liter and 8.8 liter ion chambers are independent. Yet within the limits

of our errors the two chambers gave the same ionization from sea level

to 600 gm/cm^2. From this we must draw one of two conclusions,

assuming that wall effects for the 552 liter chamber are always negligible.

If there is no significant wall effect for the 8.8 liter chamber in the lower

atmosphere, then the absolute calibrations of the two instruments are

essentially in agreement. Or on the other hand, if there is a wall effect,

then the absolute calibrations differ in such a way as to compensate for it.

We have reason to believe that the wall effect is at most rather small in the lower atmosphere, since the dominant contribution to the ionization comes from muons, which have only a weak interaction with matter. The situation is different at higher altitudes, where the radiation becomes primarily electromagnetic. After a transition region from 600 to 500 gm/cm², the 8.8 liter chamber runs consistently about 5 percent higher than the 552 liter chamber at altitudes above 500 gm/cm², an effect which we attribute to the interaction of the electromagnetic radiation with the steel wall of the 8.8 liter chamber. Lowder and Beck (5) reported no change from 4,000 to 15,000 ft in the ratio of responses of their steel walled, argon filled chamber to their aluminum walled, air filled chamber. This is consistent with our result, but we believe that if they had gone to 20,000 ft or beyond, they would have seen a change, as we did.

Lowder and Beck determined that the shape of their ionization vs. depth curve was the same as that of Millikan and Cameron, the truth of which is easily seen in Fig. 11. The absorption coefficient changed fairly gradually with increasing depth, and they attributed the difference between the two curves purely to differences in the absolute calibrations of the two instruments. Actually the Lowder and Beck instrument was not calibrated absolutely at all, but instead the relative values were made to agree with a calculated ionization of 2.10 ion pairs/(cm³ sec atm) at sea level. However, the shape of the two curves of the present work, which can be considered identical at depths of more than 600 gm/cm², is quite different from that of the other two. Thus it is indicated that the problem of discrepancies among the various results is not so simple as

just disagreements among the absolute calibrations. Our absorption

coefficient changes rapidly in the region 600 to 750 gm/cm ^{2}, but at

deeper depths much less rapidly than in the other two curves. At sea

level it is in good agreement with the absorption coefficient of Shamos

and Liboff, but the absolute value of our ionization is about 11 percent

higher than theirs. It is perhaps significant that the region where the

greatest change occurs in our absorption coefficient is near the region

where the change occurs in the relative responses of the two ionization

chambers, indicating the transition of the radiation from mostly electrons

to mostly muons.

The value of 2.10 ion pairs/(cm^3 sec atm) was calculated by Lowder

and Beck in two steps. First they give 1.48 ion pairs/(cm^3 sec atm) for the

ionization due to sea level cosmic ray muons, which is backed up by

many references. They admit that they have not taken cosmic ray time

variations into account and thus imply that this value may be too low,

since their results are supposed to apply to the solar minimum year of

1965. However, they later state that this value does apply to 1965 and

may be even lower for other years. Second, the muon ionization value is

divided by the ratio I(muons)/I(total). To get this ratio, Lowder and

Beck quote four references (14, 15, 16, 17), and then the value 0.70 ±

0.03 appears. This writer checked the last three of these references and

noted the following. The paper by Clay (15) was not thought to be very

applicable to this problem, but a paper immediately following by him (18)

presents a graph (Figure 1) showing the decrease of cosmic ray intensity

with increasing lead shielding and leads to the value I(muons)/I(total) =

0.46. The value of 0.67 is derived from Carmichael's (16) fluxes of

(1.68 and 0.84) $\times 10^{-2}$ cm^{-2} sec^{-1} for muons and electrons, respectively.
The data given by Rossi (17) do lead to the result I(muons)/I(total) = 0.70,
but that is under 2.3 gm/cm^2 of brass. If we try to extrapolate to zero
absorber thickness, we get 0.66. The point we want to make here is that
the value that one obtains experimentally for I(muons)/I(total) depends
rather critically on how the experiment is done, and the value used by
Lowder and Beck may be considerably too high. If they had used 0.59,
the average of the 3 values quoted above, they would have obtained I =
2.51 ion pairs/(cm^3 sec atm) at sea level, not in bad disagreement with
our value.

Shamos and Liboff quote I = 2.18 ion pairs/(cm^3 sec atm) for
their sea level value, which we assume refers to air at 20°C (NTP).
Converted to STP, their result is 2.34 ion pairs/(cm^3 sec atm), 10 per-
cent lower than our measurement with the 552 liter chamber. There are
three facts concerning their measurements which we regard as possible
weaknesses. 1) Their ionizations depend on the ratio I(air)/I(freon),
which they claim to be independent of the ion chanber and type of radia-
tion being used. However, their measurements of this quantity were all
made in radiation environments that consisted mainly of γ-rays. The
situation for cosmic rays may be quite different. In the next section we
will show that the ratio I(air)/I(argon) may be expected to be 10 percent
or more higher for cosmic rays than for γ-rays, and we do not expect
freon to behave fundamentally differently. 2) The relation between ion
chamber saturation and α -particle contamination manifests itself some-
what differently in their data from what we have observed, and they
attempt to operate their chamber at a voltage where they collect all of

the ions from minimum-ionizing particles and none of the ions from the heavily-ionizing α-particles. We believe this to be a rather tricky thing to do, since great care must be taken to separate the two effects properly at all radiation levels. 3) Absolute ionization calibrations were made by Shamos and Liboff in two ways. One method depended on the use of calibrated radiation sources and was therefore subject to errors due to radiation scattered from nearby objects and modification of the radiation by the ion chamber walls. The other method measured the actual ion current by measuring the voltage across a high resistance, which we describe for our own system in connection with Figure 1, where we also mentioned some ways in which errors can enter in, especially under field conditions. We believe our null method with a standard capacitor, followed by the use of a sealed Neher electrometer, is a much more accurate way to measure absolute ion currents.

We will report as our sea level ionization value, given by the thin walled, air filled, 552 liter ion chamber,

$$I = 2.60 \pm .03 \text{ ion pairs/(cm}^3 \text{ sec atm)},$$

where the estimated standard deviation now includes errors from all sources, including the absolute calibration. This result is lower than previously reported Caltech values, 2.77 ion pairs/(cm³ sec atm) by Millikan and Cameron (3) and 3.22 ion pairs/(cm³ sec atm) by Millikan and Neher (19), corrected for wall effect to 3.06 ion pairs/(cm³ sec atm) by Neher (20). (See note on page 3 regarding standard atmospheres.) However, our new value is still considerably higher than the more recently reported results of 2.34 ion pairs/(cm³ sec atm) by Shamos and Liboff (4) and 2.10 pairs/(cm³ sec atm) by Lowder and Beck (5).

Comparison of the Response of Different Ionization Chambers

A. Results with ^{60}Co γ-Rays.

During the development of the 552 liter ion chamber certain data were obtained regarding the response of our two different kinds of chambers containing various fill gases in a radiation field of ^{60}Co γ-rays, usually at a strength of several hundred ion pairs/(cm^3 sec atm). While the data are not necessary for the interpretation of the cosmic ray results already presented, they are of interest with regard to the intercalibration of various ion chambers, which is often done with γ-rays. The data are summarized in Table 5. For convenience, all the results have been reduced to the same radiation field and normalized so that the ionization given by the 552 liter chamber is 100 arbitrary units. These experiments were done with two or more γ-ray sources of known relative strength. The ion chambers were placed between the sources at the position where $\frac{\partial I}{\partial x} = 0$ for x = any position coordinate.

It is now of interest to mention the work of Johnston (6) regarding the Caltech ion chamber calibrations. He made an independent absolute value calibration using an 8.8 liter chamber filled with 1 atm of air. If

Table 5

Comparison of ion chambers exposed to ^{60}Co γ-rays

Ion Chamber	Ionization
552 liter, air filled, with masonite cover (400 mg/cm^2 wall)	95.0
552 liter, air filled, w/o masonite cover (13 mg/cm^2 wall)	100.0
8.8 liter, argon filled, 400 mg/cm^2 steel wall	120.1
Berkeley 4" (0.55 liter), argon filled, aluminum wall	108.8

proper account was taken of the different standard atmospheres used, his new ionization, measured in a flux of ^{208}Tl, ^{226}Ra, or ^{60}Co γ-rays, agreed with that given by the old Caltech calibration to within less than his estimated error of 0.5 percent. The same calibration has been carried on through the years at Caltech and is still used to calibrate the 8.8 liter balloon chambers, including those used in the experiments described here and in the previous sections. However, this calibration has been normalized to standard air inside the ion chamber. Therefore it does not give the correct result for the ionization in the air outside the chamber unless the intensity and character of the radiation are not significantly altered by the chamber walls. Johnston went on to measure the γ-ray wall effect for argon filling with walls of various equivalent Z. He found the ionization per atmosphere to increase 6 percent for 1 atm argon filling compared with 8 atm argon filling when steel walls were used. He did not state a corresponding result for air filling, but the value of 19 percent can be inferred from his data. He also determined that the wall effect was negligible for filling pressures of 8 or more atmospheres. Thus we might expect the present 8.8 liter chambers to read 19 percent too high in γ-rays of the type Johnston used, provided that we consider the air outside the chamber to be our standard reference. If we assume that the ionization measured by the uncovered 552 liter chamber is indeed indicative of the air outside the chamber, then from Table 5 we see that the 8.8 liter chamber actually ran 20.1 percent too high when ^{60}Co γ-rays were used. We regard these results to be in substantial agreement in view of the fact that Johnston used different radiations. Thus we have further evidence for the agreement of the absolute calibrations of the two ion chambers.

Additional information on the variation of internal chamber ionization with wall thickness is to be found in the data of Workman (21), who studied the response of a 630 cm³, air filled ion chamber. He observed the ionization to increase over the value at zero wall thickness from 15 to 89 percent for 400 mg/cm² steel walls, depending on the spectrum of the γ-rays used. Corresponding results for 400 mg/cm² aluminum walls were 2 to 57 percent. In general we might expect his increase to be higher than what we observe in the 8.8 liter chamber for a similar spectrum because our chamber has a much larger volume.

Some of the ion chambers used for the University of California IMP satellite experiments (22) were run in our standard calibration position and compared with the 8.8 liter chamber results. Their absolute calibration is in terms of STP argon; to convert to STP air one must know the ratio I(air)/I(argon). The normalized result given in Table 5 is based on Johnston's value of I(air)/I(argon) = 0.655 for γ-rays. The fact that the Berkeley chamber gives an ionization intermediate between the 552 liter and 8.8 liter chambers is reasonable because of the aluminum wall, but we do not have enough information to predict precisely what the relative responses should be.

B. The Ratio of Ionization in Air to that in Argon.

We have just mentioned an example in which it is necessary to know the ionization in air relative to that in argon. Johnston discussed this problem in considerable detail. He predicted the ratio I(air)/I(argon) should be 0.685 for penetrating charged particles and 0.620 for γ-rays which produce only Compton interactions in the gas. If photoelectric

absorption of the γ-rays in the gas is also considered, a ratio more like 0.55 to 0.60 is expected. Thus if this ratio is measured in an ionization chamber with γ-rays, we should expect the result to depend on the thickness and material of the chamber wall, the pressure and volume of the gas, and the spectrum of the γ-rays. Johnston's result of 0.655 for γ-rays was obtained in the 8.8 liter, steel walled chamber using argon and air at 1 atm pressure. From this ratio it must be assumed that a significant portion of the ionization in the chamber is due to electrons ejected from the chamber walls, the quantity of which is independent of the type or pressure of filling gas inside the chamber. However, as one goes to higher filling pressures, the effect of wall electrons becomes relatively less important because of the increased number of secondary electrons in the gas itself. If Johnston had made his measurement at a higher pressure, a lower value of $I(air)/I(argon)$ should have been obtained. In practice the high pressure measurement becomes difficult to make because of the problem of ion recombination in compressed air.

The use of the 552 liter ion chamber to measure the air/argon ionization ratio offered the advantage of eliminating wall effects. However we had composition problems. Commercial argon has been found sufficiently pure for use in all regular Caltech ionization chambers, which are first baked under vacuum for several hours at about 340° C. Because of the very thin walls of the 552 liter chamber, we could not pump it out. The only way we could fill it with argon was simply to force the argon in and let the air out. Purity of the order of 99 percent is not too hard to achieve in this manner, but probably 99.99 percent is desirable, and this becomes impractical, since a very large amount of

argon is required in order to flush all the air out. The problem is further compounded by the fact that we could not de-gas the chamber beforehand. After flushing the chamber for more than two days with over 10 volumes of argon, we did seem to obtain some consistent results. Comparison of the ion current with previous runs in air using the same ^{60}Co source configurations yielded an average value

$$I(air) \,/\, I(argon) = 0.612 \pm .002.$$

This value is believed to be consistent with Johnston's predictions. There is still an effect of secondary Compton electrons entering the chamber from the outside air, since such an electron may have a typical energy of 400 keV and a range of one meter, the order of the chamber dimensions, in air. The ratio of photoelectric to Compton interactions in the argon is only about 10^{-4} for the primary (1.17 and 1.33 MeV) γ-rays but considerably larger for the secondary Compton γ-rays.

Finally, the air/argon ionization ratio is known to depend on the velocity of the ionizing particles, even at relativistic velocities. Johnston also discussed this effect and predicted $I(air)/I(argon)$ ratios for the various cosmic ray components. These will be used in the following discussion.

C. Results for Cosmic Rays.

The fact that Johnston's value of $I(air)/I(argon)$ for cosmic ray muons (0.652) is nearly the same as his value for lab γ-rays (0.655), together with agreement in the absolute calibrations and negligible wall effect for muons, leads to the prediction that our two ion chambers

should give the same ionization for cosmic rays in the lower atmosphere. Indeed this is what we observe, as has been shown in Fig. 11 and the associated discussion.

The situation will be different in the 100 to 500 gm/cm^2 region, where the electronic component predominates. The 8.8 liter chamber should read higher due to wall effects, which Johnston estimated to be 1.4 $\pm$ 1.4 percent for the electronic component. We get another 1.7 percent or so from the ratio I(air)/I(argon) for high velocity electrons (0.641) relative to that for muons (0.652), and in reality this will probably account for an even greater increase in ionization in the argon chamber due to the presence of hard γ-rays. We believe our observed difference of about 5 percent between the two chambers above 500 gm/cm^2 is consistent with these predictions.

The 10 to 100 gm/cm^2 region was the area of greatest interest to Johnston. Here the argument of the previous paragraph tends to reverse, and we might expect the ionizations given by our two chambers to become nearly the same again. However, recombination losses also become important in this region, due to nuclear stars, slow protons, and finally heavier nuclei. Columnar recombination will doubtless become quite severe in the air filled chamber and may render its output meaningless at the highest altitudes. Therefore we do not feel that continuation of our experiment to altitudes much above 188 gm/cm^2 would have been justified.

Summary

During the development of a large volume, very thin walled ionization chamber it was found that α-particles from the external atmosphere made an important contribution to total ion current. Thus we had an α-particle source which helped us study the saturation characteristics of the ion chamber when filled with air which had been aged long enough to allow for the decay of any radon gas that it might have contained. When the wall thickness was increased to 12.7 gm/cm^2, α-particles could no longer be detected, and 99.9 percent saturation was achieved at 900 volts collector potential in an ion chamber of volume 552 liters. We therefore concluded that the contribution to the ion current from α-particles originating in the ion chamber itself was negligible. This conclusion was reinforced by the observation that the chamber saturation characteristics did not change with radiation strength except for effects due to volume recombination.

Absolute ion currents were measured by observing the time required to charge a standard capacitor to a well known voltage. Once the ionization was accurately determined, it was then used to calibrate a sealed Neher quartz fibre electrometer for use for measurements in the field. The electrometer was sealed in glass and filled with argon, so that it could operate inside the air filled ion chamber without damage to the electrical conductivity of the quartz fibre. The absolute calibration of the 552 liter ion chamber was therefore independent of that used for previous ionization measurements at Caltech.

The 552 liter ion chamber, along with a chamber used for balloon

flights and based on the old calibration, was flown in a C-135 aircraft at altitudes from 1000 to 40,000 feet to measure the ionization vs. atmospheric depth. The lower altitude measurements were made over water in order to eliminate radiation from the ground, but we concluded that there was a background radiation due to the airplane, and some independent sea level measurements were undertaken to determine the airplane contribution. We again had to cope with the problem of atmospheric radon, since we were still sensitive to β- and γ- radiations. Using the small balloon-type ion chamber on an oil drilling platform off the Southern California coast, we found that the ionization varied with time and reached a minimum value after the wind had been blowing from the sea for many hours. This minimum value of 2.59 ion pairs/(cm^3 sec atm) is claimed to be the ionization due to cosmic rays only. In a different measurement on a long wooden pier over the ocean, we found that the independently calibrated 552 liter ion chamber read 0.01 ion pair/(cm^3 sec atm) higher than the balloon chamber when the ionization was only a few percent higher than the lowest value measured on the oil platform Therefore we give 2.60 ion pairs/(cm^3 sec atm) as the sea level value given by the 552 liter ion chamber, and we interpret the agreement of the two chambers in terms of agreement of the independent absolute calibrations within 1 percent, since there should be negligible wall effect in either chamber for sea level cosmic radiation. The ionization for each ion chamber to be subtracted from the airplane data was then determined so that the airplane data agreed with the sea level results. The agreement between the two chambers was found to extend up to 600 gm/cm^2, while above 500 gm/cm^2 the balloon chamber read approximately

5 percent higher than the 552 liter chamber, a fact which is attributed to shower multiplication in the steel wall of the balloon chamber. The airplane data are shown to be in agreement with balloon data at the higher altitudes. Our results are also compared with those of other observers, where some discrepancies are shown to exist.

An experiment was done to compare the responses of the 552 liter and balloon type ion chambers in the same flux of ^{60}Co γ-rays. The results have been interpreted as further evidence for the agreement of the absolute calibrations of the two instruments, in spite of the fact that the responses are different because of wall effects. We have then given a discussion about the ratio I(air)/I(argon) and how it applies to the measurements made in the lower atmosphere.

Figure Captions

Figure 1   Circuit for measuring absolute value of the ion current, for use with vibrating reed electrometer.

Figure 2   Saturation characteristics of 1168 liter air filled ion chamber for lab background radiation. Data accurate to 0.1 scale unit.

Figure 3   Saturation characteristics of 1168 liter air filled ion chamber for ^{60}Co γ-rays of ionization strength approximately 15 times the lab background. Data accurate to 0.05 scale unit.

Figure 4   Relation of slopes and intercepts of saturation curves of 1168 liter ion chamber for background radiation.

Figure 5   Geometrical design for 552 liter ionization chamber. Each of the 45 edges is 53.18 cm long, and the length (top to bottom, excluding neck) is 146.5 cm. The Neher electrometer is inserted through the neck at bottom. Gas inlet/outlet is provided at the bottom/top.

Figure 6   Sealed electrometer (Neher type) for use in 552 liter air filled ion chamber. See references 7, 8, 11.

Figure 7   Saturation characteristics of 552 liter air filled ion chamber. Errors in data points are approx. 0.1 percent.

Figure 8   Route of C-135 aircraft flight, January 10-11, 1968. Line segments indicate data acquisition portions of the flight, with times and altitudes. 29,000 and 40,000 ft runs were made on January 11, all others January 10. Later sea level measurements were made at San Clemente and Huntington Beach, California.

Figure 9   Ionization vs. atmospheric depth as measured in the C-135 aircraft with two different ion chambers.

Figure 10   Ionization vs. date and local time (PST) on off-shore oil drilling platform, $2\frac{1}{4}$ miles off the coast of Huntington Beach, California

Figure 11   Cosmic ray ionization in the atmosphere as determined at different times by various observers.

Part II

THE QUIET TIME IONIZATION IN SPACE

AT ALTITUDES FROM 430 TO 1540 KILOMETERS

Introduction

Data on the cosmic ray ionization at high altitudes in the atmos-
phere, obtained by use of integrating ionization chambers which were
built at Caltech and all referred to the same calibration, now exist over
a period of time which includes three solar cycles (23). For about the
first half of this period, ending with the 1954 solar minimum, these data
and similar results from other institutions represented the only way that
was possible to observe the spectral changes that were taking place in
the primary cosmic radiation. However, certain quantities derived from
the data, for example the absolute ionization or particle flux in regions
far from the earth as determined with the omnidirectional ion chamber,
required a correction to account for upward moving secondary, or
"splash albedo", particles, which was not known. During the last solar
cycle more direct methods have become available for study of the prop-
erties of the primary cosmic rays, but the balloon ion chamber data still
provide a way of monitoring a large portion of the cosmic ray spectrum
with a minimum amount of effort, and they provide useful comparisons
with the earlier years.

Beginning with the first earth orbiting satellites in 1957, it became
possible to extend upper atmosphere cosmic ray measurements into the
near-earth region of outer space. A few years later interplanetary probes
returned the first data from regions of space far away from the earth's
magnetosphere. One of the more successful of the early interplanetary
missions was the Mariner II Venus fly-by in late 1962. The Mariner II
spacecraft carried, along with several other scientific experiments, an

ionization chamber of the type previously used for Caltech upper atmosphere balloon experiments, although smaller (24, 25). The Mariner II ion chamber provided information on the time variations of the interplanetary cosmic radiation, the change of cosmic ray intensity with distance from the sun, and, by comparison with balloon measurements over Thule, Greenland, the fraction of the ionization at the top of the atmosphere due to splash albedo particles. Another ion chamber provided similar information on the Mariner IV mission to Mars in 1964-65 (23, 26).

The albedo estimates derived from comparison of interplanetary and balloon ionization results were subject to errors due to time differences between the balloon and spacecraft measurements in the case of Mariner II and to problems in extrapolating the balloon data to the top of the atmosphere in the case of Mariner IV. The measurements of the radial gradient (dependence on distance from the sun) depended on the use of an earth-based monitor for comparison with the interplanetary results in order to account for time variations in the cosmic radiation (26). Because of the problems just mentioned, the balloon ionization data did not prove to be very useful as such a monitor, so that more dissimilar cosmic ray detectors had to be used. An ionization chamber in a polar orbit would provide fairly continuous cosmic ray data without being subject to extrapolation problems in the atmosphere. Therefore the POGO ion chamber experiment was intended to obtain such near-earth data simultaneously with the Mariner IV flight to Mars. The first POGO was launched too late, however, and this objective was not achieved. But in many other ways the POGO ionization data should serve to improve our understanding and interpretation of the balloon data.

A better measurement of the ionization albedo can be obtained by determining the altitude dependence of the cosmic ray ionization near the earth over the polar regions, where the cosmic ray flux is essentially unmodified by the geomagnetic field. In the analysis of the polar data which follows, we will show that we must find approximate solutions to problems involving spacecraft radioactivity, time variations in the cosmic radiation, and possible systematic errors in the absolute calibration of the ion chamber in order to determine the ionization as a function of altitude. The data will then be fit to an analytical function for the altitude dependence, and the albedo will be derived by extrapolating this function to the top of the atmosphere and to infinity. The results will be compared with the Mariner results and with particle flux measurements of other observers. The derivation of an accurate analytical function for the altitude dependence at lower latitudes is an extremely complex problem which is not to be attempted in this thesis. However, we will show qualitatively that there is agreement between the satellite and balloon data at low latitudes.

The POGO ion chamber would be particularly useful for observing the position of the cosmic ray "knee". A few months' part-time operation of one polar orbiting ionization chamber would be equivalent to several thousand balloon flights during the same time period, which would involve a costly expenditure for equipment and personnel. In the case of balloon observations, the knee has been of interest as an indicator of the spectral changes in the primary cosmic radiation at different times during a solar cycle. We will show that the satellite knee cannot be observed directly but can easily be determined by extrapolating the high and mid-latitude

portions of the ionization vs. latitude curves until they intersect. Thus the knee is defined as the position where the mid-latitude ionization, as it increases with approach to the geomagnetic pole, becomes equal to the polar ionization value, which is independent of position. The knee is interpreted to be the position in the geomagnetic field where the cosmic ray cutoff rigidity has a particular value, a little greater than 1 BV, assuming that the cosmic ray spectrum does not change significantly during the period of observation. Current theory and data lead to models of the magnetosphere with open field lines at high latitudes, which predict that the cutoff rigidity at a fixed location with respect to the earth varies with local time near the transition region between open and closed field lines. Calculations done by Gall, Jimenez, and Camacho show that the cutoff point for 500 MeV protons is expected to shift by about one degree of latitude between noon and midnight (27). For lower energies the shift in the cutoff point becomes larger. Therefore we will look for a possible local time variation in the position of the knee, which, at this energy, we should probably expect to be less than one degree but perhaps greater than zero between noon and midnight. Such local time variations have been observed at higher latitudes but not in the region of the knee, near $60°$ geomagnetic latitude, well within the closed field line region.

There are other problems which can be studied with the POGO ion chamber data that will not be discussed in this thesis. These include ionization spikes in the outer radiation zone, the variation of the boundary of trapped radiation with local time, dumping of particles from the radiation belts and subsequent injection of new particles, and the propagation of solar particles through the magnetosphere, all of which are under investigation by collaborators at Rice University.

The POGO Ion Chamber Experiment

A. **Spacecraft and Orbits.**

The Orbiting Geophysical Observatory (OGO) satellite series was conceived by the National Aeronautics and Space Administration to meet three primary objectives, all of which represented major advances over spacecraft being used in the early 1960's: 1) to provide a platform on which a large number of integrated scientific experiments could be performed simultaneously, 2) to provide full-time, three-axis stabilization for those investigations which required a well-determined look angle, and 3) to provide a data handling system capable of very high bit rates of real time data telemetry and/or data storage onboard, to be played back later. Three of these spacecraft, the Polar Orbiting Geophysical Observatories (POGO) were scheduled for low altitude polar orbits. OGO-II was launched on October 14, 1965 into an orbit with perigee height 413 km, apogee 1512 km, inclination 87.4 degrees, and period 104.3 minutes. The perigee moved 3.048 degrees/day from its initial position at 144° (36° N geographic latitude on the southbound side) in the direction opposite to the orbital velocity, and the right ascension of the ascending node (northbound equator crossing) moved westward 0.284 degrees/day from its initial location at 280.5 degrees. OGO-IV was launched on July 28, 1967, and its respective orbital elements were 412 km, 908 km, 86.0 degrees, 96.9 min., 3.452 degrees/day, 154 degrees, 0.492 degrees/day, and 224.1 degrees. The third POGO had not been launched at the time of this writing but was not scheduled to carry an ionization chamber.

Because of the motion of the position of perigee, it was possible to make observations over any given position on the earth at all altitudes within the range of the satellite in a time span of about two months. The precession of the ascending node, together with the earth's motion around the sun, enabled the spacecraft to sweep out all local times in about five months.

B. The POGO Ion Chamber.

Ion chambers of the the type used on POGO have already been mentioned in Part I of this thesis. In particular, we are interested in the 1 liter chamber whose properties are described in detail in Ref. 12. The POGO chambers were filled with 10 atm of argon, compared with 4 atm for the Mariner II and IV chambers, and they were equipped with a dual sensitivity quartz electrometer (11) in order to be able to respond to spatial variations in the ionization expected in a polar orbit. The ion chambers were built at Caltech, and the electronics were designed at the Jet Propulsion Laboratory. Calibrations and environmental testing of the units were done at JPL.

The POGO chambers were calibrated with ^{60}Co sources in a standard configuration at JPL. The ionization was originally determined with the four Caltech standard ionization chambers, the same ones used to calibrate the 8.8 liter balloon chambers, in October, 1961. A graph of ionization vs. time was then constructed, based on a half-life for ^{60}Co of 5.27 years. Thus for any subsequent calibration run the ionization for the appropriate date could simply be read off the curve. The standard chambers were run again in June, 1964 and gave an ionization that was

within 0.1 percent of the value predicted by the decay curve. One of the Mariner-type chambers was flown to the top of the atmosphere at Thule, Greenland with the same balloon that carried one of the conventional 8.8 liter chambers, where the Mariner chamber was found to read 3.5 percent lower than the conventional model (24). The difference was assumed to be due to the difference in wall thicknesses between the two instruments, 0.25 mm for the 1 liter chamber, 0.5 mm for the 8.8 liter chamber. It is assumed that the POGO chamber would behave similar to the Mariner chamber; it has the same wall thickness but 2.5 times the filling pressure. The average path length inside the ion chamber is approximately 0.07 gm/cm^2 for Mariner and 0.18 gm/cm^2 for POGO. The wall effect must be mainly particles that penetrate the entire volume of argon, since particles which penetrate only partially and thus lose all their energy in the argon would produce an ionization difference in the other direction.

The chambers are sensitive to protons of energy greater than 10 MeV and electrons of more than 0.7 MeV. They also respond to non-penetrating electrons through the bremsstrahlung process, with approximately six orders of magnitude less sensitivity in the 40-100 keV range. The γ-ray sensitivity falls off rapidly below 30 keV, peaks at 50 keV, drops a factor of two near 300 keV, and then begins to rise again. The details of these response functions are given in Ref. 12, as is the response of the chambers to changes in temperature, operating voltage, and gravity or acceleration.

The ion chamber and a small preamplifier were mounted at the end of a spacecraft boom, roughly 3 meters long, in order to minimize the effects of spacecraft shielding of the radiations being measured. No

correction is applied to the data for such shielding, but it is believed to be less than 1 percent. The main experiment power supply and logic unit was mounted on the inside of one of the doors to the spacecraft main body. The experiment could be controlled by four possible commands from the ground: power on, power off, low sensitivity, and high sensitivity.

C. Performance of Spacecraft and Experiment.

The OGO-II spacecraft lost 3-axis stabilization during the tenth day of operation and subsequently went into a slow spin. The ion chamber being an omni-directional sensor, our data were not adversely affected. However, the loss of attitude control resulted in considerably less than optimum solar panel orientation and corresponding loss of spacecraft power. This severely limited all experiment operations, especially during periods of large eclipse duration times. Thus very little data were acquired during passes along the noon and midnight meridians.

The orbital injection velocity for OGO-II was too fast, resulting in an apogee of over 1500 km vs. the intended value of approximately 900 km. The spacecraft therefore found itself well into the trapped radiation belts during portions of each orbit. Thus the ion chamber had to deliver many more pulses than originally anticipated, running at saturation perhaps 20 percent of the total operating time. Saturation occurs when the pulse rate approaches the mechanical resonant frequency of the quartz fiber, typically about 80 cps, and there is a region of non-linearity at somewhat lower pulse rates. The ion chamber failed on April 1, 1966 after operating for about 1100 orbits out of a total of 2326, reaching its

expected lifetime of the order of 3×10^8 pulses. The spacecraft itself continued to function for many more months at diminishing performance levels as the battery deteriorated.

The OGO-IV ion chamber was somewhat more disappointing, operating successfully for only the first 160 orbits of the spacecraft. The reason for failure is not known, but the data obtained during the first 160 orbits are of good quality and should provide some interesting comparisons with the OGO-II data. The OGO-IV spacecraft as a whole was far more successful than OGO-II, retaining its attitude control for more than its planned lifetime of one year.

D. Data Handling.

The spacecraft main commutator contains 128 nine-bit data words, of which Nos. 19 and 83 are assigned to the ionization chamber, Experiment 5007. Thus there are 63 words between 19 and 83, and 63 more between 83 and the return to 19. Telemetry bit rates used for POGO are 64, 16, or 4 thousand bits per second, which result in the ion chamber word being sampled at intervals of 9, 36, or 144 milliseconds respectively. There are two separate data equipment groups, which allow data to be tele-metered directly to the ground in real time while simultaneously being recorded on the spacecraft tape recorder. In the following analysis we will be concerned almost entirely with tape recorded data, which are always at the low bit rate. The tape is played back at the high bit rate, so that a whole orbit of data can be played back during one pass over a tracking station. Real time data can be obtained only while the space-craft is within range of a tracking station and thus are available only for

short periods of time.

It is sobering to consider the sheer quantity of data which is generated by this kind of experiment. At one word per 144 ms, we get over 43,000 words per orbit. If the total amount of data recorded is equivalent to 700 complete orbits, this adds up to the order of 3×10^7 data words from the experimental measurement alone, and the ion chamber is one of the simpler experiments on the spacecraft! Then in addition to the experimental measurement, a great deal of other information is needed, such as Greenwich time, geographic coordinates, geomagnetic parameters, and spacecraft engineering data. The process by which all these data are reduced to physically meaningful quantities is outlined briefly in the following text.

The data from all experiments in the main commutator sequence are recorded on magnetic tape at the various tracking stations around the world together with readings from the spacecraft clock and engineering data. The tapes are then sent to Goddard Space Flight Center, where the spacecraft clock readings are converted to Greenwich time and the data tagged accordingly. This sounds like a trivial job, but in reality it has its problems, among them the fact that the spacecraft clock resets itself to some arbitrary value every time the spacecraft batteries reach under-voltage condition, which happened frequently on OGO-II because of low available power. The data for each experiment are now separated out, put on separate tapes, and sent to the individual experimenters. NASA also assembles "Orbit-Attitude" tapes, containing spacecraft position, velocity, attitude, geomagnetic parameters, etc. as a function of Greenwich time, and sends a copy of each tape to each experimenter.

The ion chamber tapes go to Rice University, where Dr. Hugh Anderson is in charge of initial reduction, which consists of three steps. 1) the raw data words are converted to Δt (see Eq. 7) and approximate ionization as a function of Greenwich time. At high ionization rates, averages are taken over ten data words in order to reduce the volume of data to be handled. The data are printed out by the computer and scanned by eye. 2) Cards are punched to delete data values which are obviously erroneous. A new tape is generated in which the bad data are deleted and the remaining data corrected for temperature variations and for non-linearity of the ion chamber at high ionization rates. 3) The corrected data are merged with the orbit-attitude data, using the Greenwich times common to the two tapes. Two output tapes are generated, one of which is sent to Caltech. The data are now ready for analysis. The above procedure is described in more detail by McCoy (28). A total of 210 tapes have been received at Caltech containing OGO-II data, and an additional 15 tapes containing OGO-IV data.

E. Properties of the Data.

Plots of a complete orbit of data during a time of quiet solar activity, showing ionization vs. geographic latitude, are given in Figure 12. Also shown are spacecraft altitude and the McIlwain parameter L as a function of latitude. This is only a representative orbit; many variations occur at different longitudes. It is primarily designed to illustrate how the data can be divided into four categories. 1) The polar ionization plateau, where the ionization is independent of position except for statistical fluctuations. Typically $I \approx 800$ ion pairs/(cm^3 sec atm)
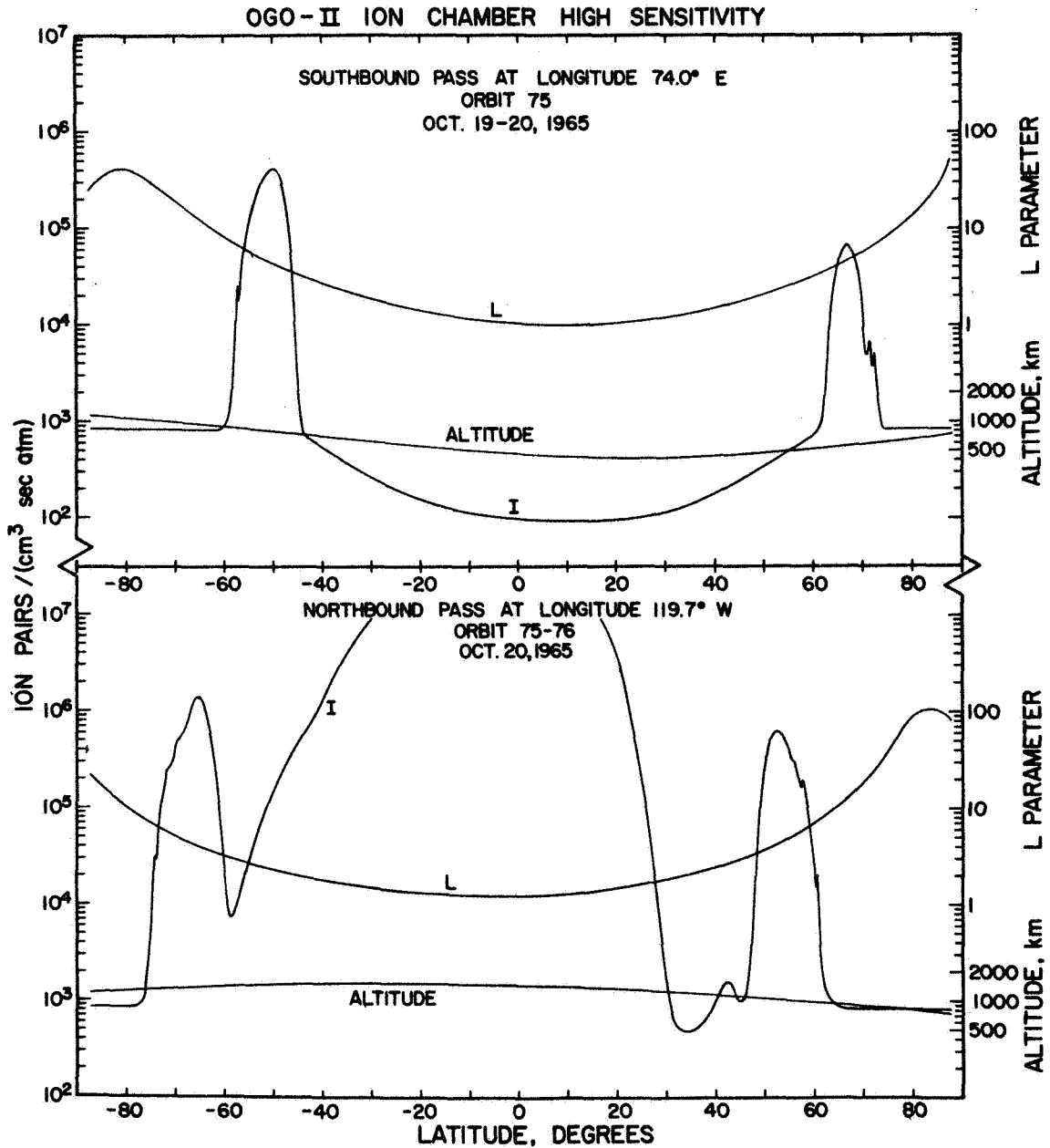
Figure 12

Plot of ionization vs. geographic latitude for OGO-II Orbit 75, North Pole, 23:35 GMT Oct. 19, 1965 to Orbit 76, North Pole, 01:19 GMT Oct. 20. Also shown are L parameter and spacecraft altitude vs. latitude.

and $L > 7$ to 10. 2) Low and mid latitude galactic cosmic ray ioniza-
tion, showing an increase in ionization from ≈ 100 ion pairs/(cm^3 sec atm)
at the geomagnetic equator ($L \approx 1$) up to near the polar level near $L = 3.5$.
This phenomenon is visible only in the southbound pass in Fig. 12, on the
perigee side of the orbit. The curve often contains spikes and wiggles,
probably due to small quantities of trapped radiation which reach the
spacecraft at certain longitudes. 3) The outer radiation belt, detectable
on all orbits in the range $3 < L < 7$. Typical values of I run from 10^4
to 3×10^6 ion pairs/(cm^3 sec atm). Narrow ionization spikes on the high
latitude edge of the outer belt have been discussed by Anderson, Hudson,
and McCoy (29). 4) The inner radiation belt, which shows up below $L = 3$
on all passes except those at the lowest altitudes in the Eastern Hemi-
sphere. The ionization can run from less than 10^3 up to 10^8 or more ion
pairs/(cm^3 sec atm). The values of I in the most intense portions are
higher than what is required to saturate the ion chamber, approximately
3×10^6 (4×10^7) ion pairs/(cm^3 sec atm) in high (low) sensitivity.

The following analysis will deal with only categories 1 and 2 above.
Particular emphasis will be placed on the polar data, the understanding
of which is necessary for the accurate analysis of solar particle fluxes at
high latitudes. We will attempt to determine the variation of ionization
with altitude, from which we should be able to derive the fraction of the
ionization which is due to upward moving "splash albedo" particles. We
will be able to draw a conclusion regarding the symmetry between the two
poles. The position of the cosmic ray "knee" will be determined, and a
possible variation of this position with local time will be investigated.

Ionization Over the Geomagnetic Poles

A. __Nature of the Observations__.

The motions of cosmic ray particles in the earth's magnetic field were first analyzed in detail by Störmer (30). His theory led to calculations of cutoff rigidities as a function position on the surface of the earth in order to describe the exclusion of particles of lower rigidity (31, 32). These calculations used a dipole-like model for the geomagetic field but attempted to account for higher-order terms, and they all predicted a decreasing cutoff rigidity and a corresponding increase in the incident cosmic ray flux as one approached the geomagnetic poles.

More recent measurements have led to the interpretation that the earth's field lines above an invariant latitude of about 65 to 80 degrees, depending on local time, are not closed as in a dipole field but stream away from the earth in a magnetic "tail" for great distances, due to the interaction of the solar wind with the geomagnetic field (33, 34). Invariant latitude is defined as

$$\Lambda = \cos^{-1}(L^{-\frac{1}{2}}), \tag{8}$$

where L is the McIlwain parameter (35). For the reader who is unfamiliar with invariant latitude, for a pure dipole field it is just the magnetic latitude where the field line through the point of observation intersects the surface of the earth. In the real case calculations of invariant latitude take into account the non-dipole parts of the field, whereas the geomagnetic latitude does not. The nature of the connection of the field lines in the tail to each other or to the interplanetary medium

is not yet known, but it is believed to occur at distances of more than 100 earth radii.

A consequence of the open field line model is that the cosmic ray cutoff rigidity will be zero over a large portion of the polar region, hence the existence of the polar ionization plateau. Thus we should expect the cosmic ray ionization to be independent of position within the polar plateau, the boundaries of which may be somewhat variable with local time and geomagnetic acitivity. It will, however, vary with altitude because of the increased shielding by the physical earth at low altitudes. Because trapped radiation can exist only on closed field lines, the high latitude edge of the trapped radiation belt can be considered to be the boundary of the polar plateau.

The ionization measured by POGO over the geomagnetic polar regions conforms to the above expectation if we exclude times when solar particle fluxes are present. The solar particle data do exhibit fluctuations over the poles as shown by Hudson and Anderson (36), but it is not clear from the POGO data whether some of the fluctuations may be primarily temporal in character. As for galactic cosmic radiation, six consecutive high sensitivity polar passes were analyzed statistically. The individual ion chamber Δt's, usually about 30 to 40 per polar pass, were found to have a Gaussian distribution with a standard deviation of 6.4 percent, a small part of which may be due to a systematic altitude variation. It is of interest to compare this result with that from the Mariner IV ion chamber data of Neher and Anderson, (23), which was obtained a year earlier but during a similar level of galactic cosmic ray intensity. The Mariner ion chamber has the same volume as the POGO chamber but is

less sensitive by a factor of about 25. Thus we might expect the Mariner

data to have a standard deviation about a factor of 5 smaller. Indeed

standard deviations from 1.2 to 1.4 percent were typical for the Mariner

data.

B. Polar Pass Ionization Averages.

The first step of our polar ionization analysis consisted of com-

puting averages of the ionization over each polar pass where data had

been recorded. First consideration was given to the high sensitivity data.

For each pass a first calculation was made by computer, scanning the

tapes for data within specified limits for I and L. Two averages were

calculated, one including all the data that appeared to be free of any

trapped radiation near the boundaries, and the other including only the

data in the region $L > 20$. The results were checked by hand to make

sure the computer indeed chose the proper end points for the polar pass.

If not, the results were corrected accordingly. Other types of mistakes

in the data were also looked for at this time, and appropriate corrections

were made. Mistakes were usually easy to correct because the time

intervals are regular, not random. The most common types of mistakes

found were: 1) Double time intervals. There is a probability of 1/64

at the low bit rate that an ion chamber pulse will be missed while the

experiment data word is being shifted out by the spacecraft. The result

is a Δt which is twice as long as most of the others being measured,

within statistics. 2) Missing time intervals. Consecutive Δt's must

be consistent with the Greenwich time difference between them. Sometimes

there is too much Greenwich time difference, which indicates that some

data have been left out. The length of the missing interval can easily be calculated, and it always turns out to be consistent with the rest of the data if we assume it is an integral number of ion chamber pulses, or it combines with an adjacent shorter-than-average Δt to form one ion chamber pulse. 3) Short time intervals. Sometimes there are two or more consecutive short Δt's whose sum is about the same as the other Δt's measured during the pass. In this case we assume that one or more effective "extra pulses" were introduced into the data somewhere during processing. Obviously if too many mistakes occur, the polar pass becomes useless.

In order to eliminate most of the altitude dependence, all the ionizations were divided by the geometrical solid angle of open space as seen from the point of observation in units of 2π steradians:

$$\Omega(h) = 1 + \left[1 - \left(\frac{R_E + t}{R_E + h}\right)^2\right]^{\frac{1}{2}}, \tag{9}$$

where h is spacecraft altitude, R_E is the radius of the earth, taken to be 6371 km, and t is the effective thickness of the atmosphere. Initially a value of 29 km was used for t, but in final calculations 40 km, the value determined by Murayama (37), was used. It will soon be shown that we expect the ionization to depend on altitude in a more complicated way than just being proportional to $\Omega(h)$, but this was thought to be a good first approximation in order to get an average ionization nearly independent of altitude. In this way we hoped to be able to look for systematic effects in the ionization averages due to possible influences other than altitude.

Of the two averages calculated for each polar pass, the L > 20

average was usually slightly lower than the grand average, but generally

the two differed by less than 1 percent. In all cases the lower of the two

was considered to be the better value and was used for further analysis.

The standard deviation for each polar pass is estimated at 1.2 percent in

the case of OGO-II and 1.5 percent for OGO-IV, where the ionization level

was considerably lower and thus fewer $\Delta t's$ were obtained during a given

pass. A total of 444 polar passes were processed for the high sensitivity

OGO-II data, and 89 passes for OGO-IV. The results have been assembled

in Appendix I.

In the case of the low sensitivity data, there are only one or two

or, at the most, three $\Delta t's$ per polar pass that seem entirely free from

trapped radiation. Also the data are much more easily destroyed by

mistakes than in the high sensitivity case. However, the low sensitivity

mode is much less affected by such systematic effects as temperature

variations, power supply voltage fluctuations, and the amount of electrical

or mechanical noise that reaches the ion chamber. For this reason the

low sensitivity data were thought to be of considerable value, and 278 low

sensitivity polar passes for OGO-II were averaged by hand. The results

are given in Appendix I.

C. Spacecraft Radioactivity.

It soon became apparent that the fluctuations among the various

polar ionization averages were far greater than what should be expected

on the basis of statistics alone. This fact along with certain other

evidence led us to consider the possibility of radioactivity being induced

on the spacecraft by nuclear interactions during passes through the high intensity portions of the inner trapped proton belt.

1) The highest polar averages tend to correspond to approach longitudes of 0° to 90° West, where the inner belt comes down to its lowest altitude and the ionization intensity is at the highest observed values. This fact is especially noticeable for the first polar cap after apogee is passed where apogee is near the equator.

2) Consider the experiment of Stone, of Caltech in cooperation with the University of Chicago, No. 5008 on the same spacecraft (38). A schematic of the detector arrangement is shown in Fig.13. Considering only events which do not trip the V_3 scintillator, the V_1 and $V_1 V_2$ rates are, respectively, measures of proton fluxes in the 1 to 40 and 10 to 40 MeV energy ranges. No correlation is found between these rates and the ion chamber fluctuations at low flux rates, where no solar particles are present. On the other hand there is a correlation with the V_2 rate, which is sensitive to electrons of a narrow energy range near 1 MeV that do not trip the V_1 detector, neutral particles or γ-rays that get converted in the V_2 detector or in the absorber directly below it, or β-particles which originate in the absorber. Fig. 14 shows a sample plot of ionization vs. V_2 rate.

3) Consider a low altitude pass over the equator, as in the south-bound portion of Fig. 12. If we plot I vs. the V_3 rate, which is sensitive to all protons above 10 MeV and electrons above 1 MeV, for all the data between the radiation belts, we get a hysteresis effect as shown in Fig.15. The V_3 rate seems to include a contribution that is decreasing with time through the entire pass, which indicates a contamination of the V_3 rate but not necessarily of the ion chamber.

OGO-II, IV PARTICLE TELESCOPE
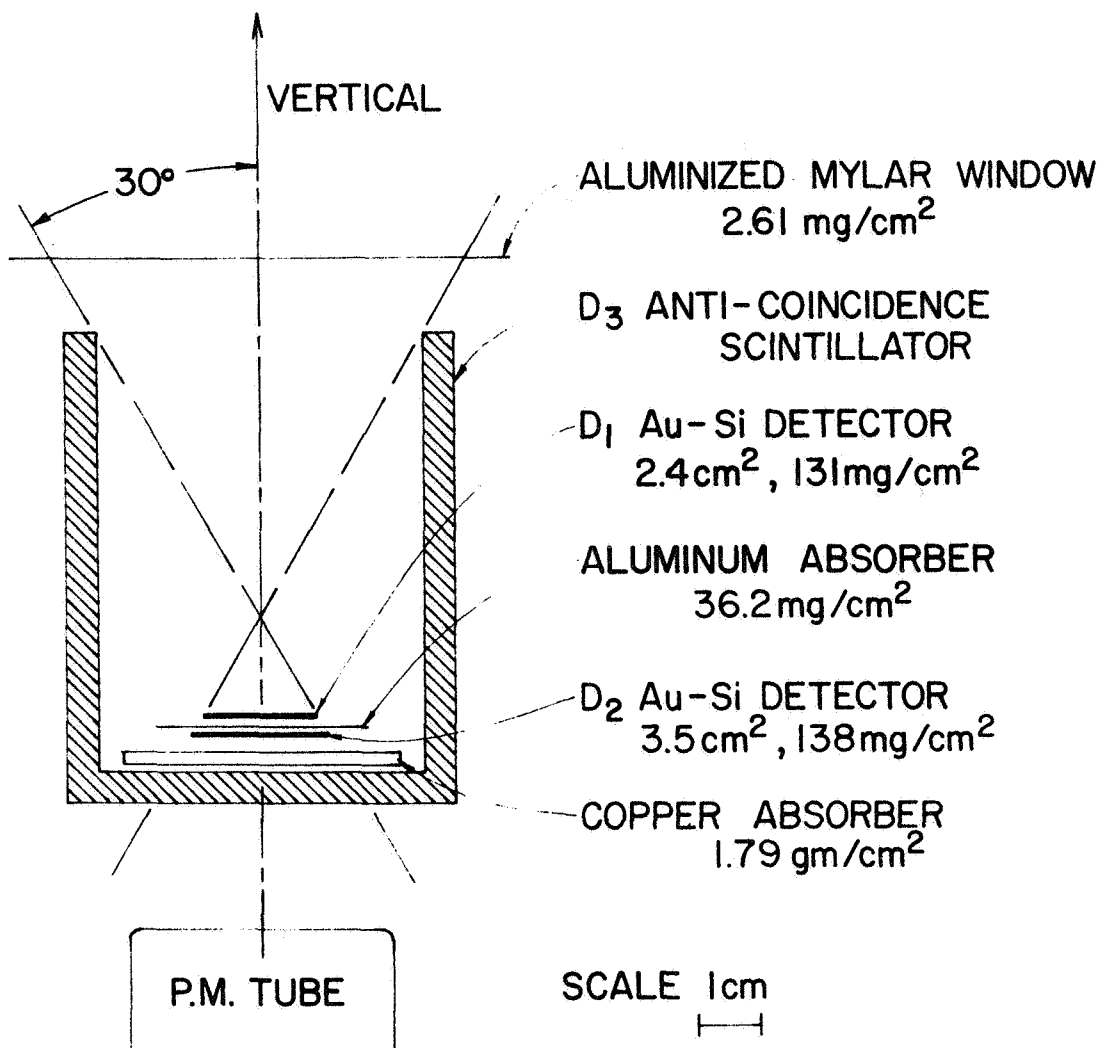
VERTICAL

30°

ALUMINIZED MYLAR WINDOW
2.61 mg/cm^2

D_3 ANTI-COINCIDENCE
SCINTILLATOR

D_1 Au-Si DETECTOR
2.4 cm^2, 131 mg/cm^2

ALUMINUM ABSORBER
36.2 mg/cm^2

D_2 Au-Si DETECTOR
3.5 cm^2, 138 mg/cm^2

COPPER ABSORBER
1.79 gm/cm^2

P.M. TUBE

SCALE 1 cm

Figure 13

POGO Experiment 5008 vertical detector arrangement. D_1, D_2, D_3 detectors correspond respectively to V_1, V_2 and V_3 counting rates mentioned in text.

OGO-II
REVS. 8-68 LOW SENSITIVITY
o NORTH POLE
+ SOUTH POLE
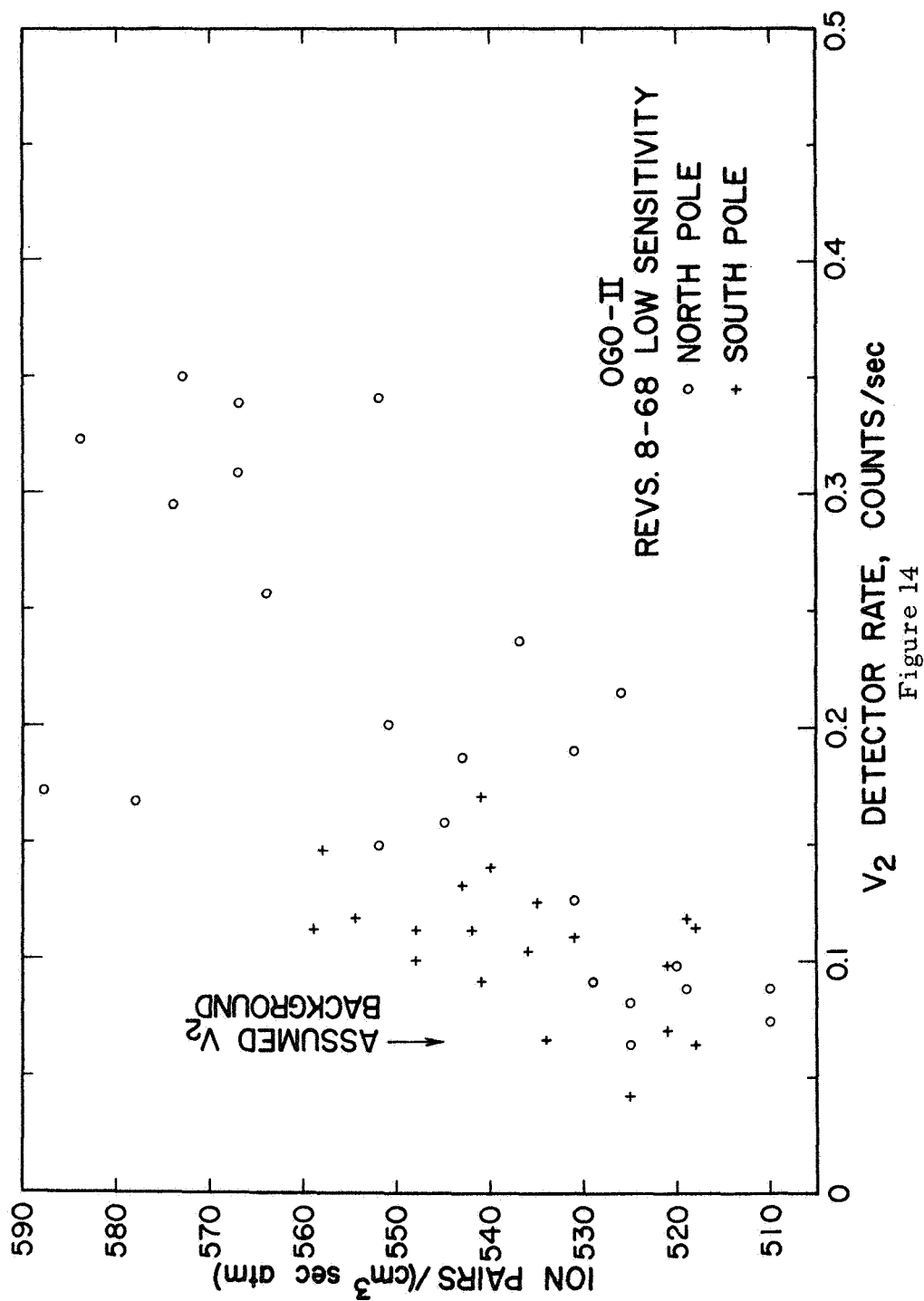
Figure 14

Experiment 5007 ionization vs. Experiment 5008 V_2 rate.
Data points are polar pass averages;
uncertainties are 1.5 to 2.0% in ionization, 10 to 20% in V_2 rate.
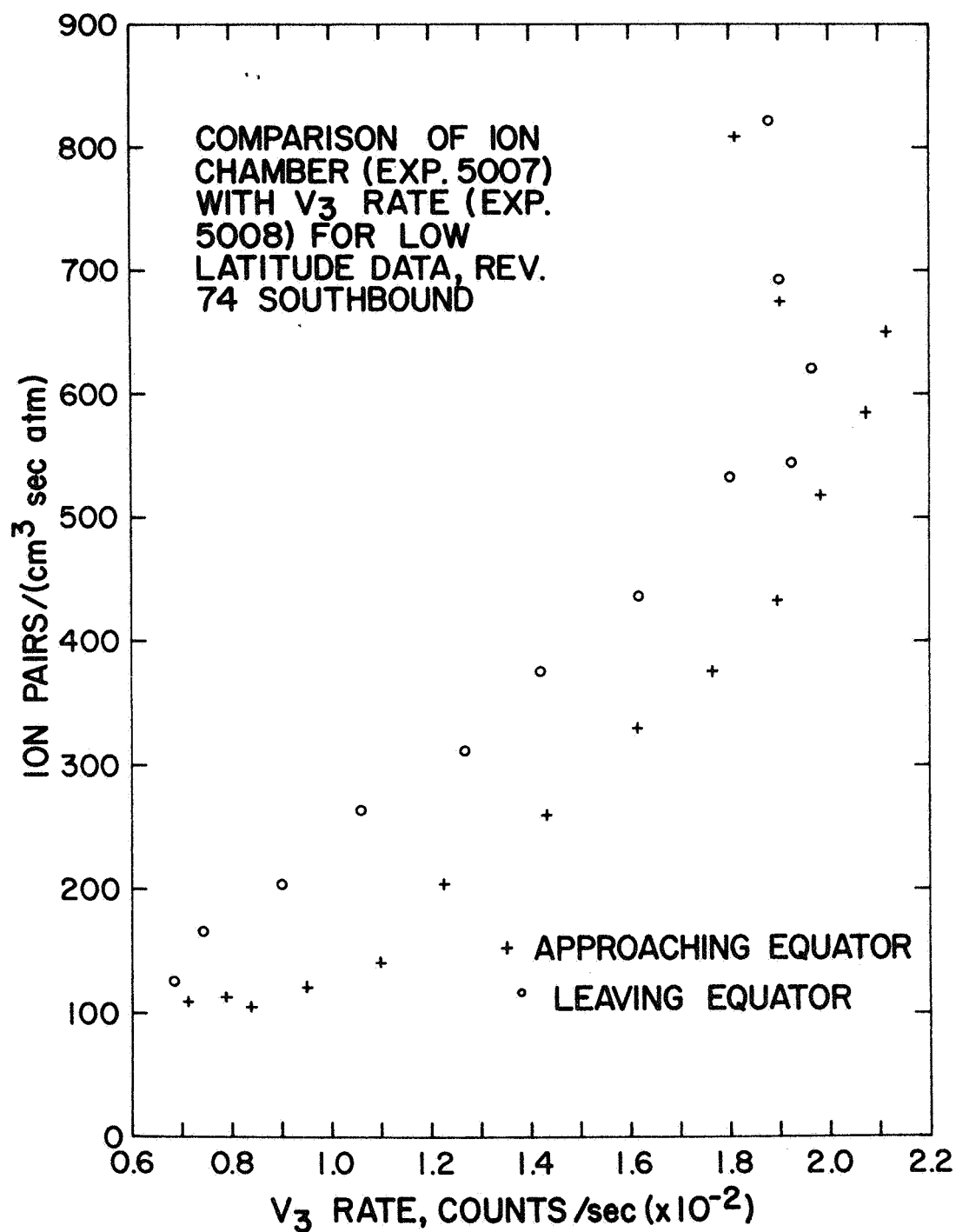
Figure 15

Ionization vs. V_3 rate for equatorial pass.
V_3 rates above 180 counts/sec are not reliable
because of scaler saturation.

4) Contamination in the ion chamber can be looked for by plotting I vs. L for a pass where no trapped radiation is present and where the altitude vs. latitude curve is symmetric with the L vs. latitude curve, which means h can be expressed as a function of L. In this way the effect of earth shielding will not destroy the symmetry between I and L. Only one complete pass that meets these specifications is available, and the plot is shown in Fig. 16. A hysteresis is observed, in the direction of a decaying contribution to the ionization but relatively less than the contribution to the V_3 detector. This is a reasonable result in view of the fact that the Exp. 5008 detectors are located in the main body of the spacecraft and therefore surrounded by much more matter than the ion chamber.

5) If one compares the equatorial ionization at different longitudes, it is found that the lowest values observed do not correspond to longitudes where the geomagnetic cutoff rigidity is highest. In fact over India, where the cutoff is highest, the ionization is higher than over South America, where the lowest equatorial cutoffs occur. But when passing over India near orbital perigee, the spacecraft has, on the previous half of its orbit, just been over South America near apogee, where the trapped radiation intensity is highest.

6) Equatorial ionization values measured near perigee by OGO-IV are considerably less than those measured at the same position by OGO-II. The difference is far greater than what we might reasonably expect on the basis of the increased solar activity at the time the OGO-IV data were obtained. But OGO-IV, having a much lower apogee, is subject to much less trapped radiation.
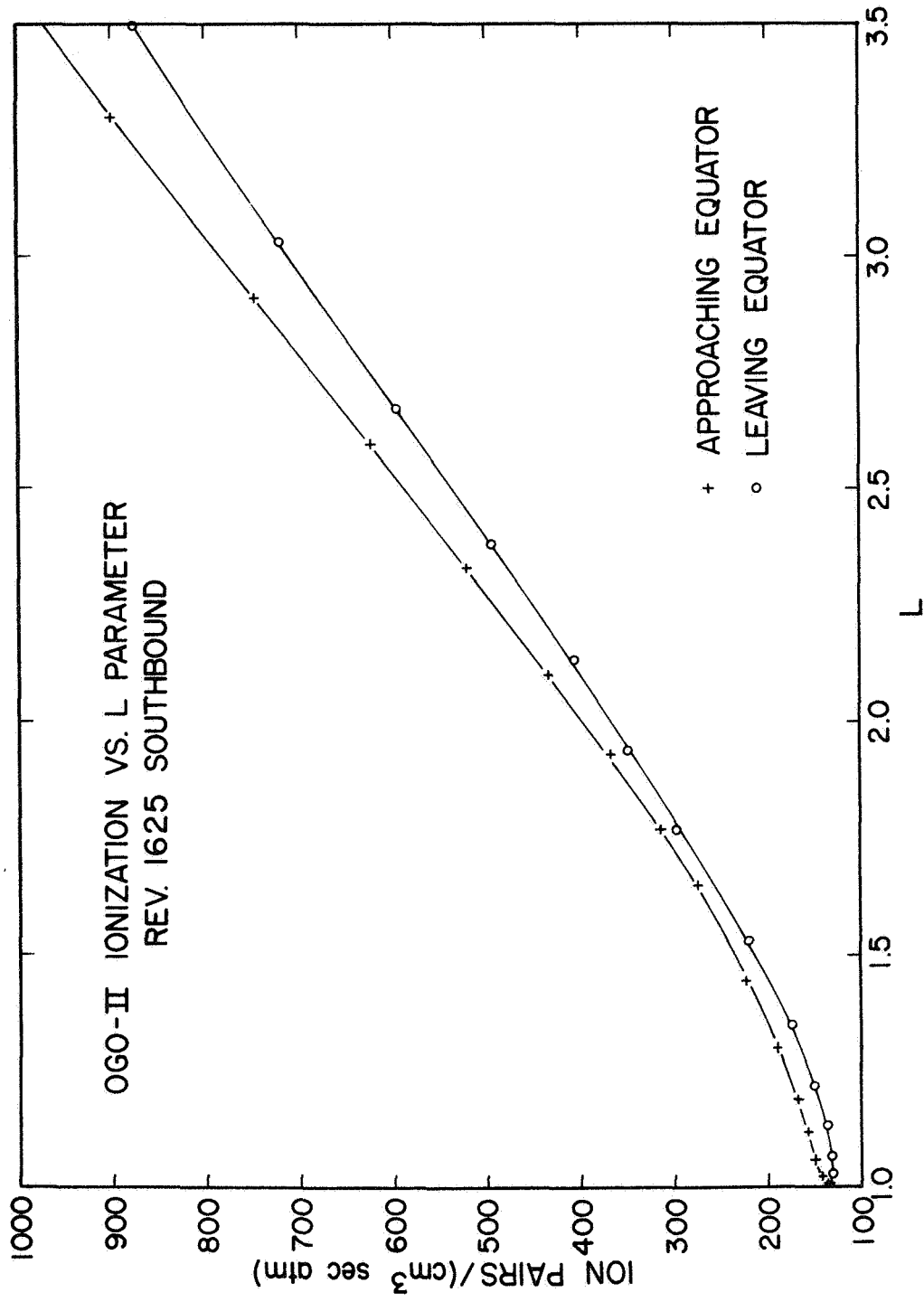
Figure 16

Ionization vs. L parameter for equatorial pass where perigee is located at minimum L.

7) Random scatter in the OGO-IV polar pass ionization averages during quiet times is much less than that in the OGO-II data. In fact, the OGO-IV results are consistent with a standard deviation of 1.5 percent for the separate averages, which indicates that the polar ionization is essentially constant with time over many orbits.

The preceding evidence points to radioactive elements on board the spacecraft with half lives on the order of a significant fraction of the orbital period, probably from 10 to 60 minutes. Radiation of shorter half life will become increasingly difficult to distinguish from the structure of the radiation belts themselves. A somewhat longer half life would lead to a diurnal variation that lags in phase behind the excitation, an effect that does not seem to be present in the data. A very long half life, several days or more, would appear as a constant background, which could not be distinguished from the galactic cosmic radiation.

Let us now consider the type of nuclear interactions that can occur. For target nuclei, we should consider all isotopes which are common on board the spacecraft. The incident particle will be a proton of energy from 10 to more than 100 MeV. One or more nucleons will be emitted, and we will look for residual nuclei with half lives within our detectable range. A list of reactions which may be of chief importance is given in Appendix II. All the products β^+ decay, so we will have both positrons and γ-rays. Let us do an order-of-magnitude calculation to see if we can make enough radioactive nuclei to account for the observed fluctuations in the ionization.

Consider the reaction $^{52}Cr(p,n)\,^{52}Mn$, which may be one of the most important which has an effect on the ion chamber. We will consider

only those reactions which occur in the chamber wall, which is about 20 percent ^{52}Cr. Our data indicate that the maximum ionization encountered on a pass through the inner belt is of the order of 10^8 ion pairs/(cm^3 sec atm) over a time period of approximately 500 seconds. If the particles are protons of typical energy 50 MeV, then the omnidirectional flux is 2.5×10^5 protons/(cm^2 sec). Integrated over the ion chamber for 500 sec, we have a total of 1.5×10^{10} protons, each of which passes through about 0.5 gm/cm^2 of wall material, or 0.1 gm/cm^2 of ^{52}Cr. If we assume a cross section of 10^{-26} cm^2 for the reaction, about 1.5×10^5 ^{52}Mn nuclei will be formed. They emit positrons with a half life of 21 minutes, so about 7×10^4 of them will be left after $\frac{1}{4}$ orbit when the polar pass occurs, decaying at the rate of 40 per second. The maximum energy of the ^{52}Mn positrons is 2.7 MeV, which corresponds to a range of slightly more than 1 gm/cm^2, or over five times the thickness of the ion chamber wall. Thus nearly half of the positrons will go through the interior of the ion chamber and will produce an equivalent ionization of the order of 10 ion pairs/(cm^3 sec atm). Probably of equal importance is the reaction ^{52}Cr(p,2n)^{51}Mn, and several others probably contribute to a lesser degree. Thus ionizations of the order of 50 ion pairs/(cm^3 sec atm), about the upper limit to the fluctuations in our data, may be produced by the radioactivation process.

Having recognized a serious problem, we must now admit that the quality of our galactic cosmic ray ionization data is not as good as we might have hoped for. Perhaps we can find a way to correct our ionization values. For example if we knew the integrated proton flux for recent passes through the inner belt, we should be able to fit these, together with an estimate of the half life, to the intensity of ionization

observed at the poles. However, our ion chamber is unreliable at these high flux values; we get essentially no data at all here. One could trace the spacecraft through B, L space (35) and look up corresponding trapped radiation fluxes measured by other observers, but this would be a very laborious process, and an estimate of the half life would still be required.

A simpler method seems to be available. Let us return to Fig.14, where I is plotted vs. the V_2 rate from Exp. 5008. Such a relation can be used to estimate the radioactivity contribution to the ionization if we made the following assumptions. 1) There is no significant contribution to the V_2 rate except from spacecraft radioactivity or radioactivity in the detector-absorber system itself. 2) Time variations in the cosmic radiation are negligible compared with the radioactivity contribution to the ion chamber. 3) Both the V_2 detector and the ion chamber are looking at radioactive decays with the same average half life. In reality we expect none of these assumptions to hold, but if we take certain precautions, they should at least become reasonable approximations. As for the first, we will have to live with 10 to 20 percent statistical errors in the V_2 rates, but we can at least estimate a constant background contribution by looking at some quiet time OGO-IV data, which should be subject to little or no spacecraft radioactivity. A value of 0.065 ± 0.010 counts/sec is thus estimated for the V_2 background. We will take care of the second approximation by treating only a few days' data at a time, quiet periods only. The third assumption becomes unnecessary if the time between activation and observation remains constant, which is nearly true if we treat North and South polar passes separately. We will then try to make a linear fit to our data of the form

$$I = A(V_2 - .065)/\Omega(h) + B, \qquad\qquad (10)$$

where A and B are constants to be determined by least squares fitting.
Remember I has already been divided by $\Omega(h)$ as defined in Eq. 9. The
constant B is then the average "corrected ionization" over the time
period selected, and it can be used for further analysis.

V_2 rates are available for most of the polar passes where we
have ionization averages, and these are listed in Appendix I along with
the ionizations. For all groups of points, a plot was made as in Fig. 14
and examined by eye. A few "bad points", far away from the rest of the
data, were deleted from the analysis. The number of such points was
small, and they were assumed to contain errors which were probably
introduced during initial data processing. Values of A were usually
found to lie between 200 and 350, with standard deviations of 20 to 50
percent. There were a few poor fits, where the standard deviation was
near 100 percent, but these were associated with data where the V_2 rates
were low, and therefore the corrections to the ionization were small. In
order to prevent extreme values of A resulting from poor fits, A was
not allowed to exceed 400 or go below 150.

For each ionization average used, a corrected value can be ob-
tained by subtracting out the first term of Eq. 10. These results are
given in Appendix I. The corrected averages still have quite a large
spread from the mean, but we will now assume this is due to original
errors in the ionization, 1.2 to 1.8 percent; statistical errors in the V_2
rates, 10 to 20 percent; faults in our approximations that make this type
of fit valid; and the fact that the V_2 rates were not determined over

exactly the same time interval as the ionization averages. Thus we think we have removed an important systematic effect at the expense of having larger statistical errors.

We can now derive an estimate of the half life by comparing ionization corrections from consecutive polar passes where no exitation occurs in between. For example, we determine ΔI (North pole)/ΔI (South pole) for a perigee pass at longitudes near India, so that all the exitation occurred on the previous northbound pass. Here ΔI means the amount of ionization that is attributed to spacecraft radioactivity. In this way we estimate that ΔI decays by a factor of 4.3 $\pm$ .5 during the 50 minute period between the poles, which corresponds to a half life of 23.8 $\pm$ 1.7 minutes. A similar comparison of the V_2 rates, subtracting out the .065 count/sec background, yields a decay factor of 4.9 $\pm$ .7 and a half life of 21.8 $\pm$ 2.1 minutes. We must be aware, however, that we are really calculating only an effective half life which is the result of the decay of many isotopes with different half lives. Therefore the fact that the two results turn out to be nearly equal is not regarded as particularly significant.

The results for the constants A and B are given in Table 6 for the different groups of data that were processed, including average altitudes. Also included are IMP-III interplanetary ionization data for the applicable time periods from the University of California ion chamber experiment, which we hope to use to eliminate time variations from our data. The uncertainties for the constants A and B are the results of the least squares fit.

Table 6

Orbits OGO-II	Pole	Altitude km	A ion pairs/ (cm³ atm)	B ion pairs/ (cm³ sec atm)	IMP-III ionization pulses/hr
Low Sensitivity					
8- 68	N	796	268 ± 54	522.5 ± 5.8	2.66
8- 68	S	1098	322 ± 133	527.5 ± 4.6	2.66
122- 224	N	573	241 ± 74	531.9 ± 6.9	2.66
122- 224	S	1367	150 ± 192	528.9 ± 7.6	2.66
352- 450	N	439	357 ± 78	542.7 ± 3.8	2.80
352- 450	S	1520	150 ± 80	536.3 ± 4.4	2.80
608- 620	N	640	150 ± 185	545.5 ± 8.9	2.90
608- 620	S	1302	150 ± 72	551.3 ± 7.8	2.90
1387-1425	N	1303	264 ± 68	520.5 ± 5.6	2.64
1387-1425	S	554	400 ± 221	527.2 ± 8.8	2.64
1446-1528	N	1188	193 ± 67	514.1 ± 5.5	2.61
1446-1528	S	708	270 ± 254	512.6 ± 7.7	2.61
1568-1754	N	756	179 ± 130	550.2 ± 13.8	2.78
1568-1754	S	1096	307 ± 178	535.3 ± 8.2	2.78
High Sensitivity					
74- 110	N	698	286 ± 39	555.6 ± 3.8	2.64
74- 110	S	1211	272 ± 144	558.5 ± 5.2	2.64
380- 444	N	440	200 ± 112	547.1 ± 4.3	2.81
380- 444	S	1524	216 ± 78	543.4 ± 4.2	2.81
572- 703	N	655	202 ± 124	558.1 ± 4.4	2.87
572- 703	S	1328	195 ± 54	567.7 ± 5.0	2.87
1201-1279	N	1496	150 ± 307	565.9 ± 5.6	2.93
1201-1279	S	486	223 ± 78	583.6 ± 2.7	2.93
1372-1411	N	1364	205 ± 113	539.0 ± 8.5	2.62
1372-1411	S	576	207 ± 130	544.2 ± 7.8	2.62
1426-1537	N	1205	276 ± 63	533.2 ± 4.9	2.64
1426-1537	S	734	152 ± 111	552.5 ± 6.3	2.64
1553-1646	N	906	157 ± 76	578.8 ± 8.3	2.71
1553-1646	S	1005	150 ± 224	586.1 ± 9.3	2.71
1742-1824	N	563	400 ± 101	581.0 ± 8.8	2.74
1742-1824	S	1374	400 ± 175	581.1 ± 11.2	2.74

D. Time Variations in the Data.

The cosmic radiation is not constant but shows variations over a wide range of characteristic times due to the solar modulation. During solar minimum, however, when our OGO-II data were obtained, such fluctuations tend to be also at a minimum. In most cases the radiation changes by less than 1 percent during periods of the order of five days in the high energy part of the spectrum, although low energy particles can change somewhat more. We would like to make sure that time changes in the OGO-II ionizations do not introduce any systematic errors into the altitude dependence that we wish to derive.

Conveniently available are the data from the University of California ion chamber experiment on the IMP-III satellite, which operated during the same period with OGO-II. The IMP-III was in a highly elliptical orbit, so that most of the time it was in the interplanetary medium, where it could measure particle fluxes independent of geomagnetic effects. The IMP ion chamber (22) operated on the same principle as the OGO model and had nearly the same response to the cosmic radiation, although its wall was aluminum. The time resolution of the IMP experiment is rather poor, being on the order of 5 $\frac{1}{2}$ minutes compared with 144 milliseconds for OGO-II. Thus we have to average the IMP data for the order of one day in order to obtain statistical accuracy of less than 1 percent. Therefore we cannot look for time variations shorter than one day, but these are not likely to be important anyway. The IMP ionizations, averaged over the same time periods as our OGO values, have been listed in Table 6.

The determinations of B in Table 6 can be considered as the

average ionizations over the orbits indicated, with spacecraft radio-activity subtracted out. Hereafter the B values will be called ionizations and used as such in analysis. Now we plot the OGO-II ionizations vs. the IMP-III results in Fig. 17. Immediately we notice that the low sensitivity data seem to form a linear relationship, while the high sensitivity values show much more scatter and lie generally higher on the OGO ionization scale. A least squares straight line fit, which includes the low sensitivity data only, is shown in the figure.

Before discussing the odd behavior of the high sensitivity data, we will mention another problem. The slope of the line in Fig. 17 is such that for a 1 percent change in the IMP ionization the OGO ionization changes by only 0.57 percent. We should expect the two rates to be proportional to each other (the line should pass through the origin), since the two instruments should respond in the same way to changes in the cosmic radiation. We also have some data available from the University of Minnesota ion chamber (39) on the OGO-I satellite, which is also in a highly elliptical orbit. Without presenting a lot of data here, we note the following results. Between October 20 and November 15, 1965 the IMP-III ionization increased by 6.4 percent, while the OGO-I value increased by only 0.9 percent. Over a longer time period and a larger change in the radiation, between November 15, 1965 and March 30, 1966 the IMP-III ionization decreased by 18.5 percent while the OGO-I measurement decreased by only 12.7 percent. Clearly there are significant disagreements here concerning the changes in the ionization in space. It is not likely that spectral changes in the cosmic radiation, coupled with differences in the ion chamber responses to various parts of the spectrum, can
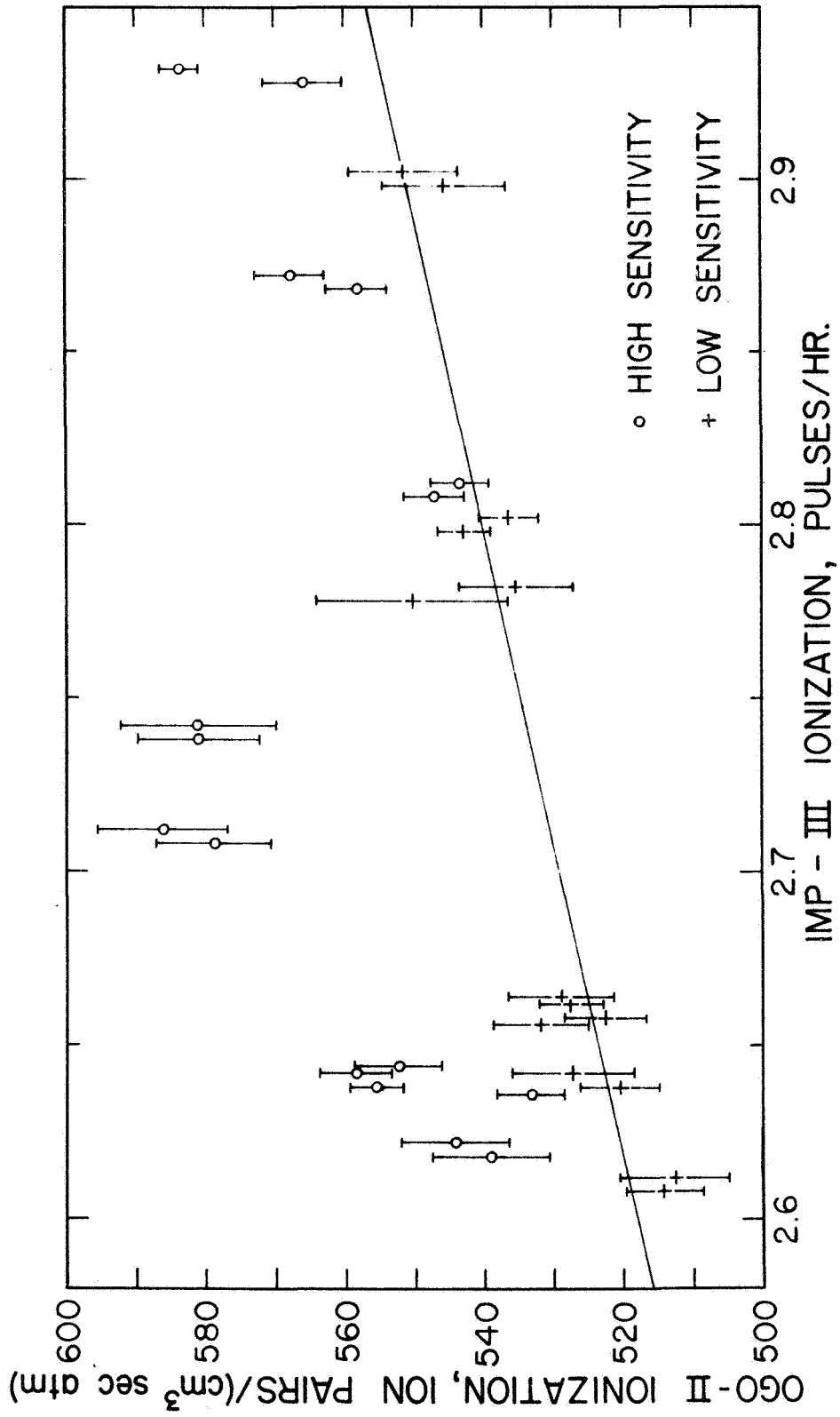
Figure 17

OGO-II ionization vs. IMP-III ionization, quiet time data.
Straight line fits low sensitivity data only.

account for disagreements of this magnitude. We do not have a good OGO-II ionization for March 30 because no V_2 rates are available for the subtraction of spacecraft radioactivity. Perhaps this is a problem which should be investigated in the future, but we do not propose to deal with in any more detail in this paper. Suffice it to say that we get a good fit with the IMP-III data, and by use of Fig. 16 it is easy to correct the OGO-II data to constant IMP-III ionization level, for example 2.75 pulses /hr. The results will be presented in Table 7.

We now turn our attention back to the high sensitivity data, which appear to be affected by something other than time and altitude variations. The high sensitivity ion chamber constant was observed to fluctuate by a few percent during laboratory calibrations, but the spread of the data in Fig. 17 is a little more than what we might expect from this cause. No obvious conclusions are possible, but temperature fluctuations may well be responsible for the high data values. The dependence of ion chamber sensitivity on temperature is known, and an attempt has been made to correct for it during data processing. Of course an input temperature is required, which is measured in the electronic assembly attached to the base of the ion chamber. The temperature in the ion chamber itself may be somewhat different, however, especially since the ion chamber sphere contains much less mass and much more surface area than the base assembly, so that it may be expected to respond to environmental changes considerably faster. The Mode II sensitivity of the OGO-II ion chamber decreases by approximately 0.08 percent per 1 degree increase in temperature, so that the data in Fig. 17 indicate that the ion chamber may be running somewhat colder than what our measured temperature indicates.

Both the absolute value of the ionizations and the difference be-
tween the simultaneous averages at opposite poles, which are generally
at different altitudes, contain information regarding the altitude depend-
ence of the ionization. Since the high sensitivity absolute values appear
to be unreliable, it seems best to ignore the measured absolute values
and assign new ones which agree with the low sensitivity results, but we
will retain the same differences between the simultaneous measurements
at opposite poles. Thus the high sensitivity data will contribute new in-
formation to the altitude dependence only through the differences between
simultaneous measurements at different altitudes. We must still worry
about possible systematic errors in these differences. For six out of
our eight pairs of high sensitivity averages in Table 6, the spacecraft
passes through eclipse while traveling from North to South, while there
is no eclipse at all during the periods covered by the other two pairs.
Thus we might expect the ion chamber to be colder at the south pole, pro-
ducing higher ionization values there than at the north pole. There is
some evidence for this in our data. To try to correct for it, we assume
that the temperature induced ionization difference depends linearly on
eclipse duration time. (This of course is a crude approximation, since
radiation losses are usually proportional to the fourth power of the tem-
perature, but we do not believe the quality of the data or the magnitude of
the correction justify a better approximation.) From the data the coefficient
of proportionality is estimated to be 1 ion pair/(cm^3 sec atm) per 2.8 minutes
of eclipse duration, which corresponds to a temperature decrease of about
30°C during a 35 minute eclipse. We should worry that this kind of
adjustment of the data may be bad because it alters the very relation that

is going to give us the altitude dependence. If we look at the altitudes, however, we find that we are in a rather fortunate situation. Of the six pairs of data values involved, three have their higher altitude at the south pole, and the other three are higher at the north pole. Thus if there is a systematic altitude dependence in the ionization differences, an adjustment of the type just described will add to it in three cases and subtract from it in the other three cases, so that in reality we cannot bias our altitude dependence very far one way or the other.

E. Polar Ionization as a Function of Altitude.

The ionization averages, after the above adjustment have been applied for time and temperature variations, are presented in Table 7. One slight further adjustment has also been made. The value for the thickness t of the atmosphere in Eq. 9 has been changed from 29 km to 40 km.

The method of analysis to be used will be similar to that employed by Murayama (37), except that we will attempt to fit data over a range of altitudes instead of at two discrete altitudes. We assume the measured ionization is the sum of two components due to the primary particles and the splash albedo particles:

$$I = I_p + I_A. \tag{11}$$

The two components should have different altitude dependences, so we can write Eq. 11 in the form

$$I(h) = \left[C_p F_p(h) + C_A F_A(h) \right] / \Omega(h), \tag{12}$$

where C_p and C_A are constants, $\Omega(h)$ is the geometrical solid angle as defined in Eq. 9, and the functions $F_p(h)$ and $F_A(h)$ describe the altitude dependence of the primary and albedo cosmic rays, respectively. $I(h)$ has already been divided by $\Omega(h)$ for reasons previously described. We must find the forms of $F_p(h)$ and $F_A(h)$. If we then normalize each of these functions to have the value unity at $h = 40$ km, the constants will be in the same absolute ionization units as our data, and

$$I(40) = \left(C_p + C_A \right) / \Omega(40), \tag{13}$$

$$I(\infty) = 2C_p/\Omega(\infty), \tag{14}$$

$$\text{fractional albedo} = \frac{C_A}{C_p + C_A}. \tag{15}$$

Note that $\Omega(40) = 1$ and $\Omega(\infty) = 2$.

To find $F_p(h)$, we must find the solid angle of allowed trajectories of cosmic ray particles as a function of energy and altitude. Then we integrate over all energies, folding in the primary energy spectrum and the response function of the ion chamber. Integration of the equation of motion of a charged particle in the earth's magnetic field in order to find the allowed cosmic ray trajectories has become a highly developed technique, notably through the efforts of Shea and Smart (13). Essentially all calculations, however, have been done for positions at the top of the earth's atmosphere, not for higher altitudes. Murayama did it for the two altitudes of interest to him, 165 and 540 km, at $70°$ and $85°$ geomagnetic latitude.

We do not intend to get involved in trajectory calculations of such a complicated nature, but instead we shall argue that it is sufficient to

Table 7

Orbits OGO-II	Pole	Altitude km	I ion pairs/(cm³ sec atm)*
			Low Sensitivity
8- 68	N	796	533.6 ± 5.8
8- 68	S	1098	538.4 ± 4.6
122- 224	N	573	543.4 ± 6.9
122- 224	S	1367	539.6 ± 7.6
352- 450	N	439	538.9 ± 3.8
352- 450	S	1520	531.4 ± 4.4
608- 620	N	640	530.2 ± 8.9
608- 620	S	1302	535.4 ± 7.8
1387-1425	N	1303	533.4 ± 5.6
1387-1425	S	554	540.9 ± 8.8
1446-1528	N	1188	527.2 ± 5.5
1446-1528	S	708	526.0 ± 7.7
1568-1754	N	756	548.1 ± 13.8
1568-1754	S	1096	532.9 ± 8.2
			High Sensitivity
74- 110	N	698	534.2 ± 4.5
74- 110	S	1211	536.7 ± 4.5
380- 444	N	440	542.4 ± 4.2
380- 444	S	1524	527.2 ± 4.2
572- 703	N	655	537.1 ± 4.7
572- 703	S	1328	533.6 ± 4.7
1201-1279	N	1496	531.2 ± 4.4
1201-1279	S	486	538.3 ± 4.4
1372-1411	N	1364	537.0 ± 8.1
1372-1411	S	576	533.4 ± 8.1
1426-1537	N	1205	529.9 ± 5.7
1426-1537	S	734	541.0 ± 5.7
1553-1646	N	906	534.5 ± 8.8
1553-1646	S	1005	536.7 ± 8.8
1742-1824	N	563	535.6 ± 10.0
1742-1824	S	1374	534.7 ± 10.0

*Standard deviations include statistical errors only.

take the low rigidity limit and evaluate the solid angle of the allowed cone
as a function of altitude. By the low rigidity limit, we mean that the
gyration radius of the particle is much less than the scale of the field
geometry, so that the solid angle becomes independent of rigidity. If we
look at Murayama's results, we observe the following. 1) The solid angle
of the allowed cone remains within 1 percent of the low rigidity limit up to
rigidities of the order of 7 BV. For high rigidities the allowed solid angle
approaches the geometrical solid angle $\Omega(h)$, which is a few percent
smaller. From the 1965 latitude survey (1) we estimate that roughly 80
percent of the total ionization is accounted for by particles of rigidities
less than 7 BV. 2) The approximation gets better as one goes to higher
altitudes and higher geomagnetic latitudes. We are interested in altitudes
generally higher than Murayama's range and geomagnetic latitudes gen-
erally above 77°.

The low energy calculation is easy. We do not even have to know
the absolute value of the magnetic field; only its altitude dependence,
which we shall assume to be $(R_E + h)^{-3}$. Consider a particle observed at
altitude h to have a direction of motion which makes an angle θ with
the magnetic field lines ($\theta = 0$ means vertically upward). The equations
which describe the motion of a particle in a magnetic field whose intensity
is a function of distance along the field lines are derived in many texts on
electrodynamics, for example Jackson (40). In particular, we want to
know how the angle θ changes with field strength. Jackson gives

$$\sin^2\theta = \frac{B}{B_0} \sin^2\theta_0 \ , \tag{16}$$

where θ_0 is the angle at a different altitude where the field strength is

B_0. In our situation, when θ_0 becomes $90°$, the particle mirrors; that is to say the particle reverses the vertical component of its velocity vector. To find the limit of allowed trajectories, we require the mirror point to be at the top of atmosphere. Setting $\sin^2 \theta_0 = 1$ and inserting the altitude dependence for B, we get

$$\sin^2 \theta_c = \left(\frac{R_E + t}{R_E + h} \right)^3 , \tag{17}$$

where θ_c is the value of θ below which the particle has mirrored below the top of the atmosphere. It will be convenient to define the quantity

$$a = \left(\frac{R_E + h}{R_E + t} \right)^{3/2} . \tag{18}$$

Then

$$\theta_c = \sin^{-1} \frac{1}{a} . \tag{19}$$

All particles following trajectories with $\theta > \theta_c$ have not been in the atmosphere and therefore are in the allowed cone for primary particles. From Liouville's theorem we know that the particles are isotropic in this cone with the same intensity per unit solid angle as they had at infinity. If we express the solid angle in units of 2π steradians, it has the desired normalization for $F_p(h)$:

$$F_p(h) = 1 + \cos \theta_c = 1 + \left[1 - \left(\frac{R_E + t}{R_E + h} \right)^3 \right]^{1/2} . \tag{20}$$

Notice that this differs from the geometrical solid angle only in the power of the altitude dependent term, cubed instead of squared.

For the altitude dependence of the splash albedo particles, Murayama assumed a simple $(R_E + h)^{-n}$ relation, where $n = 3$ for low energy charged particles and $n = 2$ for high energy charged particles

and γ-rays. He assumed that the two components contributed nearly equally to his detector rate and accordingly took the arithmetic mean between the two altitude dependences over his altitude range. We propose to do things a little differently here. First of all, the sensitivity of the ion chamber to γ-rays is only about 1 percent of that for electrons at energies near 1 MeV, and 4 percent for energies above 50 MeV. The relative contribution of γ-rays to the total ionization will be even less, since we also have to contend with the more highly ionizing protons (gray track particles). Therefore we will neglect entirely the presence of γ-rays in the splash albedo. Furthermore, essentially all the charged albedo particles have sufficiently low energy (Larmor radii small in comparison to the scale of the magnetic field geometry) that we can set $n = 3$ for all ionizing particles. Then we have simply

$$F_A(h) = \left(\frac{R_E + t}{R_E + h} \right)^3 . \tag{21}$$

We can now predict the altitude dependence for the ionization as given by Eq. 12. Plots of ionization vs. altitude are given in Fig. 18 for no albedo and for fractional increases over the primary ionization at 40 km due to albedo particles of 5, 10, 15, and 20 percent. We see that for fractional albedo contributions of 0 to 10 percent we indeed have removed most of the altitude dependence in the 430 to 1540 km region by dividing the total ionization by $\Omega(h)$.

However, Eq. 21 only applies if all the albedo particles are emitted parallel to the field lines ($\theta = 0$) or if θ does not change with altitude, as is shown to be wrong by Eq. 16. Suppose all the particles are emitted at the same angle θ_0 with the field lines. Then $F_A(h)$ will
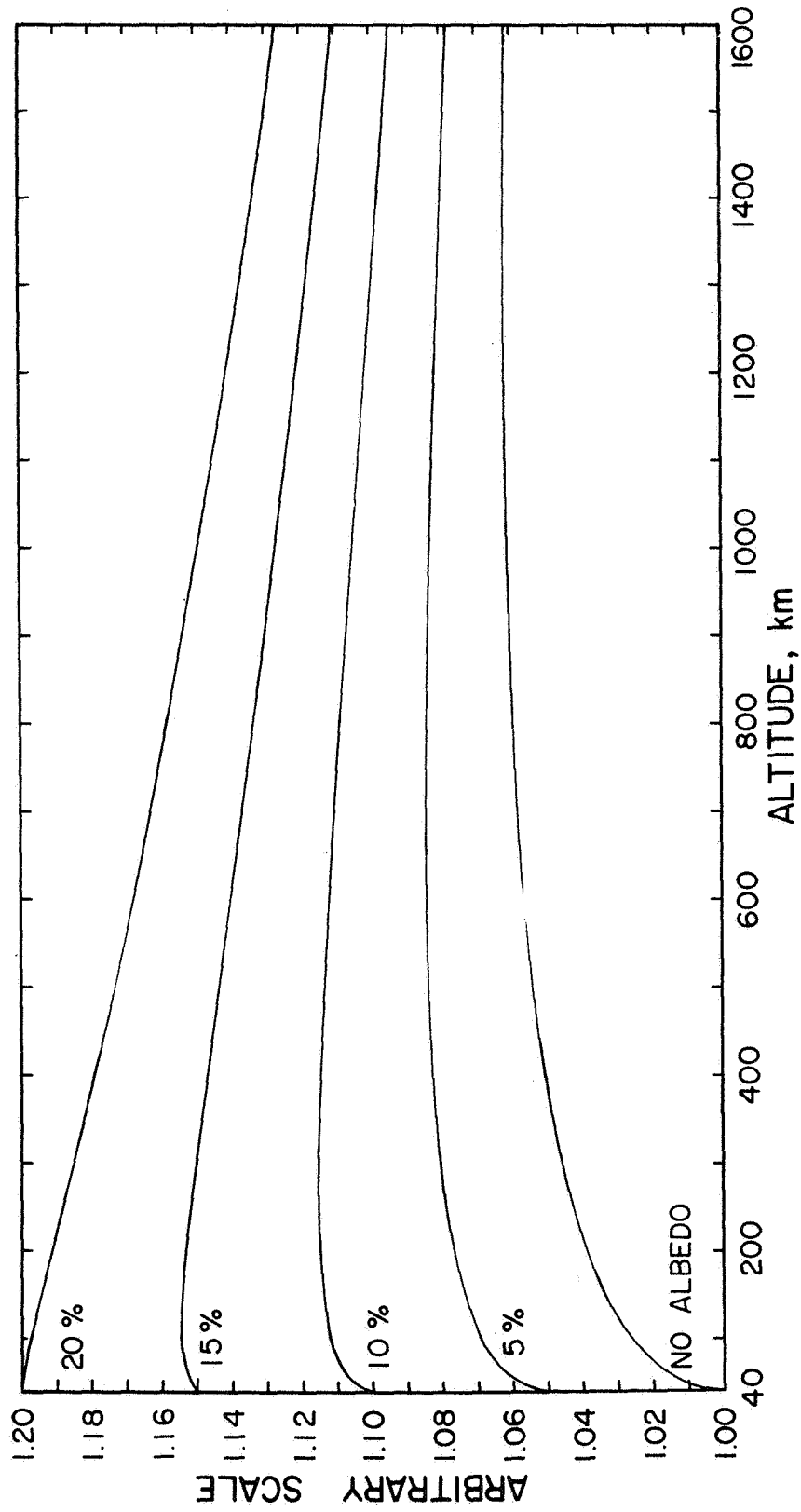
Figure 18

Predicted ionization vs. altitude curves for various additions to the primary ionization due to splash albedo.
Total ionization has been divided by the geometrical solid angle of the sky.

be proportional to $\dfrac{1}{r^3 \cos\theta}$, where $r = R_E + h$ and we must include the variation of θ with altitude according to Eq. 16. If we insert the quantity a as in Eq. 18, we get

$$\cos\theta = \left(1 - \frac{1}{a^2} \sin^2\theta_0\right)^{\frac{1}{2}} = \frac{1}{a}\left(a^2 - \sin^2\theta_0\right)^{\frac{1}{2}} \tag{22}$$

and

$$F_A(h) \propto \frac{1}{a}\left(a^2 - \sin^2\theta_0\right)^{-\frac{1}{2}} . \tag{23}$$

We must now integrate over all possible values of θ_0 to get the altitude dependence of the total ionization.

$$F_A(h) = \frac{C_N}{a} \int_0^{\pi/2} f(\theta_0)\left(a^2 - \sin^2\theta_0\right)^{-\frac{1}{2}} \sin\theta_0 \, d\theta_0 , \tag{24}$$

where $f(\theta_0)$ describes the angular distribution of the albedo particles at the top of the atmosphere and C_N is a normalization constant such that $F_A(40) = 1$. If the specific ionization of the particles also depends on θ_0, we must also account for that in the determination of $f(\theta_0)$.

The angular distribution of the splash albedo particles has not been measured experimentally, nor has it been calculated theoretically. We cannot assume it is isotropic because the integral in Eq. 24 becomes infinite for $a = 1(h = 40 \text{ km})$. This is a consequence of the fact that the $\dfrac{1}{r^3 \cos\theta}$ dependence implies that a particle with $\theta = 90°$ remains at the same altitude forever, where in reality it begins to move upward, and θ decreases, because of the divergence of the field. Therefore, we require $f(\theta_0)$ to go to zero as θ_0 approaches $\dfrac{\pi}{2}$. Let us consider five trial functions for $f(\theta)$.

$$f_1(\theta) = \delta(\theta)$$

$$f_2(\theta) = \cos\theta$$

$$f_3(\theta) = \cos\theta(1 + \sin^2\theta)$$

$$f_4(\theta) = \cos\theta(1 + \sin^2\theta + \sin^4\theta)$$

$$f_5(\theta) = \cos\theta(1 + \sin^2\theta + \sin^4\theta + \sin^6\theta)$$

The first case, where $\delta(\theta)$ is the Dirac delta function, corresponds to the altitude dependence of Eq. 21. The remaining four cases ought to be more representative of the actual angular dependence and have the additional advantage of making the integral easy to do. For the reader's convenience they are plotted in Fig. 19.

As an example let us evaluate $F_A(h)$ in Eq. 24 for $f(\theta_0) = f_3(\theta_0)$. The result is

$$F_A(h) = \frac{1}{5}(2a^2 + 3) - \frac{1}{5}(2a + 4a^{-1})(a^2 - 1)^{1/2}. \tag{25}$$

A similar expression occurs for f_2, f_4, and f_5. In all cases, if we expand $(a^2 - 1)^{1/2}$ by the Binomial Theorem and express $F_A(h)$ as a power series in a, we find that constant terms and positive powers of a cancel out, and we are left with only negative even powers of a, for example, in the case of Eq. 25

$$F_A(h) = \frac{3}{5}\left(\frac{3}{4}a^{-2} + \frac{5}{24}a^{-4} + \frac{7}{64}a^{-6} + \cdots\right). \tag{26}$$

Thus we get an altitude dependence which falls off steeper than r^{-3}; it has terms containing r^{-6}, r^{-9}, etc. in addition to the r^{-3} term.

We are now ready to fit the data in Table 7 according to Eq. 12. It is found that good fits are obtained using all five trial functions for $f(\theta)$. The results, defined by Eqs. 12-15, are presented in Table 8.

$f_2(\theta) = \cos\theta$

$f_3(\theta) = \cos\theta \, (1 + \sin^2\theta)$

$f_4(\theta) = \cos\theta \, (1 + \sin^2\theta + \sin^4\theta)$

$f_5(\theta) = \cos\theta \, (1 + \sin^2\theta + \sin^4\theta + \sin^6\theta)$
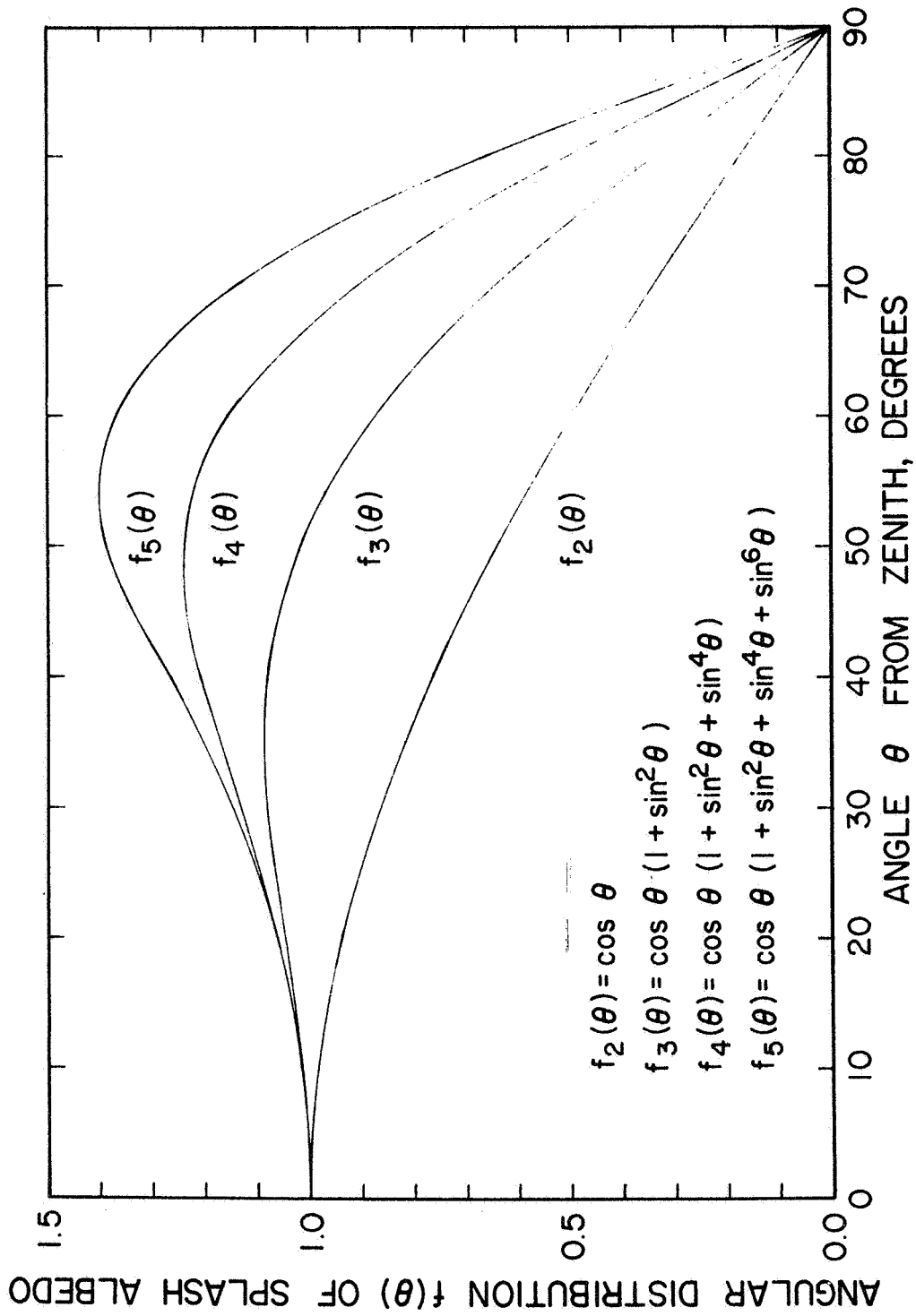
Figure 19

Trail functions used for the angular distribution of splash albedo particles.

Table 8

$f(\theta)$	f_1	f_2	f_3	f_4	f_5
C_p^*	485.8 ± 4.5	490.2 ± 3.5	490.6 ± 3.4	490.9 ± 3.3	492.6 ± 3.0
C_A^*	44.4 ± 9.9	53.0 ±11.8	55.2 ±12.6	57.1 ±12.7	57.1 ±12.7
$I(40)^*$	530.6 ± 5.6	543.1 ± 8.4	545.8 ± 9.0	548.0 ± 9.5	549.7 ± 9.9
$I(\infty)^*$	971.7 ± 8.9	980.3 ± 7.0	981.2 ± 6.8	981.8 ± 6.7	985.1 ± 6.0
Percent Albedo	8.4 ± 1.9	9.8 ± 2.2	10.1 ± 2.3	10.4 ± 2.3	10.4 ± 2.3

*Units are ion pairs/$(cm^3 \, sec \, atm)$

Note that the entire analysis that we have just explained depends on the approximation that there is a definite height to the top of the atmosphere. We have assumed it to be at 40 km altitude, the same value used by Murayama. In reality, of course, there is a more gradual transition between space and the atmosphere, which must be considered if a more accurate calculation is to be done. Such a calculation would also remove the requirement that the angular distribution of the albedo particles must go to zero at the horizon at 40 km, although obviously this eventually does happen at higher altitudes. Therefore, our approximation has the effect of requiring all of the albedo particles to be produced somewhat below 40 km.

We see from the table that the results do not depend critically on the form of $f(\theta)$, especially in the 3rd, 4th, and 5th cases, which probably come close to representing physical reality. We will consider the values in the f_5 column to be our best results, and they will be compared with other measurements. The data of Table 7 are plotted in Fig. 20 along with the best fit to Eq. 12 for the cases $f(\theta) = f_1(\theta)$ and $f_5(\theta)$. Finally, Fig. 21 shows the real ionization vs. altitude curve, obtained from Eq. 12 by multiplying $\Omega(h)$ out again. From this point on, when we talk about ionization values, we will no longer have the $\Omega(h)$ divided in.

F. Comparison with Other Results.

An estimate of the ionization albedo near the geomagnetic pole using similar instruments was made by Neher and Anderson (24) in 1962 by comparing the ionization at balloon altitude over Thule, Greenland with that measured by the Mariner II Venus probe in the interplanetary medium.

COSMIC RAY IONIZATION IN SPACE OVER THE POLAR REGIONS

OGO - II SATELLITE, OCT., 1965 - FEB., 1966

$f(\theta) = f_1(\theta)$

$f(\theta) = f_5(\theta)$

○ HIGH SENSITIVITY

+ LOW SENSITIVITY

ALTITUDE, km

ION PAIRS/(cm³ sec atm)
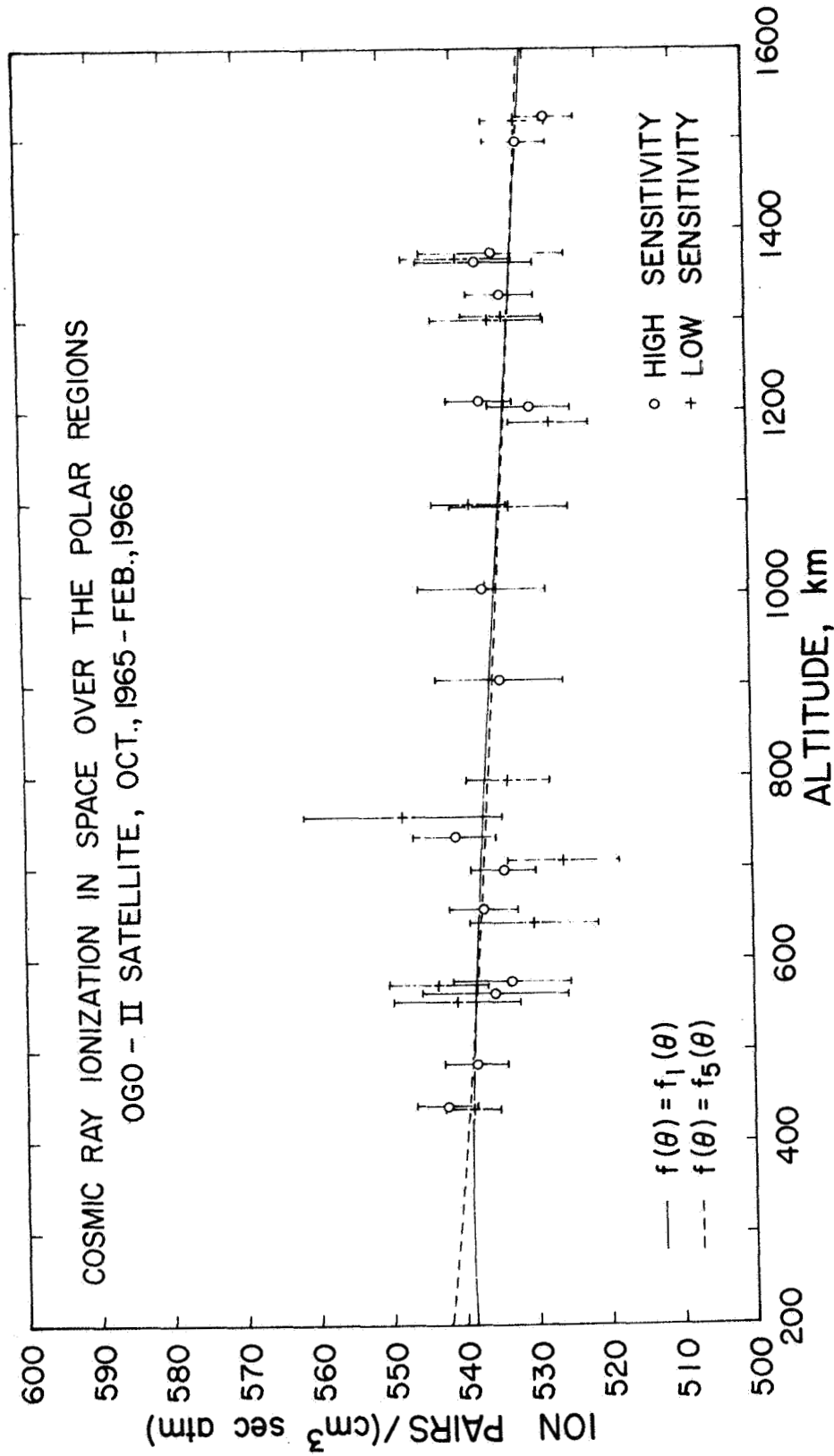
Figure 20

Plot of corrected ionization averages vs. altitude, where data have been divided by the geometrical solid angle of the sky, with top of atmosphere at 40 km. Curves show least squares fit to data according to Eq. 12.

111

ACTUAL COSMIC RAY IONIZATION VS.
ALTITUDE OVER THE POLAR REGIONS

A   GEOMETRICAL SOLID ANGLE OF SKY
B   PRIMARY COSMIC RAY IONIZATION
C   TOTAL COSMIC RAY IONIZATION,
    $f(\theta) = f_1(\theta)$
D   TOTAL COSMIC RAY IONIZATION,
    $f(\theta) = f_5(\theta)$

ALTITUDE, km
Figure 21
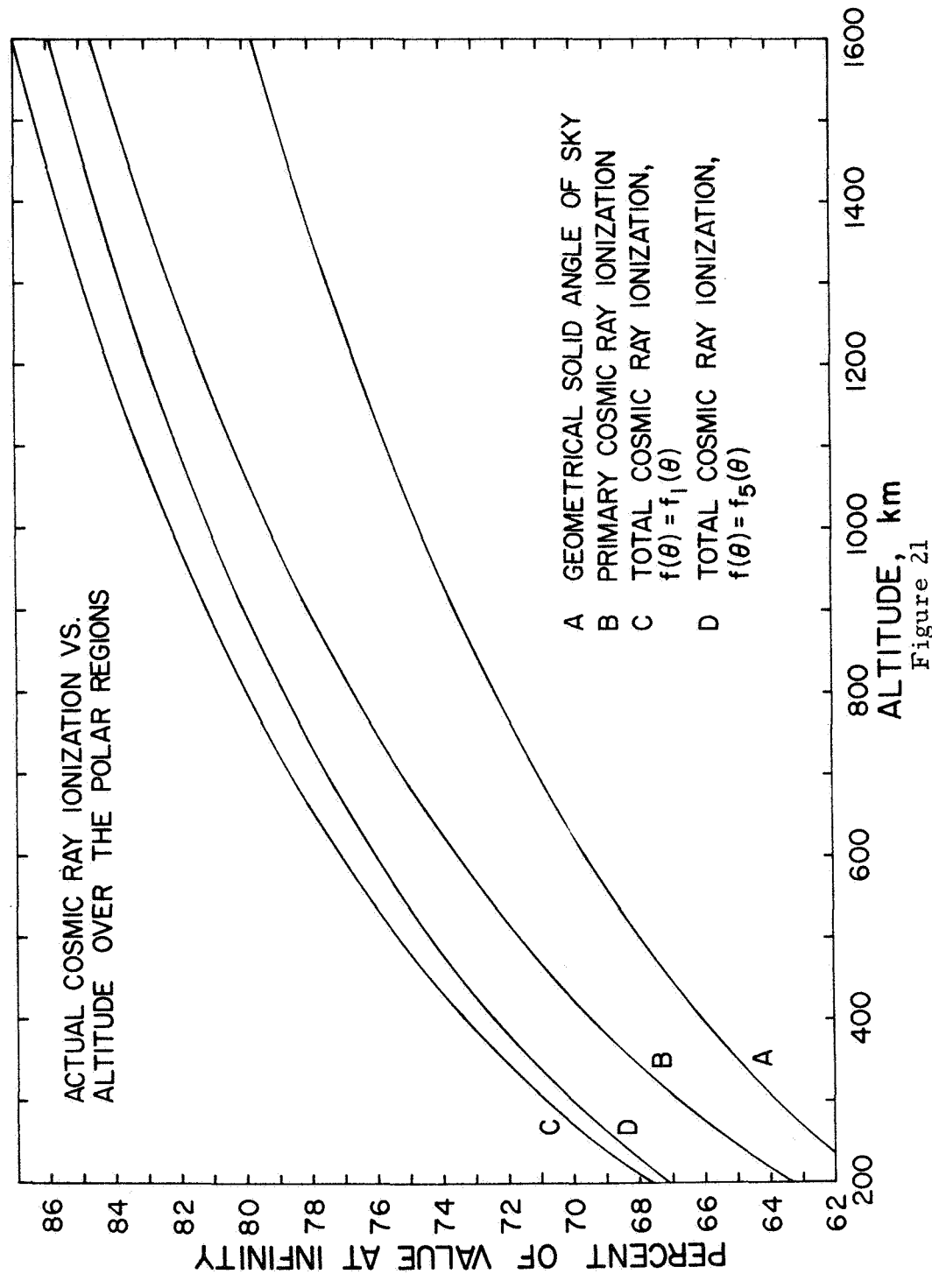
Ionization vs. altitude near the geomagnetic poles
See Table 8 for values at infinite altitude.

Their chief uncertainty was due to the fact that the measurements were not made simultaneously at the two locations. Their albedo contribution was such as to increase the ionization at the top of the atmosphere by 21 percent, which amounts to 17.6 percent of the total ionization. If we assume that the number of albedo particles remained the same between 1962 and 1965, while the observations show that the total ionization at the top of the atmosphere increased from 419 to 569 ion pairs/(cm^3 sec atm), we would predict a splash albedo contribution of 13.0 percent of the total ionization from their data, which is somewhat greater than the present result of 10.4 ± 2.3 percent. In terms of the absolute value of the albedo ionization, the Neher and Anderson value of 72 is to be compared to our result of 57 ± 13 ion pairs/(cm^3 sec atm). The reader should be reminded that in all these comparisons we have accounted for the different atmosphere used in previous Caltech publications and for the 3.5 percent difference in response of the balloon and spacecraft ion chambers to the cosmic radiation. Thus the figures quoted here might be somewhat different from those given in the references.

Similar balloon-space ionization data are available during the early portion of the flight of Mariner IV (23, 26), and in this case the balloon flights were made during the flight of the spacecraft. Here there was another difficulty, however. The slope of the ionization vs. depth curve over Thule became so steep at the upper end of the curve that it was impossible to extrapolate the ionization to the top of the atmosphere. Therefore no new albedo estimate was derived, but certain comparisons can be made with the POGO data.

The OGO-II data have been normalized to a cosmic ray intensity

typical for early November, 1965. According to the Deep River Neutron Monitor, the intensity was very nearly the same in late December, 1964, when Mariner IV was still close to the earth. At that time the Mariner IV ion chamber was fluctuating between 970 and 992, which is in excellent agreement with the OGO-II extrapolated I(∞) = 985 $\pm$ 6 ion pairs/(cm³ sec atm). Therefore we conclude that the OGO-II ionizations are consistent with the interplanetary results within the uncertainty that is caused by the fact that a neutron monitor is not always a good measure of the total ionization, since the spectrum of the cosmic rays can change in such a way as to change the total ionization while the neutron monitor remains unchanged. For example, on February 16, 1965 Mariner IV gave 994 ion pairs/(cm³ sec atm), about 1 percent higher than in late December, 1964, while the neutron monitor was about 0.4 percent lower. For a comparison with balloon results, we note that on February 16 the ionization at 2.2 gm/cm² over Thule reduced by 3.5 percent was 549 ion pairs/(cm³ sec atm). If we estimate the extrapolated value at 0 gm/cm², which we consider equivalent to 40 km altitude, to be 2 percent higher, and if we then take away 1 percent to account for the fact that Mariner was 1 percent higher on that date than in late December, we estimate that the value for I(40) in late December as predicted by the balloon measurement is 555 ion pairs/(cm³ sec atm). This compares favorably with the OGO-II value of I(40) = 550 $\pm$ 10 ion pairs/(cm³ sec atm). We conclude that the OGO-II ionizations are in good agreement with both balloon and Mariner IV results within limitations imposed by time variations and extrapolation problems.

It is also of interest to compare our absolute ionization, 57 $\pm$ 13

ion pairs/(cm^3 sec atm) for the splash albedo particles, with the fluxes
of upward moving particles measured by other observers. Using the
albedo proton spectrum measured at Fort Churchill, Canada by Wenzel
(41) in 1966, we calculate that his integrated flux from 10 to 500 MeV would
produce an ionization of 21 ion pairs/(cm^3 sec atm) in our instrument, with
negligible contribution from protons with energies greater than 500 MeV,
assuming the protons are isotropic over the lower hemisphere. Wenzel
repeated his experiment in 1967 and obtained the same differential spect-
rum within the limits of his errors. In the case of electrons, measure-
ments of upward moving electrons have been made by Israel (42) in 1967.
He reports 170 electrons m^{-2}sec^{-1}ster^{-1} between 12 and 1000 MeV. Again
assuming isotropy over the lower hemisphere, we calculate from this flux
8 ion pairs/(cm^3 sec atm), which, when added to the proton contribution,
gives a total of 29 ion pairs/(cm^3 sec atm). There are other contributions
that will increase this calculated ionization. 1) There is probably a sig-
nificant contribution due to electrons in the 1 to 10 MeV energy region.
Rice (43) has data on the daytime flux of return albedo electrons at Ft.
Churchill which show a steep increase in the electron spectrum toward
low energies. If we assume the splash albedo electrons to behave in a
similar manner, it seems reasonable to expect another 8 ions pairs/(cm^3
sec atm) due to these electrons, increasing our calculated ionization to
37 ion pairs/(cm^3 sec atm). 2) The angular distribution of the albedo
particles, especially the high energy electrons, may be peaked at large
angles from the vertical, so that the integrated flux is somewhat larger
than 2π times the flux per steradian measured within 31° or less of the
vertical in the experiments mentioned above. There exist data on the

angular distribution of albedo γ-rays, which may provide a clue to the electron situation. Measuring 100 to 500 MeV γ-rays from the earth on board the OSO-III satellite at an altitude of 550 km, Borken (44) found the γ-rays to be strongly peaked at the horizon, so that the total flux was about a factor of 3 more than 2π times the flux per steradian in the vertical direction. The photons in the peak had generally higher energies than those coming from near the vertical. Let us now assume that the electrons behave similarly to the γ-rays, and we multiply the 12-1000 MeV electron ionization contribution by 3 while we let the low energy electrons and the protons remain isotropic. Then we get another 16 ion pairs/(cm³ sec atm) to add to our calculated value. 3) Muons have not been considered. They will be present at balloon altitudes, but almost all of them will have decayed before reaching the satellite altitude. Some of the decay electrons will re-enter the atmosphere and thus not appear at all in the POGO ion chamber; so that here we can argue that the ionization at the top of the atmosphere should in fact be slightly higher than what is estimated by extrapolation downward from satellite altitudes. Perhaps this is sufficient to explain the somewhat higher albedo from the balloon-Mariner II result in comparison to the OGO-II result. When all the above facts are accounted for, our calculated albedo ionization will probably be slightly greater than 53 ion pairs/(cm³ sec atm). The OGO-II result of 57 ion pairs/(cm³ sec atm) therefore appears to be consistent with the present knowledge of the fluxes of splash albedo protons and electrons.

Murayama's fractional albedo extrapolated to balloon altitude is 29 ± 5 percent, considerably higher than the Neher and Anderson result

or the OGO-II result. There are two reasons why this should be so. First, his instrument had a non-negligible response to γ-rays; second, his measurements were made in 1961, when the fractional albedo probably was higher than in 1962. We might add that his result is based on comparing the numbers of particles, not the ionization, so the two values should not be expected to be the same. However, if Murayama had used an altitude dependence for the albedo particles similar to the one we used with $f(\theta) = f_5(\theta)$, he would have obtained a lower result, about 14 percent at 165 km and 23 percent at the top of the atmosphere.

To get an idea of how the fraction of albedo particles should compare with the ionization albedo, assume that all of the 57 ion pairs/(cm^3 sec atm) except the proton contribution is due to minimum ionizing particles, which means we have 12 times as many of these as protons. We get an equivalent omni-directional flux of 0.558 cm^{-2}sec^{-1}. For the primary cosmic rays we take the average of the values from the 1965 latitude survey and from Mariner IV (45), 4.15 cm^{-2}sec^{-1} at infinity. This corresponds to a fractional albedo of 21 percent for particles which can penetrate 0.2 gm/cm^2, probably somewhat of an overestimate but still considerably higher than the ionization albedo of 10.4 percent.

The ionizations observed on OGO-IV were strongly variable in time, probably due to solar particle fluxes. During revolutions 128-160, however, the ionization fluctuations appeared to be small, and the data for that period, August 6-8, 1967, were analyzed in the same way as the OGO-II data. Corrections for spacecraft radioactivity amounted to only a few ion pairs/(cm^3 sec atm). The two averages for $I/\Omega(h)$ obtained were 402.7 $\pm$ 2.2 ion pairs/(cm^3 sec atm) at 461 km altitude over the

North Pole and 400.9 ± 2.6 ion pairs/(cm³ sec atm) at 875 km over the South Pole. These were high sensitivity data and therefore might be subject to the limitations previously discussed, although there was no eclipse of the spacecraft during this period. From the two averages we derive values of 407 ± 20 and 740 ± 16 ion pairs/(cm³ sec atm) for I(40) and I(∞), respectively, and a fractional albedo of 9 ± 7 percent of the total ionization, based on the use of $f_5(\theta)$ for the angular distribution of the albedo particles. This albedo is rather low in the light of the comparisons previously made, but we do not attach very much significance to it because of the large standard deviation.

Some of the 1967 balloon flights at Thule were made within two hours of a pass of OGO-IV near the North geomagnetic pole. The balloon flights indicated that the ionization over Thule in 1967 was very nearly the same as in 1962, when the extrapolated value at the top of the atmosphere was 419 ion pairs/(cm³ sec atm). The above I(40), when multiplied by 1.035 to make it compare properly with balloon data, is 421 ion pairs/(cm³ sec atm), in excellent agreement. However, the value for I(∞) = 740 ion pairs/(cm³ sec atm) does not agree with the Mariner II result of 668 ion pairs/(cm³ sec atm). The 1967 balloon data have not yet been published and further comparisons with the OGO-IV data will be left for a later paper.

Other POGO Ion Chamber Observations

A. The Ionization at Low Latitudes.

The analysis of the dependence of the ionization on altitude, or alternatively on latitude for constant altitude, at low or middle latitudes becomes much more complicated than what we have just done for the polar regions. One must first integrate trajectories to determine the solid angle of the allowed cone as a function of altitude and primary energy. At each altitude it is then necessary to integrate over all energies above the Störmer cutoff, folding in the charge and energy distributions of the cosmic rays according to the response of the ion chamber. If we knew all of these things except the energy spectrum, it would be possible to derive the spectrum by fitting experimental data.

The albedo situation is also more complex. We now have to worry, in addition to splash albedo, about return albedo, which is due to splash albedo particles from one hemisphere spiraling along magnetic field lines and re-entering the atmosphere in the opposite hemisphere. More precisely, we have to consider albedo particles which come from each of the two areas in which the field line through the point of observation intersects the atmosphere. The effective size of the albedo production areas for a given observation point thus increases with increasing energy of the albedo particles. Near the equator the high energy part of the return albedo will be due to returning particles which have been locally generated. Ray (46) has done some calculations on the intensity of return albedo particles, and these have been improved by Wenzel (41). The calculations which are necessary for the complete analysis of the

ionization intensity would require a very large effort and are beyond the scope of the present work. We shall be content to describe the observations and suggest things that can be done with them.

For observations of galactic cosmic rays with the POGO ion chambers we are limited to the high sensitivity data, since the time resolution in low sensitivity is too poor at the low radiation levels involved. Thus we are subject to the limitations which have already been discussed concerning the high sensitivity data. Even in high sensitivity the data points near the cosmic ray equator are separated by the order of 10 degrees of latitude. We cannot average the data over a large geographical area as we did with the polar data because each position is different. Thus any kind of analysis must deal with a very large number of individual data values. Mistakes in the data of the type discussed for the polar data will be much more difficult to recognize, since we are no longer dealing with nearly constant Δt's. The problem of spacecraft radioactivity will also be more difficult. The best way to handle that will probably be to use the results for the preceding and succeeding polar passes in order to interpolate the correction as a function of latitude. The relative errors that result will be the order of five times those for the polar data, so that we cannot expect to be able to work with very high precision.

All of the high sensitivity data have been plotted as a function of geographic latitude, which does not necessarily provide the best representation of the data but has the advantage that the spacecraft altitude can be expressed as a function of geographic latitude that changes slowly with time only (see Fig. 12). As an alternative, Dr. Anderson at Rice University has plotted the data vs. invariant latitude (see Eq. 8), which is

especially useful for trapped radiation studies. As an example of what can be done with the geographic plots, we select the arbitrary position 10°N, 40°E, where the vertical cutoff rigidity is 16.03 BV, essentially on the cosmic ray equator. We read off the ionization at 10°N latitude for consecutive orbits which bracket 40°E longitude. Then a linear interpolation is made to get the ionization at the desired position. Going through all of our plots we determine values in this way for many different altitudes. The results are plotted as a function of altitude in Fig. 22. The curves have been drawn by eye only to indicate the general run of the data; they are not analytical fits. The OGO-IV curve has been drawn with exactly the same shape as, but 30 ion pairs/(cm³ sec atm) lower than, the OGO-II curve. Most of the difference is probably due to spacecraft radioactivity on OGO-II, but some of it may be due to increased solar modulation of the cosmic rays in 1967 over the 1965 level. Plots of ionization vs. V_3 rate of the type shown in Fig. 15 show much less hysteresis for the OGO-IV data than was the case for OGO-II, which means there should be very little or no radioactivity present at low latitudes in the case of OGO-IV. Perhaps the data indicate that the two curves in Fig. 22 should diverge slightly as one goes to lower altitudes. This is reasonable, since at the lower altitudes OGO-II was higher on the other side of the earth, going through more trapped radiation and accumulating more radioactivity.

Also shown in Fig. 22 is a rough plot of the data obtained from a balloon flight in 1965 off the coast of Peru (1) where the vertical cut-off rigidity is 13.53 BV. The balloon data have been divided by 1.035 in order to make them comparable with the satellite data. This particular balloon flight reached 3 gm/cm²; thus it is easy to extrapolate the curve to the
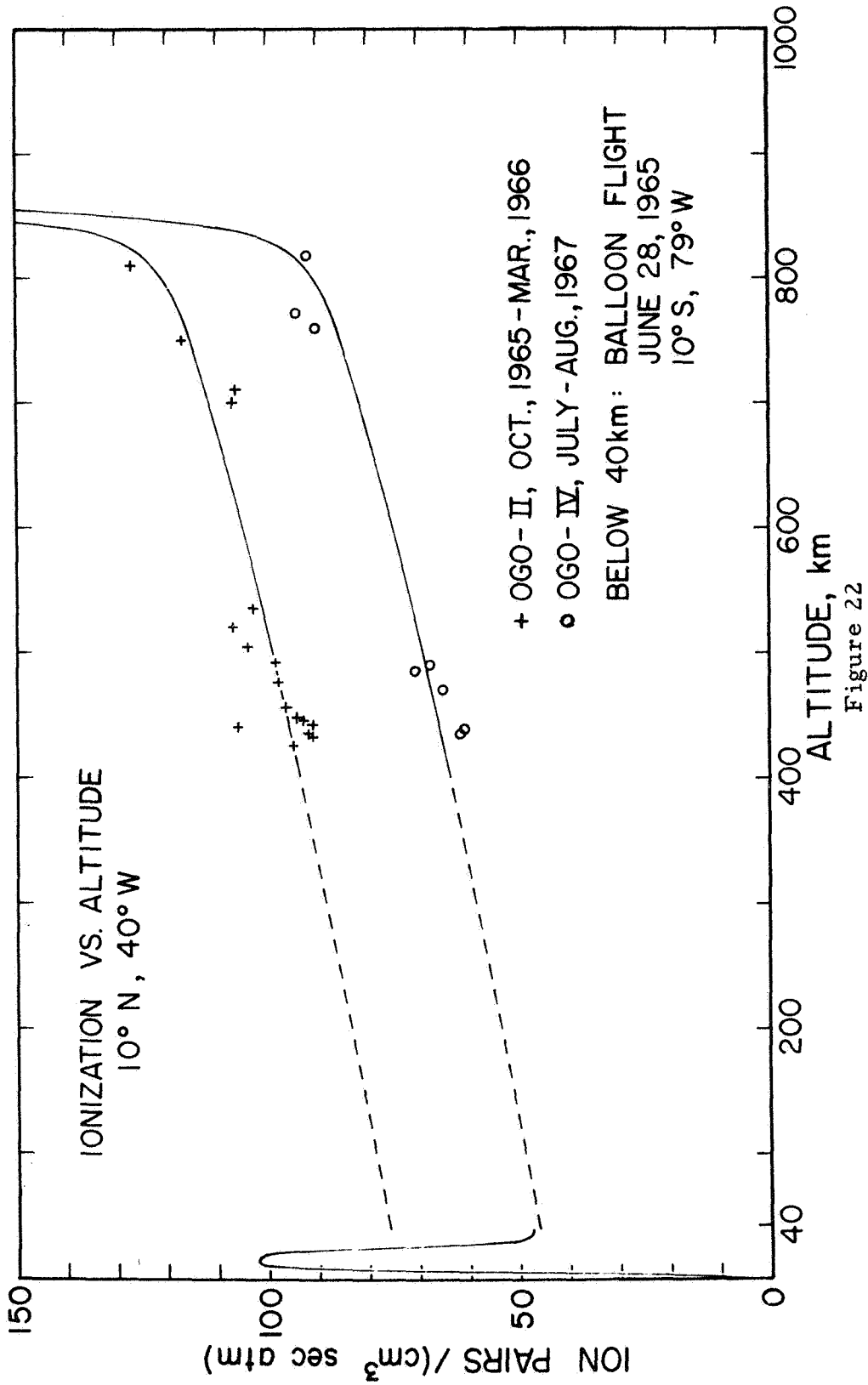
Figure 22

Example of ionization vs. altitude for position near the cosmic ray equator.
Curves are identical except for separation by 30 ion pairs/(cm³ sec atm).

top of the atmosphere, obtaining 48 ion pairs/(cm³ sec atm). At the
location of the satellite data this will be lower, say 40 ± 3 ion pairs/(cm³
sec atm) based on extrapolation of data at lower rigidities, due to the
increased cut-off rigidity. We believe the satellite data, if it could have
been measured to lower altitudes, would have been found to be in good
agreement with the balloon data.

The ionization vs. altitude curve at 10° N, 40° E turns up sharply
above 800 km, where the trapped radiation belt is entered, and rises
quickly to greater than 2×10^6 ion pairs/(cm³ sec atm) at 1400 km altitude.
At 10° S, 79° W, where the balloon flight was made, the radiation belt is
entered at 500 km altitude. That is why we have not tried to compare the
balloon results with satellite data measured over the same position.

B. The Cosmic Ray Knee.

The cosmic ray knee, definition, measurement, and interpretation
thereof, has been discussed at length by Neher (1, 47, 48) with regard to
cosmic ray latitude surveys made in the atmosphere with balloons. In
the case of satellite observations above the atmosphere, the knee may
manifest itself differently, or it may not exist at all as a sharp transition
according to his definition. In our situation with the POGO data, we can-
not observe the knee directly because of the presence of the outer trapped
radiation belt, which always masks the cosmic ray data near the knee
position, as is illustrated in Fig. 12. However, it is easy to define the
knee position for satellite observations in the following way. Suppose we
extrapolate both the mid-latitude and polar plateau parts of the ionization
vs. latitude curve, as illustrated in the low-latitude half-orbit of Fig. 12,

under the outer radiation belt until they intersect. The point of inter-
section is then taken to be the knee position. In practice the mid-latitude
extrapolation is done by eye and usually extends over only two or three
degrees of latitude. The polar extrapolation runs over a longer distance,
but it can be done accurately because we can base it on our computed
polar ionization average, taking proper account of altitude variations.
The geographic position of the satellite knee as found in this way is
shown in Fig. 23 for a block of OGO-II data, Orbits 74-110. In the case
of the Southern Hemisphere, we can only determine the knee for about
half the longitudes, because the inner trapped radiation belt covers the
mid-latitude part of the cosmic ray curve at the other longitudes. In
order to account for changing spacecraft altitude, the points in Fig. 23
actually denote the position where the magnetic field line through the
observed knee intersects the surface of the earth. Whether or not this
is the same knee that is observed at balloon altitudes, it ought to deter-
mine a characteristic position in the earth's magnetic field and is there-
fore worthy of study.

Before continuing with the observations on the cosmic ray knee
position, let us review very briefly the current picture of the magneto-
sphere and how it relates to our data. Figure 24 shows the configuration
of the geomagnetic field lines in the plane of the magnetic dipole and the
earth-sun line according to the model of Williams and Mead (49). In our
discussion of the polar ionization plateau we have already mentioned the
geomagnetic tail, open field lines, and the predicted zero geomagnetic
cutoff rigidity along these lines. We see immediately from the figure
that the closed field lines extend to higher geomagnetic latitudes on the
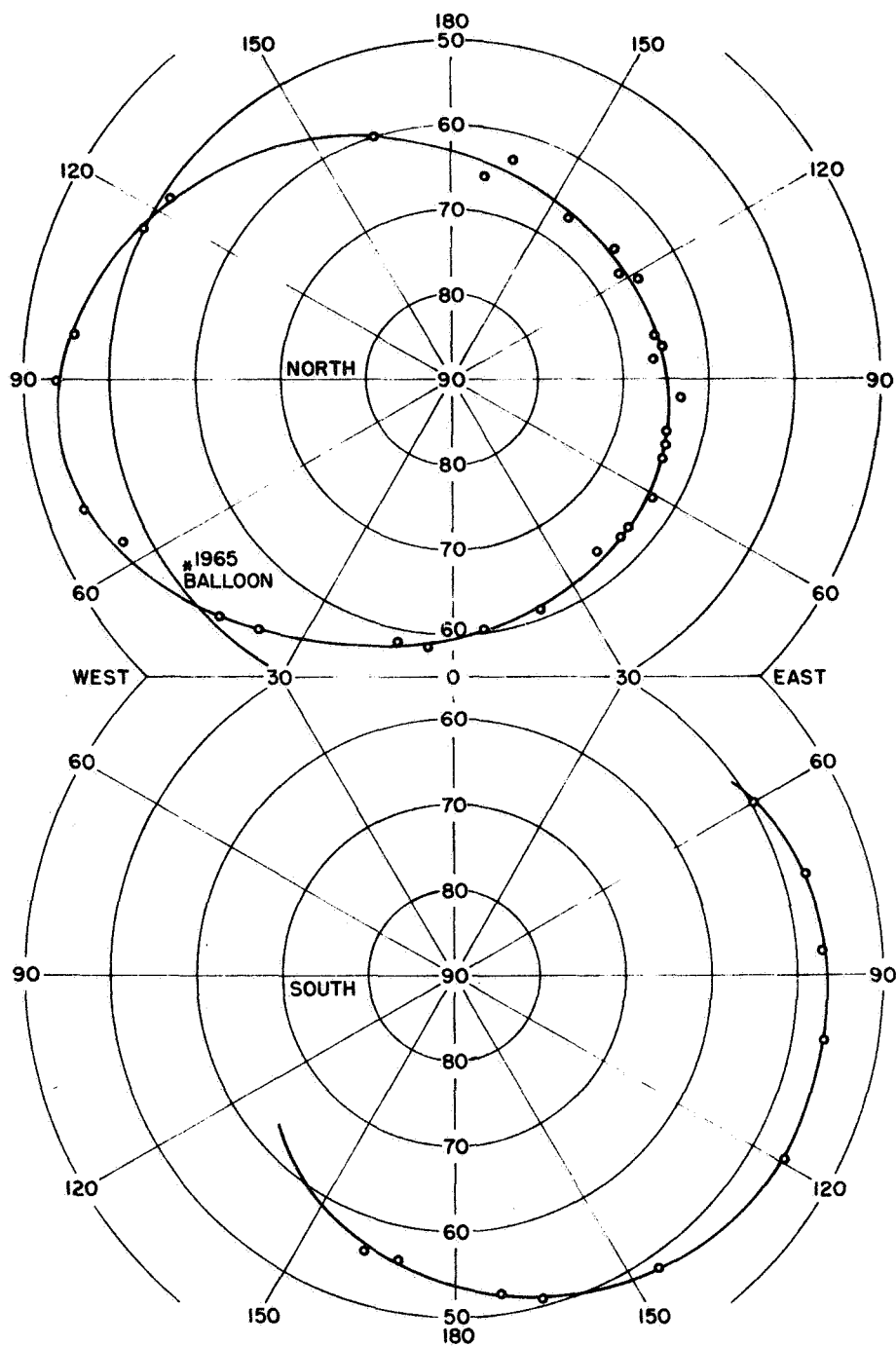
Figure 23

Geographic location of cosmic ray knee at 700 km altitude.
OGO-II Revs. 74-110, Oct. 19-22, 1965.
The solid line has been drawn through the data by eye;
it is not an analytical fit.
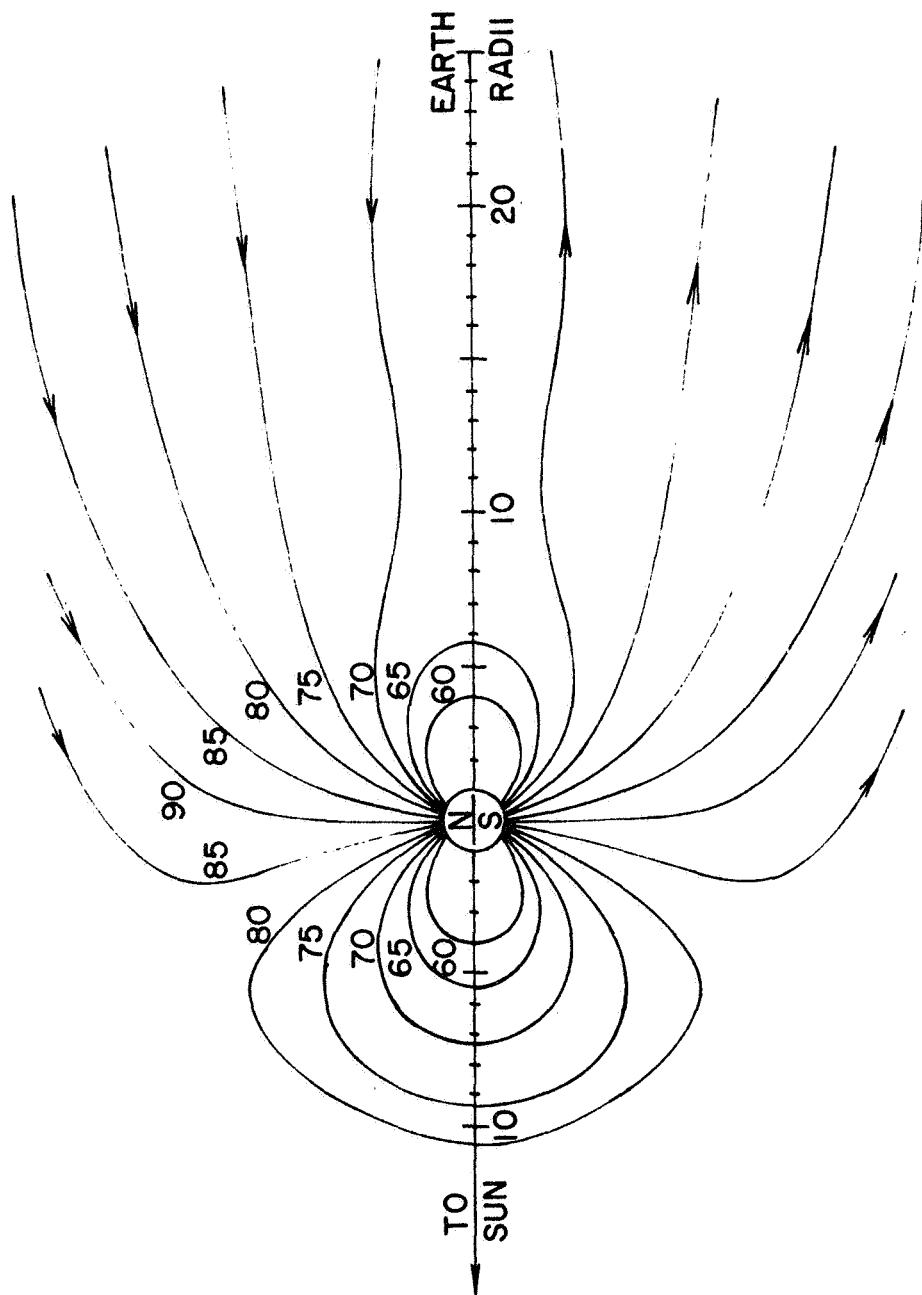
Figure 24

Configuration of geomagnetic field lines.

Lines are labeled with the geomagnetic latitude at the point of intersection with the earth.

daytime side of the earth than on the night side. The observational con-
sequence of this fact is a diurnal variation of the geomagnetic cutoff
rigidity at a given point of observation, which was first suggested by
Reid and Sauer (50). The variation will be quite significant at 70° geo-
magnetic latitude and will be small or nonexistent at 60° and below.
Such expectations are verified in calculations of particle trajectories
done by Gall, Jimenez, and Camacho (27). Among the first experimental
observations of direct relation to the theory is the work of Stone (51).
Many other observations have been made since that time, generally
dealing with protons and electrons of energies between 1 and 500 MeV.

An equivalent expression of the theory is the diurnal movement,
toward and away from the geomagnetic poles, of the position associated
with a particular physical cutoff phenomenon. However, since the L
values are calculated for a static, internal field line model and therefore
form a coordinate system which is fixed in the earth, we will observe
characteristic geomagnetic phenomena to occur at different values of L
for different times of the day, generally higher L during the day, lower
L during the night. The cosmic ray knee is such a cutoff related feature
and therefore should be expected to remain independent of L in the
internal case, but in reality we might expect the knee position to show a
small diurnal variation in L. The results of Gall, Jimenez, and
Camacho (27) indicate a shift of about one degree of latitude between
noon and midnight for the position of the cutoff for 500 MeV protons, near
L = 5. We will be interested in typical L values of 3.6, which corres-
ponds to an invariant latitude of 58° and a geomagnetic cutoff rigidity of
1.2 BV, considerably higher than the applicable value for other observers.

Anderson and Hudson at Rice University are doing a similar analysis for the high latitude boundary of the outer radiation belt, near $L = 7$. Hereafter we will talk about positions in terms of invariant latitude, which is calculated from the L parameter by use of Eq. (8).

We return now to the data. Only high sensitivity data can be used; the low sensitivity data do not provide sufficient time resolution to allow us to draw a smooth curve. Four possible knee positions can be observed for each complete orbit of data, but usually trapped radiation in the mid-latitude region obscures one or more of them, especially at the higher altitudes. Hereafter the notations NN, NS, SS, and SN will be used to denote, respectively, the North Pole, northbound approach; North Pole, southbound departure, etc.

The data were divided into groups of orbits, very much as was done for the analysis of the polar averages. The spacecraft altitude and local time at a given latitude changed very little for each group of orbits, and the average values were used for the whole group. Experiment 5008 data were used to rule out from the analysis all observations where any trapped radiation was present within 20° latitude below the sharply defined low-latitude edge of the outer radiation belt. We then evaluated the average invariant latitude of the knee position for each of the four positions and associated with each the proper altitude and local time. Thus we averaged over all longitudes. No recognizable longitude dependence was found for the knee positions. Geographic local times were used. We should really evaluate the local time with respect to the geomagnetic dipole axis, but for the invariant latitudes under consideration the two times differ by 1.6 hours or less and average to zero over all longitudes, so we did not believe

it to be worth the trouble to make the conversion. We could always go back and do it if a large diurnal variation were found. The average knee positions found in this way are summarized in Table 9.

At this point it seems appropriate to add a few comments concerning the extrapolations that have been made in order to find the knee positions. The extrapolation from the polar region was based on the computed polar ionization average over the 30 to 40 degrees of the polar plateau. The ionization vs. latitude line, which would be flat if the spacecraft altitude were not changing, was then given a small slope to account for the changing altitude. The slope was calculated from the change of the geometrical solid angle, which we have already shown to be a good first approximation to the ionization intensity vs. altitude. The polar plateau level was thus extrapolated the order of 10 degrees under the outer radiation belt. The extrapolation from the mid-latitude region usually only two or three degrees of latitude, and we always used orbits where we had at least 20 degrees of good data, free of trapped radiation, below the radiation belt. Since the distance to be extrapolated was therefore short, we felt that it was sufficient to do this extrapolation by "eyeball fitting" a smooth curve, which turned out to be nearly straight, to the data. The mid-latitude extrapolation depends on there being no abrupt change in slope of the galactic part of the ionization curve in the region of the extrapolation. If in fact that happens, then the knee as we have defined it is not necessarily indicative of a particular cutoff rigidity.

There is a possibility that some of the Greenwich times that NASA has attached to the ionization are erroneous. Such errors cause the relevant orbit data to be shifted with respect to the ionization which

Table 9

Knee Positions	NN	NS	SS	SN
		OGO-II		
Revs. 74-110				
# observations	7	20	8	0
Inv. latitude	57.3 ± 0.3	58.5 ± 0.2	57.8 ± 0.4	
Altitude, km	960 ± 180	480 ± 90	900 ± 160	
Local time	17:20 ± :16	5:00 ± :16	5:20 ± :16	
Revs. 379-444				
# observations	11	8	1	2
Inv. latitude	58.6 ± 0.4	57.8 ± 0.4	54.9 ± 1.0	54.8 ± 0.4
Altitude, km	470 ± 130	530 ± 170	1440 ± 160	1360 ± 190
Local time	15:20 ± :21	3:00 ± :21	3:20 ± :21	15:00 ± :21
Revs. 574-703				
# observations	10	2	0	3
Inv. latitude	57.6 ± 0.6	56.9 ± 0.8		57.4 ± 0.9
Altitude, km	460 ± 230	930 ± 340		940 ± 340
Local time	13:50 ± :34	1:30 ± :34		13:30 ± :34
Revs. 1201-1279				
# observations	0	0	2	7
Inv. latitude			58.2 ± 0.8	58.5 ± 0.3
Altitude, km			450 ± 130	540 ± 190
Local time			21:50 ± :24	9:30 ± :24
Revs. 1372-1466				
# observations	0	8	13	2
Inv. latitude		56.5 ± 0.6	57.0 ± 0.2	55.9 ± 0.7
Altitude, km		890 ± 280	480 ± 180	980 ± 290
Local time		20:10 ± :27	20:30 ± :27	8:10 ± :27

Table 9 - cont'd.

Knee Positions	N N	NS	SS	SN
Revs. 1516-1564				
# observations	0	7	5	0
Inv. latitude		58.1 ± 0.6	57.0 ± 0.2	
Altitude, km		750 ± 190	550 ± 140	
Local time		19:40 ± :18	20:00 ± :18	
Revs. 1613-1648				
# observations	0	7	6	0
Inv. latitude		57.3 ± 0.6	56.2 ± 0.5	
Altitude, km		600 ± 130	680 ± 140	
Local time		19:10 ± :16	19:30 ± :16	
Revs. 1742-1824				
# observations	4	7	0	0
Inv. latitude	57.2 ± 0.2	58.4 ± 0.3		
Altitude, km	840 ± 240	440 ± 100		
Local time	6:20 ± :23	18:00 ± :23		

OGO-IV

Revs. 128-160				
# observations	9	14	7	2
Inv. latitude	57.1 ± 0.5	57.4 ± 0.3	55.7 ± 0.7	57.2 ± 0.4
Altitude, km	560 ± 50	420 ± 10	760 ± 50	920 ± 10
Local time	18:00 ± :19	5:10 ± :19	6:00 ± :19	17:10 ± :19

Note: The figures after the ± sign denote standard deviations in the case of invariant latitude and range over which values were averaged in the cases of altitude and local time.

results in the knee position being shifted up or down in latitude depending
on the direction of satellite motion and the sign of the time error. Hudson
and Anderson (private communication) have investigated this problem at
Rice University and have passed along their estimated corrections to this
author. The worst case involved a latitude shift of 1.8 ± 0.6 degrees for
orbits 572-703. These corrections have already been applied to the data
in Table 9.

When we plot invariant latitude of the knee position vs. altitude,
as is done in the upper portion of Figure 25, we get a surprising result.
The knee latitude moves lower as we go to higher altitudes. This cannot
be a systematic effect due to trapped radiation at higher altitudes, since
we have already eliminated those passes where trapped radiation is
present, except for the well-defined outer belt. Nor should we expect
the geomagnetic cutoff to change with altitude, since that depends only on
the invariant latitude. Therefore we interpret the variation with altitude
to be a shadow phenomenon. Probably the best trajectory calculations
for cosmic rays arriving at observation points well above the atmosphere
have been done by Kasper (52). Qualitatively, his calculations show that
for a given altitude and particle rigidity, the cone of allowed trajectories
tends to increase as the observation point moves from the polar region
toward lower latitudes until the cutoff point is approached, where, of
course, it rapidly decreases. This effect is more pronounced for higher
altitudes. Figure 26 is a schematic which illustrates the shape of the
intensity vs. latitude curve for two altitudes and two rigidities, but only
in a qualitative way. Thus the ionization will increase with altitude
faster below the knee than above the knee, and the observational result

Figure 25

Position of cosmic ray knee.
Upper: invariant latitude vs. altitude.
Middle: deviation from altitude curve vs. local time.
Lower: same as middle but after correction for North-South effect.

INVARIANT COLATITUDE
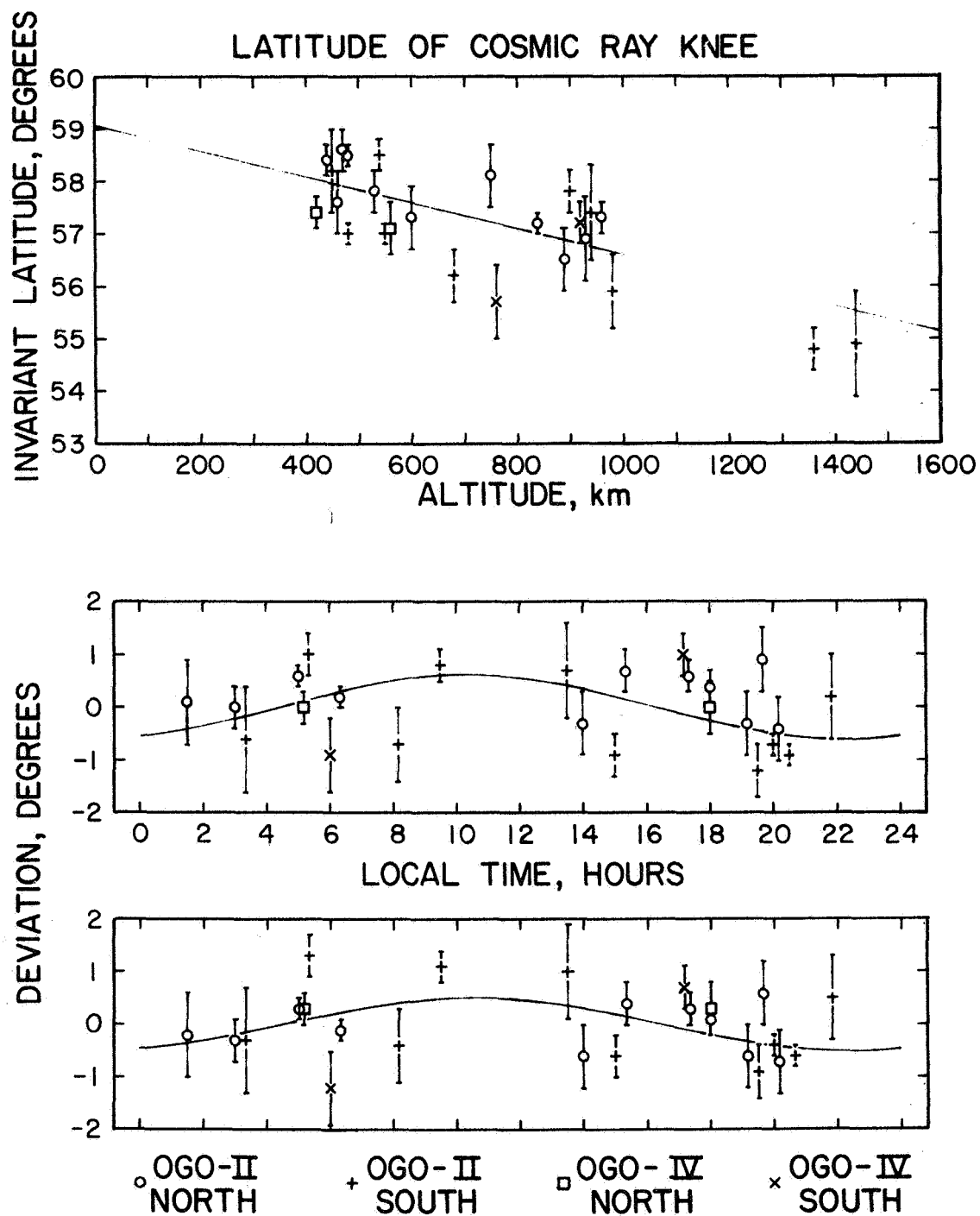
Figure 26

Intensity vs. latitude for rigidities $P_1 < P_2$ and altitudes $h_1 < h_2$.

A: P_1 at h_1. B: P_1 at h_2. C: P_2 at h_1. D: P_2 at h_2.

The relative intensities at high latitudes have no significance; we only want to show the effect of altitude on the intensity near the cutoff point relative to the polar level.

will be a movement of the knee toward lower latitudes at higher altitude.
We do not have to worry about what happens exactly at the knee, since we
cannot see that part of the curve. The variation of the knee position with
altitude has not been mentioned by other observers. However, if we look
at Murayama's plot of counting rate vs. vertical cutoff rigidity (37) and
use our extrapolation technique to find the knee, we find that the altitude
effect is indeed there. The location of the northern knee corresponds
roughly to $L = 3.05$ at nearly 200 km altitude, and the southern knee is
at $L = 2.80$ at 500 km. His data also indicate that the knee is not sharp
according to our definition but is somewhat rounded. This fact does not
alter our conclusion, however, since we are really interested not in the
shape of the knee but in the location of a characteristic position in the
geomagnetic field. Murayama's knee positions, measured in 1961, are
farther away from the poles than our 1965-66 positions, but we attribute
that to the stronger influence of the solar activity in 1961 on the cosmic
rays.

Seward and Kornblum (53) also used data from some of the 1961
Air Force satellites to measure knee positions from polar orbit, but they
claim to define it somewhat differently than Neher (47) and thus call it
the "edge". However, their definition for the "edge" is exactly the same
as what we have used for the definition of the "knee" in this report when
considering satellite data, so we assume the two words can be used inter-
changeably. They give geographic polar plots which show their knee
positions to be approximately 5 degrees farther from the pole than those
in our similar plots in Figure 23. The difference in position is again
attributed to the increased level of solar activity in 1961 and is compatible

with shifts observed by Neher with balloons. From Solar Maximum in 1958 to Solar Minimum in 1965, Neher observed the knee to shift from 56° to 63° geomagnetic latitude at 5 gm/cm^2 atmospheric depth, a difference of 7 degrees (1,47). Seward and Kornblum observed a longitude dependence for their knee positions which we do not observe in the POGO data except for a tendency to be one or two degrees higher near the Greenwich Meridian in the Northern Hemisphere. They look for local time effects and find the knee positions to be the same at noon and midnight, but the flux vs. L curves have different shapes between the knee (L $\simeq$ 3) and the polar plateau (L $\simeq$ 9). However, in their flux vs. L curves at two different altitudes (300 and 1000 km) we again see the difference in knee position that appears in Murayama's and our own data, but no specific mention is made of this fact. They finally proceed to talk about the altitude dependence of the flux over the polar regions, but their discussion is not nearly as detailed as the one given in this paper.

In the absence of a more detailed theory, we choose to fit the knee latitude vs. altitude data with a least squares straight line, which turns out to have a slope of -0.0025 degrees/km and is shown in Fig. 25. The line fits the OGO-II points only; the four OGO-IV points are then found to average 0.6 degrees below the line, in the right direction to be consistent with the increased solar activity at the time of the OGO-IV measurements.

The points in Fig. 23 have been shifted according to this altitude dependence in order to correspond to an altitude of 700 km. Also shown in Fig. 23 is the position of the knee as observed by Neher in the 1965 latitude survey (1), very close to 52° N, 55° W. The balloon observation is 3.5° closer to the pole. About half of this difference is accounted for

by the difference in altitude. The remainder must be due to return albedo particles which cannot penetrate to balloon altitude (~ 5 gm/cm^2 atmospheric depth) but can be observed by the satellite in the upper mid-latitude region.

We are now ready to look for a local time dependence in our knee positions. To do this the deviation $\Delta \Lambda$ of each point from the knee latitude vs. altitude line is plotted vs. local time, as is shown in the second plot in Fig. 25. It is not obvious to the eye that any local time dependence exists. However, in order to be more objective, we will make a least squares fit to the simplest possible periodic function of local time

$$\Delta \Lambda = A \cos \left[\frac{\pi}{12} (t + t_0) \right] , \qquad (27)$$

where A is the amplitude of the oscillation, t is the local time in hours, and t_0 is a possible phase shift. We find A = -0.6 degree, t_0 = 1.7 hours, but the fit is rather poor. When we draw in the curve in the second part of Fig. 25, we find that most of the North points are above the curve and the South points tend to be below the curve. Therefore we find a North-South effect, which can possibly be interpreted as a seasonal variation. The OGO-II data were all obtained during the four months centered on Northern Hemisphere winter. Therefore it is suggested that the field lines get pushed slightly away from the pole during summer and toward the pole in winter by 0.3 $\pm$ 0.2 degree. The OGO-IV results show no North-South effect, but only four data points are involved.

Next we shift the points by 0.3 degree in the appropriate direction to eliminate the North-South effect and make a new plot of $\Delta \Lambda$ vs. local

time, which is given in the lower graph of Fig. 25. The fit is somewhat better than before, but the remaining scatter in the data points plus the scarcity of data near noon and midnight lead us to place rather conservative error limits on the results. We present

$$A = -0.5 \pm 0.4 \text{ degree},$$

$$t_0 = 1.4 \pm 1.0 \text{ hours}$$

as our best values for the local time variation of the knee position. In other words, we can just barely detect an oscillation of the knee position with an amplitude of the order of half a degree, the knee moving closest to the pole about 1.4 hours before noon and farthest away 1.4 hours before midnight. Of course the sinusoidal variation is not necessarily the best representation of the diurnal effect, but our data do not warrant searching for a more accurate theory. It is probably not possible to detect such a small shift in the data of Seward and Kornblum (53), so it is easy to understand why they reported no diurnal variation at all for the knee position. In fact, any variation which may apply to their data is probably smaller than what we have found, because their measurements were made at lower invariant latitudes.

In order to estimate the effect on the above results if the altitude dependence of the knee position were non-linear, the analysis was repeated with the inclusion of a quadratic term in the Λ vs. altitude fit, which gave a concave-downward curve. The quality of the fit was not significantly better except that the two points near 1400 km were much closer to the curve. The results were:

North-South shift = 0.2 degree (from average),

$$A = -0.5 \text{ degree},$$

$$t_0 = 1.2 \text{ hours}.$$

These are not significantly different from the values that we obtained with the linear altitude dependence, which the author considers to be the better results because of the following reasons. 1) The linear altitude dependence is the simplest possible fit that we can make to data that scarcely justify a higher order fit. 2) The extrapolated Λ at the top of the atmosphere is 57.6° for the quadratic fit, which disagrees with the balloon results (shown in Fig. 23) more than the 59.0° obtained with the linear fit. 3) It is hard to justify a slope for Λ vs. h which falls off more steeply at higher altitudes, as the quadratic fit predicts. In fact, we may even expect the curve to become less steep at altitudes sufficiently high that the earth shadow cones become small.

Finally, in order to check for possible systematic effects due to the distribution of altitudes and local times, we can make a scatter plot of local time vs. altitude using the values in Table 9. For a given altitude range the data points are found to be essentially randomly distributed in local time, except for the relative absence of points near noon and midnight.

Summary

Initial efforts toward analysis of the POGO ion chamber data concentrated on obtaining plots of ionization vs. latitude and averages of the ionization over the polar regions. It was found that radioactive isotopes were being produced on board the spacecraft during passes through high trapped proton fluxes. We could then observe fluctuations in the ion chamber data due to the radioactive decay of those isotopes whose half-lives are of the order of a fraction of the orbital period. In the case of the polar regions the radioactivity contribution to the ion chamber was estimated by comparing the ionization fluctuations with the V_2 detector rate of Experiment 5008. No such corrections have been determined for the low and middle latitude parts of the ionization data.

In order to account for time variations, the polar ionization averages were plotted vs. the data from the University of California IMP-III ion chamber outside the magnetosphere. A good fit was obtained for the low sensitivity polar averages, but the high sensitivity data did not fit well, a fact which is attributed to systematic effects on the high sensitivity calibration due to temperature variations and other possible causes. We found that significant discrepancies exist among the relative changes that occur in the galactic cosmic radiation as measured by the ion chambers of different observers, a problem that probably cannot be resolved without a coordinated effort among all the observers involved. All the polar ionization data, after correction for spacecraft radioactivity, time variations, and temperature effects, were assembled into one plot of ionization vs. altitude. From the expected altitude dependence of the

primary and splash albedo components of the ionization, we made a least squares fit to the data. By extrapolating the curve to 40 km altitude, the effective thickness of the atmosphere which was used by Murayama, we estimate that in 1965 the splash albedo particles contributed 10.4 ± 2.3 percent of the total ionization at the top of the atmosphere. This value for the fractional albedo depends, although not very sensitively, on what function we assume for the angular distribution of the albedo particles at the top of the atmosphere. It is somewhat lower than other results that have been reported for albedo particles but not significantly inconsistent with them if we consider how the various measurements were made and how the data were analysed. Most of our comparisons with other measure-indicate that the absolute flux of albedo particles does not change nearly so much as does the primary radiation under the influence of the solar modulation.

The absolute ionization measured by OGO-II, when extrapolated to the top of the atmosphere, is consistent with balloon results near the geomagnetic North Pole with due regard for time variations in the cosmic rays. When extrapolated to infinite altitude it agrees with the ionization in interplanetary space as measured by a similar instrument on the Mariner IV spacecraft. The OGO-IV results are somewhat more un-certain because of the small amount of quiet time data available. One example has been given of the ionization vs. altitude for a position near the cosmic ray equator. The data are subject to large uncertainties due to spacecraft radioactivity at the low altitude end and trapped radiation at high altitudes. With these facts considered, we believe the results to be in agreement with balloon results near the equator. An analytical fit to

the equatorial data becomes a very complex problem and has not been attempted.

The cosmic ray knee in late 1965 - early 1966 denotes the position in the geomagnetic field where the cosmic ray cutoff rigidity is approximately 1.2 BV. In the case of the POGO data the knee cannot be observed directly because of the outer trapped radiation zone, but its position can be determined by the intersection of two extrapolated lines. The knee position has been found to move away from the pole with increasing altitude by 0.0025 degree/km, a fact which is attributed to the earth's shadow effect. Extrapolated down to 40 km altitude, the average knee position is 59.0° invariant latitude for OGO-II, 58.4° for OGO-IV in mid 1967. We find a small north-south effect that could be interpreted as a seasonal variation. In Northern Hemisphere winter the North knee is closer to the pole and the South knee farther away by 0.3 ± 0.2 degree. Finally, we can just barely detect a local time variation, which we fit with a simple sinusoidal function for the deviation of the knee from the average position. The amplitude is found to be 0.5 ± 0.4 degree, and the phase is such that the maximum excursion toward the pole occurs 1.4 ± 1.0 hours before local noon.

Figure Captions

12. Plot of ionization vs. geographic latitude for OGO-II Orbit 75, North Pole, 23:35 GMT Oct. 19, 1965 to Orbit 76, North Pole, 01:19 GMT Oct. 20. Also shown are L parameter and spacecraft altitude vs. latitude.

13. POGO Experiment 5008 vertical detector arrangement. D_1, D_2, D_3 detectors correspond respectively to V_1, V_2, and V_3 counting rates mentioned in text.

14. Experiment 5007 ionization vs. Experiment 5008 V_2 rate. Data points are polar pass averages; uncertainties are 1.5 to 2.0% in ionization, 10 to 20% in V_2 rate.

15. Ionization vs. V_3 rate for equatorial pass. V_3 rates above 180 counts/sec are not reliable because of scaler saturation.

16. Ionization vs. L parameter for equatorial pass where perigee is located at minimum L.

17. OGO-II ionization vs. IMP-III ionization, quiet time data. Straight line fits low sensitivity data only.

18. Predicted ionization vs. altitude curves for various additions to the primary ionization due to splash albedo. Total ionization has been divided by the geometrical solid angle of the sky.

19. Trial functions used for the angular distribution of splash albedo particles.

20. Plot of corrected ionization averages vs. altitude, where data have been divided by the geometrical solid angle of the sky, with top of atmosphere at 40 km. Curves show least squares fit to data according to Eq. 12.

21. Ionization vs. altitude near the geomagnetic poles. See Table 8 for values at infinite altitude.

22. Example of ionization vs. altitude for position near the cosmic ray equator. Curves are identical except for separation by 30 ion pairs/(cm^3 sec atm).

23. Geographic location of cosmic ray knee at 700 km altitude. OGO-II Revs. 74-110, Oct. 19-22, 1965. The solid line has been drawn through the data by eye; it is not an analytical fit.

24. Configuration of geomagnetic field lines. Lines are labeled with the geomagnetic latitude at the point of intersection with the earth.

25. Position of cosmic ray knee. Upper: invariant latitude vs. altitude. Middle: deviation from altitude curve vs. local time. Lower:

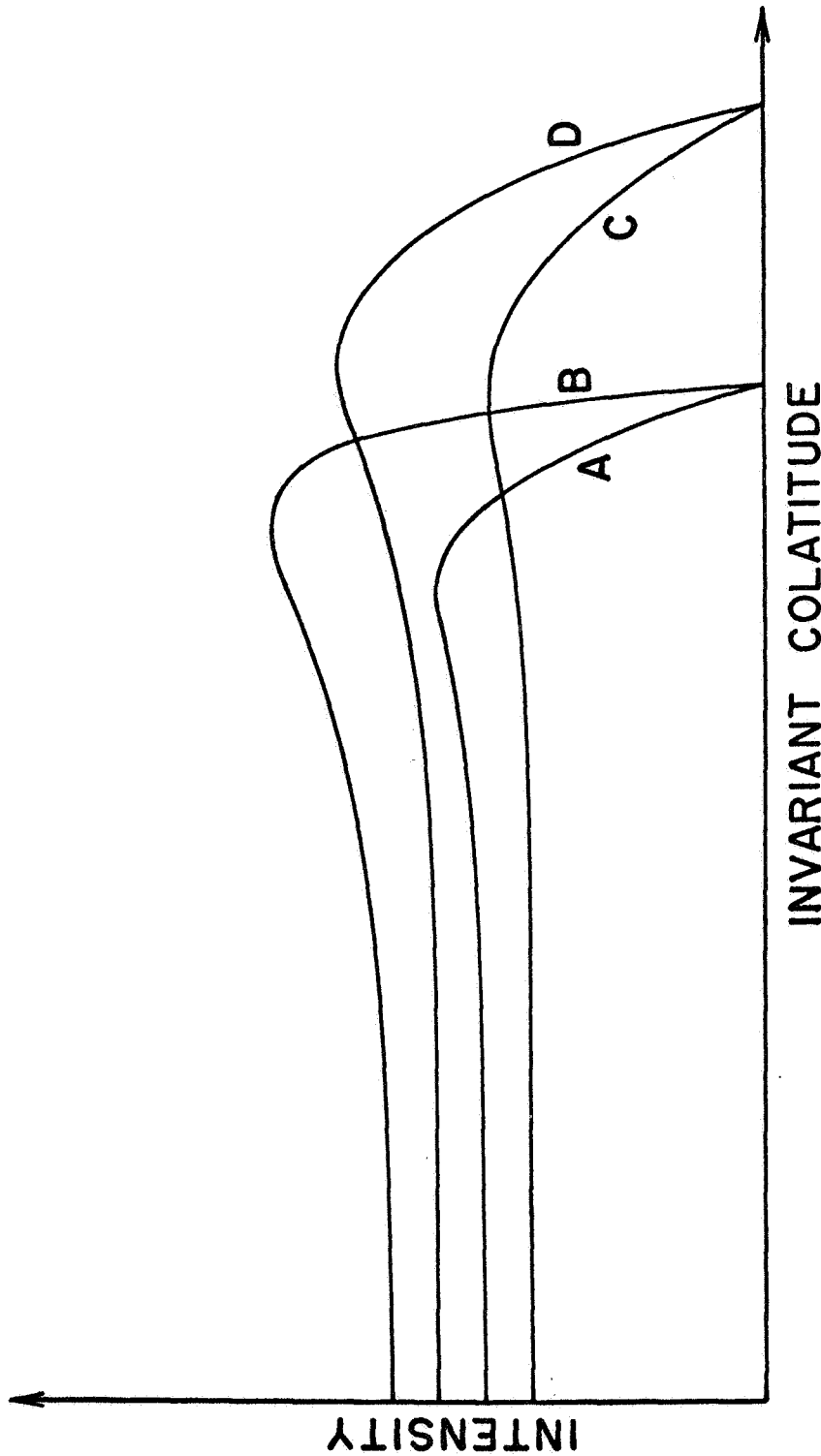same as middle but after correction for North-South effect.

26. Intensity vs. latitude for rigidities $P_1 < P_2$ and altitudes $h_1 < h_2$. A: P_1 at h_1. B: P_1 at h_2. C: P_2 at h_1. D: P_2 at h_2. The relative intensities at high latitudes have no significance; we only want to show the effect of altitude on the intensity near the cutoff point relative to the polar level.

References

1. H. V. Neher, Cosmic Ray Particles That Changed From 1954 to 1958 to 1965, J. Geophys. Res., 72, 1527-1539, 1967.

2. R. H. Callender, J. R. Manzano, and J. R. Winckler, The Response of High-Altitude Ionization Chambers During the 1954-1965 Solar Cycle, J. Geophys. Res., 70, 3189-3201, 1965.

3. R. A. Millikan and G. H. Cameron, A More Accurate and More Extended Cosmic-Ray Ionization-Depth Curve and the Present Evidence for Atom Building, Phys. Rev., 37, 235-252, 1931.

4. M. H. Shamos and A. R. Liboff, A New Measurement of the Intensity of Cosmic-Ray Ionization at Sea Level, J. Geophys.Res., 71, 4651-4659, 1966.

5. W. M. Lowder and H. L. Beck, Cosmic Ray Ionization in the Lower Atmosphere, J. Geophys. Res., 71, 4661-4668, 1966.

6. A. R. Johnston, The Absolute Cosmic-Ray Ionization in the Atmosphere at Balloon Altitudes, Ph.D. thesis, California Institute of Technology, 1956.

7. H. V. Neher, An Automatic Ionization Chamber, Rev.Sci.Inst., 24, 99-102, 1953.

8. H. V. Neher and A. R. Johnston, Modification to the Automatic Ionization Chamber, Rev.Sci.Inst., 27, 173-174, 1956.

9. L. B. Loeb, Basic Processes of Gaseous Electronics (Univ. of Calif. Press, Berkeley, 1955), p. 527.

10. J. Sharpe, Nuclear Radiation Detectors 2nd Ed. (John Wiley and Sons, Inc., New York, 1964), p. 105.

11. H. V. Neher, Variable Sensitivity Ionization Chamber, Rev.Sci. Inst., 32, 48-49, 1961.

12. H. R. Anderson, L. G. Despain, H. V. Neher, Response to Environment and Radiation of an Ionization Chamber and Matched Geiger Tube Used on Spacecraft, Nuclear Instruments and Methods, 47, 1-9, 1967.

13. M. A. Shea and D. F. Smart, Worldwide Trajectory-Derived Vertical Cutoff Rigidities and Their Applications to Experimental Measurements, J. Geophys.Res., 72, 2021-2027, 1967.

14. M. J. McHugh, Studies of the Dose to Human Beings from Natural Sources of Ionizing Radiation, M.S. thesis,University of Leeds, 1959.

15. J. Clay, The Absolute Value of Cosmic-Ray Ionization at Sea Level in Different Gases, Rev. Mod. Phys., 11, 123-127, 1939.

16. H. Carmichael, Energy Spectrum of the Soft Component near Sea Level, Phys. Rev., 107, 1401-1409, 1957.

17. B. Rossi, Interpretation of Cosmic-Ray Phenomena, Rev. Mod. Phys., 20, 537-583, 1948.

18. J. Clay, The Intensity of Cosmic Radiation under Thick Layers, Rev. Mod. Phys., 11, 128-135, 1939.

19. R. A. Millikan and H. V. Neher, A Precision World Survey of Sea-Level Cosmic Ray Intensities, Phys. Rev., 50, 15-24, 1936.

20. H. V. Neher, Recent Data on Geomagnetic Effects, in Progress in Cosmic Ray Physics, Vol. 1 (Interscience, New York, 1952), pp. 243-314.

21. E. J. Workman, Secondary Effects in Ionization by Hard Gamma-Rays, Phys. Rev., 43, 859-870, 1933.

22. K. A. Anderson, H. K. Harris, and R. J. Paoli, Energetic Electrons In and Beyond the Earth's Outer Magnetosphere, J. Geophys. Res., 70, 1039-1050, 1965.

23. H. V. Neher and H. R. Anderson, Cosmic-Ray Changes during a Solar Cycle, Proc. Ninth Intern. Conf. Cosmic Rays, 1, 153-156, 1966.

24. H. V. Neher and H. R. Anderson, Cosmic-Ray Intensity at Thule, Greenland, during 1962 and 1963 and a Comparison with Data from Mariner 2, J. Geophys. Res., 69, 807-814, 1964.

25. H. V. Neher and H. R. Anderson, Change of Cosmic-Ray Intensity with Distance from the Sun, J. Geophys. Res., 69, 1911-1913, 1964.

26. H. R. Anderson, The Radial Gradient of Cosmic Radiation Measured by Mariners 2 and 4, J. Geophys. Res., 73, 2897-2909, 1968.

27. R. Gall, J. Jimenez, and L. Camacho, Arrival of Low-Energy Cosmic Rays via the Magnetospheric Tail, J. Geophys. Res., 73, 1593, 1968.

28. J. E. McCoy, High Latitude Ionization Spikes Observed by the POGO Ion Chamber Experiment, Ph. D. thesis, Rice University, 1968.

29. H. R. Anderson, P. D. Hudson, and J. E. McCoy, Observations of POGO Ion Chamber Experiment in the Outer Radiation Zone, J. Geophys. Res., 73, 6285-6297, 1968.

30. C. Störmer, The Polar Aurora (Oxford University Press, 1955)

31. J. J. Quenby and G. J. Wenk, Cosmic Ray Threshold Rigidities and the Earth's Magnetic Field, Phil. Mag., 7, 1457-1485, 1962.

32. T. Makino, On the Cosmic-Ray Cut-Off Rigidities and the Earth's Magnetic Field, Rept.Ionosphere Space Res. Japan, 17, 173-186, 1963.

33. A. J. Dessler, Length of the Magnetospheric Tail, J. Geophys.Res., 69, 3913-3918, 1964.

34. N. F. Ness, The Earth's Magnetic Tail, J. Geophys. Res., 70, 2989-3006, 1965.

35. C. E. McIlwain, Coordinates for Mapping the Distribution of Magnetically Trapped Particles, J. Geophys. Res., 66, 3681-3691, 1961.

36. P. D. Hudson and H. R. Anderson, Non-Uniformity of Solar Protons Over the Polar Caps on 24 March 1966, Rice University preprint, to be published.

37. T. Murayama, Measurement of Primary and Albedo Cosmic Rays on a Polar Orbiting Satellite, Planet. Space Sci., 15, 1169-1180, 1967.

38. E. C. Stone, private communication; data and description of experiment to be published.

39. R. L. Arnoldy, S. R. Kane, and J. R. Winckler, Energetic Solar Flare x-Rays Observed by Satellite and their Correlation with Solar Radio and Energetic Particle Emission, Astrophys. J., 151, 711, 1968.

40. J. D. Jackson, Classical Electrodynamics (John Wiley and Sons, Inc., New York, 1962), pp. 419-424.

41. K-P. Wenzel, Primary, Secondary, and Albedo - Protons from the Cosmic Radiation, Ph.D. thesis, University of Heidelberg, 1968.

42. M. H. Israel, Primary Cosmic Ray Electrons and Albedo Electrons in 1967 at Energies between 12 and 1000 MeV, Ph.D. thesis, California Institute of Technology, 1969.

43. C. Rice, private communication; data to be included in his Ph.D. thesis, California Institute of Technology

44. R. J. Borken, A Study by Satellite of Gamma Rays from the Earth, B.S. thesis, Massachusetts Institute of Technology, 1968.

45. H. V. Neher and H. R. Anderson, Comparison of the Flux of Cosmic -Ray Particles Measured in Space to that Deduced from Balloon Flights Using Ionization Chambers, J. Geophys. Res., 72, 5515-5517, 1967.

46. E. C. Ray, Re-Entrant Cosmic-Ray Albedo, J. Geophys. Res., 67, 3289-3291, 1962.

47. H. V. Neher, Cosmic-Ray Knee in 1958, J. Geophys. Res., 66, 4007-4012, 1961

48. H. V. Neher and E. A. Stern, 'Knee' of the Cosmic-Ray Latitude Curve, Phys. Rev., 98, 845-846, 1955.

49. D. J. Williams and G. D. Mead, Nightside Magnetospheric Configuration as Obtained from Trapped Electrons at 1100 km, J. Geophys. Res., 70, 3017, 1965.

50. G. C. Reid and H. H. Sauer, The Influence of the Geomagnetic Tail on Low-Energy Cosmic-Ray Cutoffs, J. Geophys. Res., 72, 197, 1967.

51. E. C. Stone, Local Time Dependence of Non-Störmer Cutoff for 1.5 MeV Protons in Quiet Geomagnetic Field, J. Geophys. Res., 69, 3577, 1964.

52. J. E. Kasper, Geomagnetic Effects on Cosmic Radiation for Observation Points Above the Earth, J. Geophys. Res., 65, 39-53, 1960.

53. F. D. Seward and H. N. Kornblum, Jr., Near-Earth, Polar-Orbiting Satellite Measurements of Charged Particles, J. Geophys. Res., 70, 3557-3570, 1965.

Appendix I

Polar Ionization Averages

The following list has been compiled from almost all of the polar passes of OGO-II and OGO-IV where relatively noise-free ionization data were obtained. Data measured during solar particle events have been deleted if a large amount of structure was observed in the ionization. Letters following the orbit number denote the pole (North or South) and the sensitivity mode (high or low). V_2 rates have been left blank when not available. Corrected ionizations have been determined by comparison of measured ionization with the V_2 rate as explained in the text, and where blank it means the pass was not analysed because of missing V_2 rate, too many solar particles, not enough other orbits within the time period involved, or exception to the usual relation between ionization and V_2 rate. The altitude given is the average for the polar pass. Except in the case of a few low sensitivity data values, all polar passes in the list reached L values equal to or greater than 20. All ionizations have been divided by the geometrical solid angle of open sky as given by Eq. 9, with the effective thickness of the atmosphere equal to 29 km.

ORBIT NUM.	P	S	DATE M	D	Y	ALTITUDE KM	V2 RATE COUNTS/SEC	IONIZATION MEAS.	CORR.

OGO-II

ORBIT NUM.	P	S	M	D	Y	ALTITUDE KM	V2 RATE COUNTS/SEC	MEAS.	CORR.
8	S	L	10	15	65	1074	.070	521	520
9	N	L	10	15	65	800		526	
9	S	L	10	15	65	1099		525	
13	N	L	10	15	65	781	.098	520	514
15	N	L	10	15	65	832	.190	531	508
16	N	L	10	15	65	900		565	
17	N	L	10	15	65	834	.341	552	501
17	S	L	10	15	65	948	.170	541	518
18	N	L	10	15	65	929	.323	584	537
18	S	L	10	15	65	913	.132	543	528
20	N	L	10	15	65	922	.257	564	529
20	S	L	10	16	65	1035	.140	540	524
24	S	L	10	16	65	1195	.110	531	522
25	N	L	10	16	65	694	.082	525	522
25	S	L	10	16	65	1203	.064	518	518
26	S	L	10	16	65	1259	.066	534	534
27	N	L	10	16	65	810	.074	510	508
31	N	L	10	16	65	908	.309	557	523
31	S	L	10	16	65	961	.091	541	535
32	N	L	10	16	65	897	.339	567	517
32	S	L	10	16	65	987	.113	548	538
34	N	L	10	17	65	877	.159	545	528
34	S	L	10	17	65	1052	.125	535	522
35	N	L	10	17	65	841	.202	551	526
35	S	L	10	17	65	1124	.113	542	532
42	N	L	10	17	65	815	.149	552	537
43	N	L	10	17	65	741	.237	537	505
45	S	L	10	17	65	949	.147	558	540
46	N	L	10	17	65	824	.350	573	520
46	S	L	10	17	65	989	.113	553	549
47	N	L	10	17	65	861	.295	574	532
47	S	L	10	17	65	1009	.100	548	540
48	N	L	10	18	65	733	.168	578	559
48	S	L	10	18	65	1072	.118	554	543
49	N	L	10	18	65	740	.172	588	568
49	S	L	10	18	65	1179	.104	536	528
50	N	L	10	18	65	781	.187	543	520
53	N	L	10	18	65	719	.064	525	525
63	N	L	10	19	65	778	.126	531	520
63	S	L	10	19	65	1214	.118	519	508
64	N	L	10	19	65	762	.215	526	498
65	N	L	10	19	65	677	.091	529	524
65	S	L	10	19	65	1289	.098	521	514
66	N	L	10	19	65	677	.088	519	515
66	S	L	10	19	65	1257	.114	518	508
67	S	L	10	19	65	1241	.042	525	530

| ORBIT | | | DATE | | | ALTITUDE | V2 RATE | IONIZATION | |
NUM.	P	S	M	D	Y	KM	COUNTS/SEC	MEAS.	CORR.
68	N	L	10	19	65	678	.088	510	506
74	N	H	10	19	65	812	.313	596	547
74	S	H	10	19	65	1054	.147	569	554
75	N	H	10	19	65	807	.225	587	556
75	S	H	10	20	65	1102	.114	547	538
76	N	H	10	20	65	780	.186	567	543
76	S	H	10	20	65	1158	.077	541	539
77	N	H	10	20	65	745	.183	577	554
77	S	H	10	20	65	1235	.093	553	548
78	N	H	10	20	65	711	.158	562	543
78	S	H	10	20	65	1279	.157	561	545
85	N	H	10	20	65	726	.209	572	543
85	S	H	10	20	65	1095	.093	570	565
86	N	H	10	20	65	746	.312	608	559
86	S	H	10	20	65	1070	.121	571	561
87	N	H	10	20	65	776	.328	615	563
87	S	H	10	20	65	1066	.144	578	564
90	N	H	10	21	65	749	.183	579	556
90	S	H	10	21	65	1210	.114	568	559
92	N	H	10	21	65	676	.146	572	556
92	S	H	10	21	65	1317	.061	578	579
93	N	H	10	21	65	648	.092	583	578
93	S	H	10	21	65	1308	.138	586	573
94	N	H	10	21	65	629	.090	558	563
94	S	H	10	21	65	1341	.124	571	561
95	N	H	10	21	65	623	.092	557	551
95	S	H	10	21	65	1322	.062	549	550
96	N	H	10	21	65	639	.131	558	545
99	N	H	10	21	65	729	.271	605	564
99	S	H	10	21	65	1112	.113	586	577
102	N	H	10	21	65	765	.241	602	567
102	S	H	10	21	65	1139	.123	575	565
103	S	H	10	22	65	1182	.082	560	557
105	N	H	10	22	65	678		569	
105	S	H	10	22	65	1312	.088	562	558
106	N	H	10	22	65	647		562	
107	N	H	10	22	65	618	.082	557	554
108	N	H	10	22	65	564	.236	594	559
108	S	H	10	22	65	1364	.121	575	565
109	N	H	10	22	65	604	.075	569	567
109	S	H	10	22	65	1342	.155	570	554
110	N	H	10	22	65	622	.091	552	547
122	S	L	10	23	65	1369	.067	536	536
123	N	L	10	23	65	631	.106	528	521
126	N	L	10	23	65	692	.188	534	513
127	N	L	10	23	65	667	.274	538	502
127	S	L	10	23	65	1183	.176	536	525
128	N	L	10	23	65	727	.348	601	553

ORBIT			DATE			ALTITUDE	V2 RATE	IONIZATION	
NUM.	P	S	M	D	Y	KM	COUNTS/SEC	MEAS.	CORR.
128	S	L	10	23	65	1177	.112	567	563
132	N	L	10	24	65	618	.159	570	554
132	S	L	10	24	65	1320	.106	517	513
134	S	L	10	24	65	1424	.101	537	533
140	N	L	10	24	65	602	.216	560	534
211	N	L	10	29	65	616		532	
211	S	L	10	29	65	1305		531	
212	S	L	10	29	65	1334	.155	526	519
213	N	L	10	29	65	522	.063	529	529
213	S	L	10	30	65	1389	.083	511	511
215	N	L	10	30	65	528	.117	537	528
215	S	L	10	30	65	1442	.122	515	508
216	S	L	10	30	65	1501	.128	548	541
217	N	L	10	30	65	485	.084	554	551
217	S	L	10	30	65	1481	.181	538	548
218	N	L	10	30	65	495	.091	540	535
219	S	L	10	30	65	1478	.062	548	527
220	N	L	10	30	65	504	.086	523	519
222	N	L	10	30	65	497	.141	550	537
223	N	L	10	30	65	515	.193	569	546
223	S	L	10	30	65	1344	.082	518	518
224	N	L	10	30	65	534	.272	560	524
224	S	L	10	30	65	1328	.090	537	533
350	S	L	11	8	65	1518		521	
351	N	L	11	8	65	435		535	
351	S	L	11	9	65	1542		514	
352	N	L	11	9	65	431	.063	531	532
352	S	L	11	9	65	1541		533	
354	S	L	11	9	65	1533		560	
355	N	L	11	9	65	439		543	
355	S	L	11	9	65	1534		550	
375	N	L	11	10	65	432	.185	578	546
375	S	L	11	10	65	1506	.093	537	534
377	S	L	11	10	65	1539	.177	556	546
378	N	L	11	10	65	448	.079	539	535
379	N	H	11	11	65	430		545	
379	S	H	11	11	65	1543		546	
380	N	H	11	11	65	429	.060	540	541
380	S	H	11	11	65	1533	.114	553	546
382	N	H	11	11	65	434	.093	549	545
382	S	H	11	11	65	1535	.222	550	529
383	S	H	11	11	65	1497	.154	542	530
384	N	H	11	11	65	435	.093	549	545
385	N	H	11	11	65	431	.095	549	545
386	N	H	11	11	65	430	.114	543	536
388	N	H	11	11	65	429	.123	567	558
388	S	H	11	11	65	1533	.090	546	543
389	S	H	11	11	65	1530	.131	548	539

ORBIT NUM.	P	S	M	D	Y	ALTITUDE KM	V2 RATE COUNTS/SEC	IONIZATION MEAS.	CORR.
397	N	L	11	12	65	448	.099	552	543
397	S	L	11	12	65	1520	.192	542	530
398	N	L	11	12	65	453	.101	545	535
400	N	L	11	12	65	430	.091	558	551
401	N	L	11	12	65	429	.142	559	538
401	S	L	11	12	65	1539	.203	590	577
402	N	L	11	12	65	429	.156	554	530
402	S	L	11	12	65	1521	.104	560	556
404	N	L	11	12	65	430	.159	559	534
404	S	L	11	12	65	1532	.115	537	532
405	S	L	11	12	65	1528	.064	534	534
406	S	L	11	13	65	1536	.084	529	527
407	N	L	11	13	65	430	.052	546	549
407	S	L	11	13	65	1531	.092	526	523
408	N	L	11	13	65	431	.099	580	571
408	S	L	11	13	65	1505	.171	544	534
409	N	L	11	13	65	445	.085	541	536
409	S	L	11	13	65	1496	.217	537	523
410	N	L	11	13	65	449	.109	550	538
410	S	L	11	13	65	1502	.263	555	536
411	N	L	11	13	65	445	.099	550	541
411	S	L	11	13	65	1503	.181	537	526
413	N	L	11	13	65	434	.094	549	541
417	N	L	11	13	65	436	.248	586	537
417	S	L	11	13	65	1525	.106	545	541
418	N	L	11	13	65	430	.139	580	560
419	N	L	11	13	65	429	.082	566	561
419	S	L	11	13	65	1543	.055	532	533
421	S	L	11	14	65	1522	.130	531	525
422	N	L	11	14	65	435	.097	527	518
422	S	L	11	14	65	1488	.188	530	518
423	N	L	11	14	65	450	.106	551	540
425	S	L	11	14	65	1493	.176	540	530
428	N	L	11	14	65	431	.078	531	528
429	N	L	11	14	65	438	.119	571	557
429	S	L	11	14	65	1536	.105	561	557
430	S	L	11	14	65	1534	.092	522	519
431	N	L	11	14	65	446	.159	582	557
431	S	L	11	14	65	1534	.065	546	546
432	N	H	11	14	65	429	.083	549	546
432	S	H	11	14	65	1543	.058	548	549
433	N	H	11	14	65	431	.067	540	540
433	S	H	11	14	65	1536	.080	534	532
436	N	H	11	15	65	450	.088	557	554
436	S	H	11	15	65	1479	.240	584	560
437	N	H	11	15	65	463	.097	557	552
438	S	H	11	15	65	1473	.181	567	551
439	N	H	11	15	65	466	.095	577	573

ORBIT NUM.	P	S	DATE M	D	Y	ALTITUDE KM	V2 RATE COUNTS/SEC	IONIZATION MEAS.	CORR.
440	N	H	11	15	65	452	.097	548	543
441	N	H	11	15	65	445		558	
442	N	H	11	15	65	441	.101	542	537
442	S	H	11	15	65	1541	.054	547	548
443	N	H	11	15	65	438	.175	564	548
443	S	H	11	15	65	1542	.083	555	553
444	N	H	11	15	65	434	.169	550	534
444	S	H	11	15	65	1542	.085	544	541
446	S	L	11	15	65	1539	.065	540	540
448	S	L	11	16	65	1525	.074	535	534
449	S	L	11	16	65	1491	.127	554	548
450	N	L	11	16	65	466	.063	545	546
451	N	L	11	16	65	473		555	
451	S	L	11	16	65	1491		548	
452	N	L	11	16	65	461		568	
455	N	L	11	16	65	436		544	
456	N	L	11	16	65	439		557	
460	N	H	11	16	65	436		565	
460	S	H	11	16	65	1532		548	
470	N	H	11	17	65	452	.136	569	558
487	S	L	11	18	65	1509		525	
488	N	L	11	18	65	466		547	
489	S	L	11	19	65	1492		550	
490	N	L	11	19	65	534		542	
490	S	L	11	19	65	1422		548	
493	S	L	11	19	65	1350		609	
494	N	L	11	19	65	495		546	
499	N	L	11	19	65	444		566	
572	N	H	11	25	65	559	.054	557	559
574	N	H	11	25	65	605	.107	575	569
574	S	H	11	25	65	1256	.377	608	569
575	N	H	11	25	65	621	.142	574	563
575	S	H	11	25	65	1261	.288	595	567
576	S	H	11	25	65	1276	.260	605	580
577	N	H	11	25	65	608	.123	576	568
578	N	H	11	25	65	587	.067	561	561
580	N	H	11	25	65	552	.110	573	566
580	S	H	11	25	65	1462	.097	579	575
583	S	H	11	25	65	1435	.067	566	566
585	N	H	11	25	65	558	.054	604	
608	N	L	11	27	65	586	.091	531	528
608	S	L	11	27	65	1421	.113	549	545
609	N	L	11	27	65	594	.142	577	569
609	S	L	11	27	65	1403	.091	567	565
610	S	L	11	27	65	1417	.135	546	540
611	N	L	11	27	65	589	.082	551	550
611	S	L	11	27	65	1288	.080	566	565
613	S	L	11	28	65	1271	.211	564	550

ORBIT NUM.	P	S	M	D	Y	ALTITUDE KM	V2 RATE COUNTS/SEC	IONIZATION MEAS.	CORR.
614	N	L	11	28	65	621	.094	540	537
614	S	L	11	28	65	1223	.231	564	547
615	N	L	11	28	65	675	.114	548	543
615	S	L	11	28	65	1223	.337	579	552
616	N	L	11	28	65	661	.108	562	558
616	S	L	11	28	65	1176	.341	595	568
617	N	L	11	28	65	709	.135	559	552
618	N	L	11	28	65	682	.142	539	531
618	S	L	11	28	65	1294	.252	549	530
619	N	L	11	28	65	703	.117	561	555
620	N	L	11	28	65	576	.203	548	533
648	N	H	11	30	65	668	.108	565	559
648	S	H	11	30	65	1323	.235	575	554
649	N	H	11	30	65	647	.129	556	547
649	S	H	11	30	65	1358	.143	583	573
651	N	H	11	30	65	614	.107	558	552
651	S	H	11	31	65	1345	.088	585	582
674	N	H	12	2	65	750	.095	555	551
675	N	H	12	2	65	718	.116	561	554
676	S	H	12	2	65	1330	.107	578	573
677	N	H	12	2	65	685	.115	554	547
677	S	H	12	2	65	1330	.089	559	556
679	S	H	12	2	65	1280		565	
680	S	H	12	2	65	1233	.132	558	550
702	N	H	12	4	65	788	.131	565	556
703	N	H	12	4	65	764	.127	572	563
830	N	H	12	13	65	941		565	
830	S	H	12	13	65	974		572	
832	S	H	12	13	65	852		591	
834	S	H	12	14	65	745		634	
1025	S	H	12	27	65	515		654	
1026	N	H	12	27	65	1409		598	
1064	N	H	12	30	65	1393		768	
1064	S	H	12	30	65	550		746	
1065	N	H	12	30	65	1433		909	
1065	S	H	12	30	65	518		900	
1176	N	L	1	7	66	1518	.048	569	
1177	N	L	1	7	66	1521	.046	521	
1177	S	L	1	7	66	453	.124	586	
1201	N	H	1	9	66	1518	.079	569	568
1201	S	H	1	9	66	454	.058	578	579
1202	N	H	1	9	66	1512		570	
1203	N	H	1	9	66	1524	.118	553	548
1203	S	H	1	9	66	447	.075	580	578
1204	N	H	1	9	66	1524	.041	547	550
1204	S	H	1	9	66	455	.082	581	578
1205	N	H	1	9	66	1521	.057	594	595
1205	S	H	1	9	66	463	.155	595	580

ORBIT			DATE			ALTITUDE	V2 RATE	IONIZATION	
NUM.	P	S	M	D	Y	KM	COUNTS/SEC	MEAS.	CORR.
1273	N	H	1	14	66	1516		563	
1273	S	H	1	14	66	499	.074	588	587
1274	N	H	1	14	66	1479	.110	562	558
1274	S	H	1	14	66	517	.151	605	591
1275	N	H	1	15	66	1463	.040	563	566
1275	S	H	1	15	66	527	.104	589	583
1276	N	H	1	15	66	1433		560	
1276	S	H	1	15	66	523	.043	589	593
1277	N	H	1	15	66	1454	.053	577	578
1279	N	H	1	15	66	1482	.066	564	564
1305	N	L	1	17	66	1506	.062	582	
1305	S	L	1	17	66	483		577	
1307	S	L	1	17	66	519	.088	681	
1317	S	H	1	18	66	572	.141	822	
1318	N	H	1	18	66	1399	.111	761	
1318	S	H	1	18	66	555	.127	861	
1319	N	H	1	18	66	1432	.141	863	
1320	N	H	1	18	66	1463	.254	912	
1321	N	H	1	18	66	1452	.188	844	
1322	N	H	1	18	66	1464	.132	776	
1322	S	H	1	18	66	463	.106	769	
1323	N	H	1	18	66	1476	.228	824	
1323	S	H	1	18	66	460	.145	775	
1324	N	H	1	18	66	1488	.236	784	
1324	S	H	1	18	66	461	.139	750	
1325	N	H	1	18	66	1490	.124	717	
1325	S	H	1	18	66	470	.132	737	
1326	N	H	1	18	66	1482	.097	686	
1326	S	H	1	18	66	491	.134	664	
1327	N	H	1	18	66	1462	.083	662	
1330	N	H	1	18	66	1431	.110	695	
1330	S	H	1	19	66	599	.136	733	
1331	N	H	1	19	66	1384	.094	688	
1333	S	L	1	19	66	544	.133	851	
1334	N	L	1	19	66	1432	.185	1021	
1335	N	L	1	19	66	1382	.233	1082	
1336	S	L	1	19	66	468	.212	1245	
1337	N	L	1	19	66	1378	.395	1213	
1337	S	L	1	19	66	459	.200	1132	
1338	S	L	1	19	66	475	.196	1052	
1339	N	L	1	19	66	1444		1014	
1342	N	L	1	19	66	1392	.155	767	
1342	S	L	1	19	66	541	.164	751	
1343	N	L	1	19	66	1396	.160	745	
1343	S	L	1	19	66	598	.132	770	
1344	N	H	1	20	66	1358	.138	725	
1344	S	H	1	20	66	608	.139	734	
1345	N	H	1	20	66	1359	.121	719	

| ORBIT | | | DATE | | | ALTITUDE | V2 RATE | IONIZATION | |
NUM.	P	S	M	D	Y	KM	COUNTS/SEC	MEAS.	CORR.
1346	N	H	1	20	66	1367	.126	749	
1348	N	H	1	20	66	1409	.141	746	
1349	N	H	1	20	66	1428	.216	748	
1349	S	H	1	20	66	485	.178	1004	
1350	N	H	1	20	66	1440	.263	933	
1350	S	H	1	20	66	480	.247	1197	
1351	S	H	1	20	66	473	.227	964	
1352	N	H	1	20	66	1466		861	
1352	S	H	1	20	66	481		782	
1353	N	H	1	20	66	1452	.204	746	
1353	S	H	1	20	66	502	.111	748	
1354	N	H	1	20	66	1442	.111	741	
1354	S	H	1	20	66	534	.163	734	
1355	N	H	1	20	66	1416	.132	652	
1355	S	H	1	20	66	566	.209	759	
1356	N	H	1	20	66	1395	.144	649	
1356	S	H	1	20	66	581	.251	722	
1362	N	L	1	21	66	1393	.213	585	
1363	S	L	1	21	66	511	.117	570	
1364	N	L	1	21	66	1401	.233	576	
1364	S	L	1	21	66	476	.107	574	
1366	N	L	1	21	66	1437	.186	669	
1366	S	L	1	21	66	491	.132	625	
1367	N	L	1	21	66	1406	.111	561	
1368	N	L	1	21	66	1419	.100	536	
1369	N	L	1	21	66	1391	.310	574	
1369	S	L	1	21	66	576	.123	576	
1371	S	L	1	22	66	683	.099	549	
1372	S	H	1	22	66	652	.104	530	524
1374	N	H	1	22	66	1328	.102	542	537
1375	N	H	1	22	66	1358	.172	589	575
1376	N	H	1	22	66	1375	.190	568	552
1377	N	H	1	22	66	1381	.241	556	533
1377	S	H	1	22	66	502	.110	541	534
1378	N	H	1	22	66	1411	.210	535	516
1378	S	H	1	22	66	494	.098	542	537
1379	N	H	1	22	66	1428	.157	535	523
1379	S	H	1	22	66	498	.173	566	550
1383	N	H	1	22	66	1356	.154	531	519
1383	S	H	1	22	66	628	.085	559	556
1384	N	H	1	22	66	1337	.112	546	540
1384	S	H	1	22	66	658	.107	562	556
1385	N	H	1	22	66	1327	.068	538	538
1385	S	H	1	23	66	665	.083	587	
1386	N	H	1	23	66	1288	.084	553	550
1387	N	L	1	23	66	1253	.071	531	530
1388	N	L	1	23	66	1278	.086	523	519
1389	N	L	1	23	66	1306	.159	552	536

ORBIT			DATE			ALTITUDE	V2 RATE	IONIZATION	
NUM.	P	S	M	D	Y	KM	COUNTS/SEC	MEAS.	CORR.
1390	N	L	1	23	66	1307	.127	560	549
1391	N	L	1	23	66	1340	.197	526	504
1391	S	L	1	23	66	494	.080	531	526
1392	N	L	1	23	66	1357	.247	535	504
1392	S	L	1	23	66	512	.089	538	531
1393	N	L	1	23	66	1372	.151	534	519
1394	S	L	1	23	66	504	.141	565	548
1395	N	L	1	23	66	1379	.139	510	497
1396	N	L	1	23	66	1320	.133	526	514
1396	S	L	1	23	66	587	.123	534	517
1397	S	L	1	23	66	734	.086	612	
1399	S	L	1	24	66	672		523	
1400	S	H	1	24	66	685	.063	523	523
1401	N	H	1	24	66	1270		523	
1402	N	H	1	24	66	1297		527	
1403	N	H	1	24	66	1324	.210	564	545
1404	N	H	1	24	66	1346	.218	561	541
1404	S	H	1	24	66	533	.143	561	549
1405	N	H	1	24	66	1364	.237	560	537
1405	S	H	1	24	66	519	.110	571	564
1406	N	H	1	24	66	1372	.207	571	552
1406	S	H	1	24	66	505	.171	579	563
1407	N	H	1	24	66	1439	.205	560	542
1407	S	H	1	24	66	542	.164	565	550
1408	N	H	1	24	66	1389	.145	533	523
1411	S	H	1	24	66	694	.254	551	524
1413	N	L	1	25	66	1226	.082	529	526
1413	S	L	1	25	66	688	.077	508	504
1414	N	L	1	25	66	1236	.088	516	512
1415	N	L	1	25	66	1296	.261	549	516
1417	N	L	1	25	66	1265	.143	536	523
1419	N	L	1	25	66	1322	.399	592	535
1419	S	L	1	25	66	541	.152	562	537
1425	N	L	1	25	66	1282	.122	532	522
1426	N	H	1	25	66	1212	.100	543	537
1426	S	H	1	25	66	744	.127	534	527
1428	N	H	1	26	66	1210	.077	523	521
1428	S	H	1	26	66	720	.077	496	
1429	N	H	1	26	66	1237	.142	528	514
1431	N	H	1	26	66	1431	.193	549	527
1432	N	H	1	26	66	1310	.331	585	538
1432	S	H	1	26	66	560	.107	573	568
1434	N	H	1	26	66	1316	.188	600	578
1434	S	H	1	26	66	548	.094	557	554
1435	N	H	1	26	66	1342	.233	565	535
1435	S	H	1	26	66	574	.126	546	539
1438	N	H	1	26	66	1269		561	
1438	S	H	1	26	66	722	.089	559	556

ORBIT NUM.	P	S	DATE M	D	Y	ALTITUDE KM	V2 RATE COUNTS/SEC	IONIZATION MEAS.	CORR.
1439	N	H	1	26	66	1219	.117	563	554
1439	S	H	1	26	66	758	.099	568	564
1440	N	H	1	26	66	1259	.062	552	553
1440	S	H	1	27	66	779	.130	570	563
1441	N	H	1	27	66	1178	.087	529	525
1441	S	H	1	27	66	767	.072	542	541
1442	N	H	1	27	66	1269	.080	521	518
1443	N	L	1	27	66	1294	.082	560	
1445	N	L	1	27	66	1268		523	
1446	N	L	1	27	66	1260	.247	553	530
1448	N	L	1	27	66	1221	.192	523	507
1448	S	L	1	27	66	572	.085	525	521
1449	S	L	1	27	66	589	.096	511	505
1450	N	L	1	27	66	1285	.122	518	511
1451	N	L	1	27	66	1344		506	
1452	N	L	1	27	66	1233	.146	504	494
1453	N	L	1	27	66	1249	.121	510	503
1453	S	L	1	27	66	849	.102	514	507
1454	N	L	1	27	66	1161	.099	505	501
1454	S	L	1	28	66	818		514	
1455	S	L	1	28	66	747	.083	499	496
1456	N	H	1	28	66	1076	.063	530	530
1457	N	H	1	28	66	1192	.100	528	522
1459	N	H	1	28	66	1248	.279	565	527
1459	S	H	1	28	66	603	.136	552	544
1460	N	H	1	28	66	1275		578	
1460	S	H	1	28	66	590		578	
1461	S	H	1	28	66	585		567	
1464	N	H	1	28	66	1267	.142	540	526
1464	S	H	1	28	66	691	.176	604	592
1466	N	H	1	28	66	1200	.143	535	521
1466	S	H	1	28	66	755	.298	565	540
1473	N	L	1	29	66	1243	.251	546	523
1474	N	L	1	29	66	1246	.281	539	512
1474	S	L	1	29	66	532	.112	531	522
1477	S	L	1	29	66	654	.145	599	
1478	N	L	1	29	66	1254	.134	541	532
1479	S	L	1	29	66	751	.122	509	498
1480	S	L	1	29	66	837	.126	520	509
1483	N	L	1	30	66	945		508	
1483	S	L	1	30	66	811		487	
1485	N	H	1	30	66	1159		526	
1489	S	H	1	30	66	633		556	
1490	S	H	1	30	66	657		570	
1492	S	H	1	30	66	775		561	
1493	N	H	1	30	66	1222		527	
1493	S	H	1	30	66	824		554	
1494	N	H	1	30	66	1128		524	

ORBIT			DATE			ALTITUDE	V2 RATE	IONIZATION	
NUM.	P	S	M	D	Y	KM	COUNTS/SEC	MEAS.	CORR.
1494	S	H	1	30	66	865		542	
1495	S	H	1	30	66	873		546	
1496	N	H	1	31	66	1075		517	
1498	N	L	1	31	66	1104		515	
1500	N	L	1	31	66	1132		530	
1501	N	L	1	31	66	1166	.288	530	502
1501	S	L	1	31	66	621	.088	534	530
1504	S	L	1	31	66	694	.140	528	514
1505	N	L	1	31	66	1199	.168	516	503
1505	S	L	1	31	66	732	.093	514	509
1506	N	L	1	31	66	1196	.059	523	524
1506	S	L	1	31	66	862		536	
1516	N	H	2	1	66	1127	.330	577	529
1516	S	H	2	1	66	669	.170	572	561
1518	S	H	2	1	66	727	.100	556	552
1519	N	H	2	1	66	1149	.188	547	525
1519	S	H	2	1	66	800	.102	552	548
1520	S	H	2	1	66	849	.112	567	562
1521	N	H	2	1	66	1091	.151	553	537
1521	S	H	2	1	66	968	.140	546	538
1523	N	L	2	1	66	970		505	
1524	N	L	2	2	66	1025	.081	508	506
1524	S	L	2	2	66	862	.087	520	516
1525	N	L	2	2	66	1118	.023	530	535
1526	N	L	2	2	66	1074	.142	519	509
1528	N	L	2	2	66	1072	.261	558	533
1528	S	L	2	2	66	710	.120	536	526
1536	N	H	2	2	66	984	.142	548	534
1536	S	H	2	2	66	962	.114	545	540
1537	N	H	2	3	66	994	.054	546	548
1537	S	H	2	3	66	963		552	
1553	N	H	2	4	66	985	.105	586	582
1555	N	H	2	4	66	1045	.257	593	573
1556	N	H	2	4	66	1044	.312	623	597
1556	S	H	2	4	66	746	.141	613	606
1558	S	H	2	4	66	756	.117	594	589
1559	N	H	2	4	66	1103	.268	592	571
1559	S	H	2	4	66	805		626	
1562	N	H	2	4	66	1001	.138	589	581
1562	S	H	2	4	66	986	.102	602	597
1563	N	H	2	4	66	935	.199	635	621
1563	S	H	2	4	66	1014	.126	584	577
1564	N	H	2	4	66	933	.114	612	607
1564	S	H	2	5	66	1033	.095	619	617
1568	N	L	2	5	66	951	.122	585	578
1569	S	L	2	5	66	748	.155	543	524
1570	N	L	2	5	66	1016	.308	604	575
1571	S	L	2	5	66	764	.128	628	

ORBIT NUM.	P	S	DATE M	D	Y	ALTITUDE KM	V2 RATE COUNTS/SEC	IONIZATION MEAS.	CORR.
1573	S	L	2	5	66	826	.162	549	529
1575	S	L	2	5	66	1014	.179	557	534
1578	S	L	2	6	66	1083	.100	538	531
1609	N	H	2	8	66	912	.281	578	555
1613	N	H	2	8	66	922		592	
1613	S	H	2	8	66	904		603	
1617	N	H	2	8	66	878	.225	572	555
1617	S	H	2	8	66	1089	.063	577	577
1618	N	H	2	8	66	850	.205	586	571
1618	S	H	2	8	66	1130	.133	564	557
1619	N	H	2	8	66	821	.091	570	567
1621	N	H	2	9	66	762		569	
1623	N	H	2	9	66	884	.255	596	576
1624	N	H	2	9	66	906	.325	620	592
1625	N	H	2	9	66	934	.378	616	583
1625	S	H	2	9	66	873	.100	587	582
1629	N	H	2	9	66	905		617	
1631	N	H	2	9	66	852	.191	583	570
1631	S	H	2	9	66	1125	.150	591	582
1632	N	H	2	9	66	806	.179	576	564
1634	N	H	2	10	66	788		581	
1635	N	H	2	10	66	794	.124	570	564
1639	S	H	2	10	66	898	.123	590	583
1641	S	H	2	10	66	932	.174	593	582
1642	S	H	2	10	66	1003	.126	614	607
1644	S	H	2	10	66	1131	.089	583	581
1645	N	H	2	10	66	754	.159	589	579
1645	S	H	2	10	66	1174	.135	584	577
1646	N	H	2	10	66	783	.141	599	591
1646	S	H	2	10	66	1192	.132	584	577
1647	S	H	2	11	66	1219		590	
1648	N	H	2	11	66	763		570	
1648	S	H	2	11	66	1158		579	
1649	N	H	2	11	66	858		614	
1650	S	L	2	11	66	1030		538	
1653	N	L	2	11	66	870		596	
1655	S	L	2	11	66	885		568	
1657	S	L	2	11	66	1090		583	
1660	N	L	2	11	66	748	.121	536	529
1662	S	L	2	12	66	1185	.066	516	516
1742	N	H	2	18	66	622	.090	594	587
1742	S	H	2	18	66	1368	.123	600	585
1743	N	H	2	18	66	595	.090	590	583
1745	N	L	2	18	66	689	.096	563	559
1747	S	L	2	18	66	1221	.084	556	552
1748	N	L	2	18	66	670	.248	550	527
1748	S	L	2	18	66	1124	.107	589	
1749	N	L	2	18	66	698	.330	577	544

ORBIT NUM.	P	S	M	D	Y	ALTITUDE KM	V2 RATE COUNTS/SEC	IONIZATION MEAS.	CORR.
1749	S	L	2	18	66	1096	.119	561	550
1750	S	L	2	18	66	1170	.140	551	536
1753	N	L	2	18	66	618	.176	571	557
1753	S	L	2	18	66	1280	.137	566	552
1754	N	L	2	18	66	660	.128	541	533
1754	S	L	2	18	66	1336	.105	538	530
1809	N	H	2	22	66	566	.113	594	580
1809	S	H	2	22	66	1432	.085	603	598
1810	N	H	2	22	66	539	.089	604	597
1810	S	H	2	22	66	1447	.155	587	564
1811	N	H	2	22	66	523	.097	584	575
1811	S	H	2	22	66	1463	.167	566	
1812	S	H	2	22	66	1461	.113	575	563
1813	N	H	2	23	66	512	.073	569	567
1813	S	H	2	23	66	1442	.075	521	
1814	N	H	2	23	66	531		576	
1816	N	H	2	23	66	562	.309	636	565
1817	S	H	2	23	66	1273	.143	616	596
1818	N	H	2	23	66	567	.319	679	606
1818	S	H	2	23	66	1259	.196	643	609
1820	N	H	2	23	66	608	.250	623	570
1820	S	H	2	23	66	1281	.149	598	576
1822	N	H	2	23	66	595	.109	639	626
1822	S	H	2	23	66	1393	.269	629	577
1823	N	H	2	23	66	543	.116	567	552
1823	S	H	2	23	66	1451	.095	570	562
1824	N	H	2	23	66	518	.133	584	564
1824	S	H	2	23	66	1450	.126	672	
2152	N	H	3	19	66	491		602	
2183	S	H	3	21	66	1295		747	
2184	N	H	3	21	66	589		853	
2194	N	H	3	22	66	540		908	
2194	S	H	3	22	66	1286		929	
2195	N	H	3	22	66	583		887	
2197	S	H	3	22	66	1285		983	
2198	N	H	3	22	66	590		879	
2199	N	H	3	23	66	576		933	
2200	N	H	3	23	66	557	.341	873	
2201	S	H	3	23	66	1442	.131	791	
2202	N	H	3	23	66	535	.308	851	
2208	N	H	3	23	66	592		1298	
2208	S	H	3	23	66	1304	.425	1614	
2209	N	H	3	23	66	609	.543	1447	
2209	S	H	3	23	66	1285		1566	
2211	S	H	3	23	66	1276	.450	1297	
2212	N	H	3	23	66	632	.523	1156	
2213	N	H	3	24	66	574		4003	
2214	N	H	3	24	66	573	.759	4227	

ORBIT NUM.	P	S	DATE M	D	Y	ALTITUDE KM	V2 RATE COUNTS/SEC	IONIZATION MEAS.	CORR.
2228	N	H	3	25	66	595	1.619	9171	
2229	N	H	3	25	66	563	1.891	8931	
2229	S	H	3	25	66	1381		6717	
2230	N	H	3	25	66	534	1.424	7605	
2230	S	H	3	25	66	1409		5732	
2235	N	H	3	25	66	610	.786	4330	
2235	S	H	3	25	66	1312	1.367	4381	
2236	N	H	3	25	66	654	.697	3620	
2236	S	H	3	25	66	1238	1.433	3413	
2238	S	H	3	25	66	1228	1.075	2633	
2239	N	H	3	25	66	683	.525	2566	
2241	N	H	3	26	66	635	.403	1802	
2242	N	H	3	26	66	599	.338	1681	
2243	N	H	3	26	66	567	1.116	1729	
2243	S	H	3	26	66	1367	.309	1529	
2244	N	H	3	26	66	560	.549	1494	
2244	S	H	3	26	66	1385		1357	
2245	N	H	3	26	66	551	.403	1371	
2245	S	H	3	26	66	1391	.254	1331	
2246	N	H	3	26	66	547	.249	1276	
2247	S	H	3	26	66	1340		1276	
2249	N	H	3	26	66	644		1177	
2249	S	H	3	26	66	1250		1282	
2250	N	H	3	26	66	686		1062	
2252	S	H	3	26	66	1172		996	
2253	N	H	3	26	66	699		1043	
2255	N	H	3	27	66	648		864	
2256	N	H	3	27	66	626		833	
2256	S	H	3	27	66	1367		772	
2257	N	H	3	27	66	610		814	
2257	S	H	3	27	66	1386		743	
2258	N	H	3	27	66	589		743	
2258	S	H	3	27	66	1394		784	
2259	N	H	3	27	66	571		774	
2259	S	H	3	27	66	1381		745	
2260	N	H	3	27	66	583		683	
2262	N	H	3	27	66	632		663	
2262	S	H	3	27	66	1220		725	
2263	N	H	3	27	66	676		700	
2263	S	H	3	27	66	1169		779	
2264	N	H	3	27	66	656		703	
2266	S	H	3	27	66	1207		727	
2268	N	H	3	28	66	680		681	
2269	N	H	3	28	66	658		670	
2270	N	H	3	28	66	653		899	
2270	S	H	3	28	66	1352		608	
2271	N	H	3	28	66	624		631	
2271	S	H	3	28	66	1434		598	

ORBIT			DATE			ALTITUDE	V2 RATE	IONIZATION	
NUM.	P	S	M	D	Y	KM	COUNTS/SEC	MEAS.	CORR.
2272	N	H	3	28	66	602		675	
2272	S	H	3	28	66	1366		607	
2273	N	H	3	28	66	591		622	
2276	N	H	3	28	66	680		644	
2276	S	H	3	28	66	1208		744	
2277	N	H	3	28	66	694		654	
2277	S	H	3	28	66	1131		703	
2278	S	H	3	28	66	1224		971	
2279	N	H	3	28	66	750		661	
2282	N	H	3	29	66	704		668	
2283	N	H	3	29	66	679		713	
2284	S	H	3	29	66	1331		639	
2285	N	H	3	29	66	638		617	
2285	S	H	3	29	66	1255		582	
2286	N	H	3	29	66	623		599	
2286	S	H	3	29	66	1342		563	
2287	N	H	3	29	66	611		589	
2290	N	H	3	29	66	724		569	
2291	N	H	3	29	66	728		565	
2291	S	H	3	29	66	1101		601	
2293	S	H	3	29	66	1089		582	
2294	N	H	3	29	66	774		580	
2295	N	H	3	29	66	749		571	
2296	N	H	3	30	66	716		564	
2298	N	H	3	30	66	680		570	
2299	S	H	3	30	66	1326		555	
2300	N	H	3	30	66	640		562	
2300	S	H	3	30	66	1315		531	
2301	N	H	3	30	66	638		533	
2304	N	H	3	30	66	727		543	
2304	S	H	3	30	66	1090		585	
2305	N	H	3	30	66	758		543	
2305	S	H	3	30	66	1062		599	
2306	S	H	3	30	66	1034		585	
2309	N	H	3	30	66	734		569	
2311	N	H	3	31	66	721		721	
2311	S	H	3	31	66	1272		549	
2312	N	H	3	31	66	693		558	
2312	S	H	3	31	66	1299		533	
2313	N	H	3	31	66	676		546	
2313	S	H	3	31	66	1302		520	
2314	N	H	3	31	66	661		545	
2314	S	H	3	31	66	1282		536	
2315	N	H	3	31	66	664		538	
2317	N	H	3	31	66	732		542	
2317	S	H	3	31	66	1102		560	
2318	N	H	3	31	66	828		526	
2318	S	H	3	31	66	1054		571	

ORBIT			DATE			ALTITUDE	V2 RATE	IONIZATION	
NUM.	P	S	M	D	Y	KM	COUNTS/SEC	MEAS.	CORR.
2319	N	H	3	31	66	796		530	
2319	S	H	3	31	66	1019		595	
2325	S	H	4	1	66	1250		541	
2326	N	H	4	1	66	720		549	

OGO-IV

ORBIT			DATE			ALTITUDE	V2 RATE	IONIZATION	
NUM.	P	S	M	D	Y	KM	COUNTS/SEC	MEAS.	CORR.
21	N	H	7	30	67	580	.104	459	
21	S	H	7	30	67	750	.089	445	
22	N	H	7	30	67	573	.078	441	
22	S	H	7	30	67	775	.090	422	
32	N	H	7	30	67	551		626	
33	N	H	7	30	67	549		590	
33	S	H	7	30	67	750	.129	583	
34	N	H	7	30	67	557	.356	548	
34	S	H	7	30	67	747	.127	560	
36	N	H	7	31	67	564		498	
36	S	H	7	31	67	774		507	
37	N	H	7	31	67	556		458	
37	S	H	7	31	67	800		471	
38	N	H	7	31	67	545		471	
38	S	H	7	31	67	827	.103	459	
39	N	H	7	31	67	526	.067	425	
39	S	H	7	31	67	846	.094	450	
40	N	H	7	31	67	517	.077	427	
40	S	H	7	31	67	858	.061	435	
42	S	H	7	31	67	858	.057	430	
43	N	H	7	31	67	499	.091	461	
45	N	H	7	31	67	517	.172	442	
46	N	H	7	31	67	524	.124	446	
47	N	H	7	31	67	533	.133	427	
47	S	H	7	31	67	770	.067	473	
48	N	H	7	31	67	537	.145	461	
48	S	H	7	31	67	763	.169	453	
49	N	H	7	31	67	550	.138	445	
49	S	H	7	31	67	763	.101	438	
50	N	H	7	31	67	552	.171	438	
50	S	H	8	1	67	774	.087	456	
51	N	H	8	1	67	548	.105	446	
51	S	H	8	1	67	796	.118	448	
52	N	H	8	1	67	537	.065	437	
52	S	H	8	1	67	824	.101	431	
53	N	H	8	1	67	521	.133	414	
53	S	H	8	1	67	844	.129	429	
54	N	H	8	1	67	512	.103	425	
54	S	H	8	1	67	863	.077	426	
55	N	H	8	1	67	510	.073	420	
55	S	H	8	1	67	873	.131	428	

ORBIT NUM.	P	S	M	D	Y	ALTITUDE KM	V2 RATE COUNTS/SEC	IONIZATION MEAS.	CORR.
56	N	H	8	1	67	489	.085	441	
57	S	H	8	1	67	867	.083	442	
58	N	H	8	1	67	491	.052	400	
60	N	H	8	1	67	507	.060	418	
61	N	H	8	1	67	516	.121	424	
64	N	L	8	1	67	538	.580	1935	
64	S	L	8	1	67	790	.587	1950	
110	N	H	8	5	67	491		484	
110	S	H	8	5	67	854	.140	490	
111	N	H	8	5	67	475	.123	478	
111	S	H	8	5	67	874		477	
114	N	H	8	5	67	459	.125	505	
114	S	H	8	5	67	904	.164	503	
115	N	H	8	5	67	452	.144	523	
115	S	H	8	5	67	902	.092	512	
119	N	H	8	5	67	473	.100	453	
121	S	H	8	5	67	826	.087	445	
122	N	H	8	5	67	490	.183	434	
122	S	H	8	5	67	828	.111	433	
128	N	H	8	6	67	457	.068	412	412
128	S	H	8	6	67	906	.127	403	400
133	N	H	8	6	67	460	.067	407	407
134	N	H	8	6	67	467	.047	395	397
136	S	H	8	6	67	840	.087	404	403
137	N	H	8	6	67	485	.135	415	408
137	S	H	8	6	67	840	.066	404	404
138	N	H	8	6	67	486		400	
138	S	H	8	7	67	850	.068	394	394
139	N	H	8	7	67	482	.064	408	408
139	S	H	8	7	67	867	.073	400	400
140	N	H	8	7	67	475	.049	410	412
140	S	H	8	7	67	886		406	
141	N	H	8	7	67	467	.073	399	398
141	S	H	8	7	67	901	.043	402	403
142	N	H	8	7	67	456	.033	396	399
142	S	H	8	7	67	908	.065	407	407
143	N	H	8	7	67	451	.062	393	393
143	S	H	8	7	67	913	.087	409	408
144	N	H	8	7	67	443	.064	405	405
144	S	H	8	7	67	914	.086	411	410
145	N	H	8	7	67	441	.055	394	395
149	N	H	8	7	67	460		386	
150	N	H	8	7	67	466		389	
150	S	H	8	7	67	852	.078	390	389
151	N	H	8	7	67	469	.107	393	389
151	S	H	8	7	67	847	.075	403	402
153	N	H	8	7	67	505		414	
153	S	H	8	8	67	864	.075	388	387

ORBIT			DATE			ALTITUDE	V2 RATE	IONIZATION	
NUM.	P	S	M	D	Y	KM	COUNTS/SEC	MEAS.	CORR.
159	S	H	8	8	67	914		420	
160	N	H	8	8	67	437	.073	397	396

Appendix II

Nuclear Reactions Involving Spacecraft Materials

The following is a list of reactions involving protons incident on the nuclei of materials which may occur in significant quantities on board the POGO spacecraft. All of the product nuclei β^+-decay except for ^{39}Cl, which β^- decays. Only reactions leading to product nuclei with half-lives between 10 and 100 minutes have been listed. Reactions in which γ-rays or 3 or more nucleons (except for α-particles) are emitted have not been considered. If the emitted particle is a deuteron, it is not required to be bound. The energy of the incident proton will most likely be between 10 and 100 MeV.

The half-lives for the product nuclei have been obtained from R. B. Leighton, Principles of Modern Physics (McGraw-Hill Book Company, Inc., New York, 1959), Appendix G. Also given are the percent abundances of the target isotope relative to all isotopes of that element.

Reaction			Half-life of product, min.	Product decays to	% abundance of target
^{12}C	(p, d)	^{11}C	20	^{11}B	98.9
^{14}N	(p, α)	^{11}C	20	^{11}B	99.6
^{14}N	(p, d)	^{13}N	10	^{13}C	99.6
^{16}O	(p, α)	^{13}N	10	^{13}C	99.8
^{40}A	(p, 2p)	^{39}Cl	55	^{39}A	99.6
^{50}Cr	(p, α)	^{47}V	31	^{47}Ti	4.4
^{50}Cr	(p, d)	^{49}Cr	42	^{49}V	4.4
^{52}Cr	(p, n)	^{52}Mn	21	^{52}Cr	83.7
^{52}Cr	(p, 2n)	^{51}Mn	45	^{51}Cr	83.7
^{53}Cr	(p, 2n)	^{52}Mn	21	^{52}Cr	9.5
^{54}Fe	(p, α)	^{51}Mn	45	^{51}Cr	5.9
^{54}Fe	(p, d)	^{53}Fe	9	^{53}Mn	5.9
^{60}Ni	(p, n)	^{60}Cu	24	^{60}Ni	26.2
^{62}Ni	(p, n)	^{62}Cu	10	^{62}Ni	3.7
^{63}Cu	(p, d)	^{62}Cu	10	^{62}Ni	69.0
^{63}Cu	(p, n)	^{63}Zn	38	^{63}Cu	69.0